Universidad Autónoma de Querétaro
Facultad de Ingeniería
Doctorado en Ingeniería

Procesamiento de imágenes con FPGA para el modelado cuantitativo del síndrome del virus mosaico del pepino en *Cucumis sativus*

TESIS

Que como parte de los requisitos para obtener el grado de

Doctor en Ingeniería

Presenta:
M.I. Luis Miguel Contreras Medina

Dirigido por:
Dr. Roque Alfredo Osornio Ríos

SINODALES

Dr. Roque Alfredo Osornio Ríos
Presidente
Firma

Dr. Irineo Torres Pacheco
Secretario
Firma

Dr. René de Jesús Romero Troncoso
Vocal
Firma

Dr. Ramón Gerardo Guevara González
Suplente
Firma

Dr. Luis Alberto Morales Hernández
Suplente
Firma

Nombre y Firma
Dr. Aurelio Domínguez González
Director de la facultad

Nombre y Firma
Dr. Irineo Torres Pacheco
Director de Investigación y Posgrado

Centro Universitario
Querétaro, Qro.
Septiembre de 2012
Querétaro, Qro, México

RESUMEN

Las enfermedades en plantas provocan pérdidas de alrededor de 220 billones de dólares anuales alrededor del mundo lo cual conlleva problemas económicos,desempleo, ambientales, sociales y de salud, debido a la falta de comida principalmente en los países pobres. Algo que ayudaría a reducir estos efectos, sería el conocer cómo se desarrolla la enfermedad a través del tiempo de manera cuantitativa con el objetivo de conocer el daño en las plantas con más precisión, evaluar prácticas de manejo y ayudar en el desarrollo de nuevas variedades resistentes. Para conocer el desarrollo del síndrome en plantas enfermas es necesario cuantificar de alguna manera que tan saludable esta la planta en un instante de tiempo determinado, para esto se han utilizado diferentes métodos, entre los más populares están: métodos ópticos, evaluaciones visuales (EV), visión por computadora (VC), métodos basados en compuestos orgánicos volátiles. Estos métodos ayudan, en base a síntomas provocados por los agentes patógenos, a estimar el estado de salud de las plantas en un instante de tiempo dado; por lo tanto, utilizar estos métodos para conocer el estado de salud de una planta en un instante de tiempo determinado, puede ser utilizado para describir cómo se desarrolla el síndrome en una planta en particular y en epidemiologia, a través del monitoreo de varios huéspedes, para saber cómo la enfermedad se desarrolla en una cierta área cultivada.

Para cuantificar el estado de salud de una planta en un instante de tiempo determinado los métodos utilizados presentan, en conjunto, desventajas como: alto costo, necesidad de personal entrenado, son tardados, análisis no *in-situ* y algunos métodos son destructivos. Para esto, el método de VC es el que, de alguna manera, trata de superar estas desventajas, sin embargo, los trabajos que emplean este método no realizan análisis *in-situ*, solo analizan uno o dos síntomas en particular y requieren personal entrenado. Por lo tanto el presente trabajo propone un sistema para la cuantificación de síntomas en plantas enfermas basados en la cuantificación de síntomas visibles y de dispositivos de punta tecnológica, como lo son los FPGAs (Field Programmable Gate Arrays) para superar las desventajas antes mencionadas.

Palabras clave: Procesamiento digital de imágenes, visión por computadora, FPGA, enfermedades en plantas, evaluaciones visuales.

SUMMARY

The plant diseases provoke 220 billion dollar of looseness around the world year by year carrying economical, environmental, social and health problems. A quantitatively knowledge about the plant diseases development could help to deal and reduce the aforementioned consequences caused by diseases through a better and more precise estimation about the damage presented in the plants. By doing this, new resistant plant varieties could be evaluated and developed. To know the syndrome development in diseased plants it is necessary to quantify the health of the plant at a certain time instant, to accomplish this, there are several methods and the most important are: optical methods, visual evaluations (VE), computer vision (CV) and volatile organic compounds based methods. These techniques help, based on symptoms provoked by pathogens, to estimate the health of the plant at certain time. Therefore, by using techniques able to estimate the health of the plant in certain time, it is possible to obtain a quantitative description of the syndrome development specifically in a diseased plant, and in epidemiology research to know how the plant disease evolve in the crop by monitoring several host.

The quantification of the health of the plant at certain time using the aforementioned methods present disadvantages such as: high cost, trained-personal necessity, lateness, *non-in-situ* analysis and some methods are destructive. The VC based-method tries to overcome the aforesaid disadvantages; however, the so far developed works that employ this method do not realize *in-situ* analysis and analyze just one or two symptoms and also require trained personal. Therefore, the present work proposes a system able of quantifying symptoms in diseased plants based on the quantification of visible symptoms and high-technological devices such as the FPGAs (Field Programmable Gate Arrays), used to overcome the aforementioned disadvantage.

Key words: Digital Image processing, computer vision, FPGA, diseased plants, visual evaluations.

DEDICATORIAS

AGRADECIMIENTOS

Al Consejo Nacional de Ciencia y Tecnología (CONACYT) por el apoyo brindado durante mis estudios de doctorado (Núm. de beca: 201401).

Al Fondo de Investigación de la Facultad de Ingeniería FIFI-UAQ 2011 por su apoyo económico para este proyecto.

A la Universidad Autónoma de Querétaro por permitirme realizar mis estudios de posgrado en esta institución.

ÍNDICE DE CONTENIDO

ÍNDICE DE CUADROS

Cuadro **Página**

ÍNDICE DE FIGURAS

Figura **Página**

I. INTRODUCCIÓN

El alimento es una parte fundamental para la existencia de los humanos y los animales en nuestro planeta ya que gran parte del alimento disponible proviene de las plantas, que al igual que las personas, sufren de condiciones y factores adversos tal como enfermedades, condiciones climatológicas adversas y algunos otros factores que disminuyen su capacidad de supervivencia. Estudios han demostrado que enfermedades, insectos y maleza conjuntamente interfieren con la producción y provocan la destrucción del 36.5% de los cultivos alrededor del mundo, de este porcentaje, el 14.1% se debe a enfermedades, lo cual equivale a una pérdida de $220 billones de dólares anuales (Agrios, 2005; Contreras-Medina et al., 2009). En el caso de México, hasta el 2009, las pérdidas debido a organismos dañinos provocan perdidas de al menos el 25% si no se controlan adecuadamente (INIFAP, Reporte anual 2009: Ciencia y Tecnología para el campo Mexicano). Por ejemplo, en el caso de frijol, en México existen variedades que al ser atacadas por enfermedades y plagas provocan pérdidas que oscilan entre el 30% y el 50% de la producción total y en el caso de chile serrano, los geminivirus provocan pérdidas que oscilan alrededor del 25% (INIFAP, Reporte anual 2009: Ciencia y Tecnologia para el campo Mexicano). Estas patologías además de causar pérdidas monetarias, son causa de desnutrición, y desempleo alrededor del mundo. De acuerdo con la FAO (Food and Agriculture Organization of the United Nations) (2010), existen 925 millones de personas que padecen algún tipo de desnutrición alrededor del mundo, de esta cantidad, 578 millones se encuentran en Asia y países del pacifico, sin embargo, la proporción más alta de personas con desnutrición respecto al total de su población siguen siendo los países de África donde en algunos países tal como Eritrea, por mencionar un ejemplo, tienen el 65% de su población con problemas de desnutrición, por lo tanto, la humanidad no se puede dar el lujo de permitir perdidas en los campos de producción. Debido estas razones, es necesario combatir las enfermedades en plantas, para esto, el uso de pesticidas es uno de los métodos más comunes empleados y año con año se requieren millones de kilogramos de químicos para tratamiento de semillas, suelos y frutos cosechados, lo cual provoca incremento en los costos de producción, liberación

de químicos tóxicos al ambiente y limitación de la producción y la cantidad de tierra disponible para el cultivo (Blaise et al., 1999). Por estas razones, el estudio de las enfermedades de las plantas tiene la muy importante y noble tarea de proteger gran parte del alimento disponible para las personas y los animales.

El estudio de las patologías en plantas se encarga de estudiar los organismos y factores ambientales que causan las enfermedades, los mecanismos por el cual son inducidas, los métodos de prevención y control y los daños que provocan. Se dice que una planta está enferma cuando sus funciones son interferidas o afectadas de su funcionamiento normal (Cooke et al., 2006), estas afectaciones provocan que las plantas muestren síntomas las cuales se definen como los cambios visibles provocados en respuesta a infecciones provocadas por un patógeno o condiciones climatológicas desfavorables; El patógeno es el agente transmisible que provoca la enfermedad y al conjunto de síntomas específicos que identifican a un patógeno o a una cierta condición anormal que se desarrollan desde que la planta es infectada hasta que la enfermedad desaparece o la planta muere se le conoce como síndrome (Cooke et al., 2006).

Con el objetivo de disminuir las pérdidas provocadas por las enfermedades en plantas, es necesario contar con estrategias adecuadas para el combate de las enfermedades que sean viables económicamente y no tengan impacto significativo en el ambiente (De Wolf y Isard, 2007). Para esto, es necesario conocer de manera precisa el estado de salud de las plantas así como los factores determinantes que provoquen el desarrollo de ciertas enfermedades en las mismas. Diversas herramientas han sido utilizadas para conocer el estado de salud de las plantas y entre las más importantes están los: modelos matemáticos, métodos inmunoquímicos y microbiológicos, métodos ópticos, evaluaciones visuales (EV), visión por computadora (VC) y Compuesto orgánicos volátiles (VOC).

Los modelos matemáticos han sido utilizados desde antes de los años 60s cuando Ware et al. (1932) y Ware y Young (1934) presentaron curvas para

ilustrar los efectos de resistencia y tratamientos de fertilización en algodón; sin embargo, fue hasta 1960 cuando Van Der Plank (1960) desarrolló el primer modelo epidemiológico. Las herramientas matemáticas para describir enfermedades en plantas más comúnmente utilizadas son las curvas de progreso de la enfermedad, ecuaciones diferenciales ligadas (LDE, Linked Diferencial Equation), Área bajo la curva de progreso de la enfermedad (AUDPC, Area Under Disease Progress Curve), las cuales frecuentemente hacen el uso de simuladores por computadoras para obtener soluciones numéricas. Estos modelos son generados de acuerdo a las variables de interés los cuales, generalmente son formuladas en función de factores externos como por ejemplo, temperatura y humedad. Estos modelos deben incorporar variables claves en el desarrollo del síndrome en plantas que permitan conocer el comportamiento lo más cercano posible a la realidad del desarrollo de la enfermedad, sin embargo, es común que algunas veces el fitopatólogo no considere las variables clave y por lo tanto los resultados de su modelo no serán adecuados, lo cual representa un problema.

Los modelos matemáticos son utilizados, en base a variables tales como temperatura y humedad para describir el desarrollo de las enfermedades en plantas a través del tiempo; sin embargo, existen técnicas que permiten conocer el estado de salud de una planta en cierto instante de tiempo y que emplean diversos principios para hacerlo, entre las más comunes están los métodos inmunoquímicos y microbiológicos tales como PCR (Polymerase Chain Reaction) y ELISA (Enzyme Linked Immunosorbent Assay) que son los más populares, sin embargo estas técnicas son tardadas y destructivas. Los métodos ópticos son, en su mayor parte, técnicas basadas en el hecho que la energía puede ser absorbida por el proceso fotosintético, térmicamente disipada por el tejido de la hoja y reflejada por fluorescencia, de modo que un incremento o reducción en alguno de estos tres procesos permite ser captado por estos métodos (Chaerle et al., 2004), y por lo tanto, los métodos ópticos son capaces de dar información acerca del estado de salud de la planta, no obstante, estas técnicas necesitan frecuentemente equipo costoso y personal entrenado.

Las evaluaciones visuales (EV) implican el uso de personal entrenado para dar información acerca del estado de salud de la planta basado en síntomas visibles que la planta enferma presenta; este método de estimación introduce subjetividad y frecuentemente es inexacto e impreciso (Díaz-Lago et al., 2003; Bock et al., 2008; Bock et al., 2009). La visión por computadora (VC) ha sido utilizada para estimar la salud de la planta a través de los síntomas que esta presenta, debido a que ofrece estimaciones de alta precisión y exactitud, lo cual trata de superar las desventajas presentadas por las EV. Sin embargo, hasta ahora los sistemas basados en VC no son capaces de realizar una estimación *in-situ* sobre el estado de salud de la planta, algunas veces requieren arrancar la parte de la planta a analizar y solamente analizan un síntoma o dos (Wijekon et al., 2008; Camargo y Smith, 2008; Camargo y Smith, 2009). Otra técnica que ha sido utilizada para detectar problemas virales, bacterianos y fúngicos en hojas es la termografía, la cual tiene la ventaja de poder detectar síntomas horas antes de que estos sean visibles al ojo humano (Chaerle et al., 2004) sin embargo, el equipo utilizado para adquirir imágenes térmicas es costoso, necesita personal entrenado y no realiza análisis *in-situ*.

En la actualidad, los procesos biológicos tienen un cierto grado de automatización, los cuales van desde utilizar dispositivos electrónicos tales como los FPGA como interface de comunicación, pasando por el uso de dispositivos tales como microcontroladores, DSP y FPGA para el control de variables climáticas dentro de invernaderos hasta el uso de FPGA para el desarrollo de sistemas de visión para clasificar productos provenientes del campo.

Los FPGA (Field Programmable Gate Array) han ganado popularidad en diversas áreas donde las aplicaciones demandan grandes capacidades de cómputo con el objetivo de ejecutar algoritmos complicados para resolver problemas que dispositivos comunes tales como computadoras personales (PC), microcontroladores (µC) o procesadores digitales de señales (DSP) no son capaces de realizar de manera satisfactoria. Las aplicaciones en áreas biológicas no han sido la excepción tal y como lo muestra Millan-Almaraz et al. (2010), donde respuestas fisiológicas de plantas tales como transpiración,

conductancia estomatal, temperatura diferencial hoja aire y déficit de presión de vapor son estimadas utilizando técnicas de sobremuestreo con el objetivo de disminuir el ruido característico de señales provenientes de fenómenos biológicos.

El objetivo de este trabajo es desarrollar una herramienta la cual permita conocer el estado de salud, a través de un análisis *in-situ* y no destructivo, de plantas enfermas basándose en VC y los FPGA como dispositivo de procesamiento y análisis.

II. **JUSTIFICACIÓN**

En la actualidad los daños provocados por las patologías existentes producen pérdidas millonarias en el mundo además de causar hambre y desnutrición. Por lo tanto, con el objetivo de prevenir y disminuir al mínimo los daños provocados por estas patologías, es importante adoptar la estrategia más adecuada. Una herramienta importante que ayudaría a adoptar las acciones más idóneas para prevenir las enfermedades sería conocer de manera objetiva su evolución. A lo largo de la historia, se han desarrollado modelos con los cuales se ha descrito cómo evoluciona un síndrome, entre ellos los más comunes están: el monomolecular, el Gompertz y los modelos logísticos, sin embargo, éstos no son lo suficientemente satisfactorios puesto que necesitan involucrar variables que afectan el desarrollo de la enfermedad la cual al ser evaluada subjetivamente, ponen en riesgo la veracidad de los resultados, por lo tanto, son necesarias herramientas capaces de cuantificar el grado de enfermedad en plantas de manera cuantitativa.

El patologías en plantas se manifiestan con síntomas como pueden ser puntos de colores en forma de mosaico y deformaciones en las hojas, los cuales son visibles. Una de las disciplinas que puede ser utilizada para analizar y detectar estos síntomas es el procesamiento de imágenes el cual por medio de algoritmos de segmentación, análisis de textura, análisis de formas, entre otros; puede detectar y cuantificar estos síntomas. En la actualidad, una de las metodologías capaz de realizar estas tareas y que resulta atractiva debido a la robustez de sus procesos, ventajas en implementación y a la facilidad de uso

de los operadores entre otras más, es el procesamiento morfológico de imágenes, la cual basa su funcionamiento en teoría de conjuntos. El procesar una imagen en tiempo real implica el manejo de una gran cantidad de información en tiempos realmente cortos, por lo tanto, para esto se requiere rapidez de procesamiento. Un dispositivo de punta tecnológica capaz de realizar análisis y procesamiento sobre una gran cantidad de datos en tiempo real es el FPGA, ya que permite procesamientos paralelos a velocidades muy altas además de ser un dispositivo de bajo costo y altamente reconfigurable. Con el objetivo de obtener un sistema computacionalmente eficiente capaz de cuantificar los síntomas que se presentan en plantas enfermas, que ayude a proponer estrategias óptimas para aminorar los daños provocados por ciertas patologías, se justifica el uso del procesamiento morfológico de imágenes y los FPGA como herramientas principales debido a las ventajas que ambos ofrecen.

III. **DESCRIPCIÓN DEL PROBLEMA**

En la actualidad, en México las pérdidas debido a organismos dañinos provocan perdidas de al menos el 25% en los campos de cultivo si no se controlan adecuadamente, tal como se menciono el caso de frijol y el chile serrano por mencionar algunos ejemplos. Debido a esto, son necesario métodos para prevenir y controlar los daños causados por las patologías, los cuales, hasta ahora no son lo suficientemente satisfactorios debido a que la estimación acerca de la existencia y evolución de las patologías en plantas se realiza generalmente de manera subjetiva, lo cual conlleva generalmente a estimaciones erróneas y aunque existen métodos objetivos, estos no son lo suficientemente confiables para dar una estimación correcta acerca del estado de la planta. Por estas razones, es necesario un método capaz de estimar de manera objetiva y confiable la evolución de las patologías en plantas para prevenir la aparición y desarrollo de las mismas. Actualmente trabajos realizados para combatir las enfermedades en plantas no cuentan con métodos satisfactorios para medir su evolución, puesto que éstos sólo son útiles para discriminar las plantas saludables de las infectadas. Una práctica comúnmente realizada es que personal altamente experimentado emita un juicio subjetivo para determinar en qué etapa de evolución se encuentra el síndrome, lo cual

representa un problema debido a las discrepancias que pueden existir de un juicio a otro. Algunos trabajos presentan una clasificación de la severidad de la enfermedad acorde a la sintomatología observada evaluada de manera cualitativa (Anaya-López *et al*., 2003). Los tres modelos mencionados con anterioridad que comúnmente son utilizados para describir la evolución de las patologías en plantas requieren hacer suposiciones y cambios a la forma general del modelo, lo que puede provocar resultados erróneos o una mala interpretación de los mismos y por tanto no son capaces de predecir la evolución de la enfermedad de manera confiable, lo cual representa un problema. Los agentes patógenos que provocan las enfermedades en plantas se presentan en una amplia variedad de vegetales, sin embargo, en algunos de éstos, la sintomatología observada es más complicada tratarla debido a que no es evidente.

En la actualidad, los trabajos sobre patologías en plantas realizan un análisis fuera de línea con personal altamente entrenado o se auxilian de una computadora personal para hacer el procesamiento de los datos (Raupach et al., 1996; Pavlou et al., 2001; Jetiyanon et al., 2003; Lindenthal et al., 2004) esto representa una desventaja en costo, portabilidad y tiempo siendo este último el más importante puesto que a mayor tiempo mayores son los daños que se presentan en la planta y mayores son las pérdidas económicas.

Actualmente el procesamiento de imágenes se aplica a diversas áreas y el estudio de las patologías en plantas no es la excepción. Las técnicas de procesamiento de imágenes son utilizadas para análisis y de esta manera detectar plantas infectadas. Uno de los problemas principales de las técnicas comunes utilizadas en procesamiento de imágenes tradicional son generalmente los recursos computacionales que utilizan además de que no son robustas. Una metodología relativamente nueva capaz de resolver estos problemas es el procesamiento morfológico de imágenes. Esta metodología es utilizada en varias ramas de la ciencia debido a las ventajas que ofrece. De lo anterior se puede inferir, que en la actualidad no existe un sistema capaz de evaluar confiablemente de manera objetiva y en tiempo real los síntomas en plantas que además pueda servir como herramienta para evaluar de manera

cuantitativa el desarrollo del síndrome en plantas enfermas. El presente trabajo muestra una herramienta para la cuantificación de cinco síntomas comunes en plantas, estos síntomas son: clorosis, necrosis, deformación, manchas blancas y mosaicos. El sistema emite una evaluación cuantitativa acerca de cada uno de los cinco síntomas lo cual permitiría cuantificar de mejor manera los daños provocados por agentes patógenos.

IV. **OBJETIVOS E HIPÓTESIS DEL TRABAJO**

4.1 Hipótesis

Mediante el procesamiento morfológico de imágenes implementado en FPGA (*Field Programmable Gate Array*) es posible desarrollar un sistema capaz de predecir y evaluar de manera más precisa el síndrome de virus mosaico del pepino en *Cucumis Sativus* a como lo realizan los modelos epidemiológicos existentes.

4.2 Objetivo General

Mejorar robustez en la medición de variables para la alimentación de los modelos epidemiológicos existentes.

4.3 Objetivos Específicos

1. Caracterizar teórica y experimentalmente el síndrome del virus mosaico del pepino en *Cucumis sativus*.

2. Implementar los cores de los operadores morfológicos mediante estructuras FPGA para contar con las herramientas tecnológicas que permitan solucionar el problema.

3. Determinar la secuencia óptima de operadores morfológicos que permitan cuantificar el síndrome bajo estudio.

4. Generar al menos un modelo epidemiológico más preciso.

5. Comparar el modelo generado con los modelos epidemiológicos existentes.

V. **REVISIÓN DE LITERATURA**

Como se mencionó anteriormente, existen diversas herramientas y técnicas que han sido utilizadas para conocer de manera precisa el desarrollo de enfermedades en plantas. Entre las cuales se encuentran las herramientas matemáticas y técnicas tales como: métodos inmunoquímicos y microbiológicos, métodos ópticos, evaluaciones visuales, visión por computadora, compuestos volátiles. Estas técnicas son las más ampliamente utilizadas hasta ahora y a continuación se describirán cada una de ellas y lo que se ha hecho respecto a cada una de las técnicas.

5.1 Herramientas matemáticas

Las herramientas matemáticas ampliamente utilizadas para describir el desarrollo de un síndrome en plantas son:

1. Modelos de crecimiento (curvas de progreso de la enfermedad).
2. Ecuaciones diferenciales ligadas.
3. Área bajo la curva del progreso de la enfermedad (ABCPE).
4. Simulaciones por computadora.

5.1.1 Modelos de crecimiento

Los modelos de crecimiento proveen un rango de curvas que son frecuentemente similares a las curvas de progreso de la enfermedad y representan una de las herramientas matemáticas más comunes para describir epidemias de enfermedades en plantas (Xu, 2006). Los modelos de crecimiento más comúnmente usados son: Monomolecular, Exponencial, Logístico y Gompertz (Contreras-Medina et al., 2009).

Monomolecular: este modelo de crecimiento es apropiado para modelar enfermedades donde no hay infecciones secundarias dentro de un periodo de crecimiento, esto significa que la enfermedad en la planta tiene un único ciclo durante el crecimiento de la planta (Contreras-Medina *et al*., 2009) (ver Figura 5.1).

Exponencial: este modelo es conocido como logarítmico, geométrico o Malthusian y es apropiado cuando nuevos individuos esparcen la enfermedad a otros individuos. Este modelo es aplicado para describir en etapas tempranas la mayoría de las enfermedades policíclicas (Contreras-Medina *et al*., 2009) (ver Figura 5.1).

Logístico: este modelo fue primeramente propuesto por Veshuls in 1838 para representar el crecimiento de la población humana. Un segundo tipo de modelo logístico fue propuesto por Van der Plank (1963), siendo más apropiado para describir la mayoría de las enfermedades policíclicas en plantas, lo cual significa que existe un esparcimiento secundario de la enfermedad. Este modelo es el más ampliamente utilizado para describir epidemias de enfermedades en plantas (Segarra *et al*., 2001; Jeger, 2004) (ver Figura 5.1).

Gompertz: este modelo de crecimiento es apropiado para enfermedades policíclicas como una alternativa a modelos logísticos. El modelo Gompertz tiene una curva absoluta que alcanza un máximo más rápidamente y decae mas gradualmente que el modelo logístico (Contreras-Medina *et al*., 2009). La Figura 5.1 muestra la diferencia entre la curva logística y la Gompertz, las cuales tienen características sigmoidales y un punto de inflexión lo cual significa que existe inoculación secundaria.

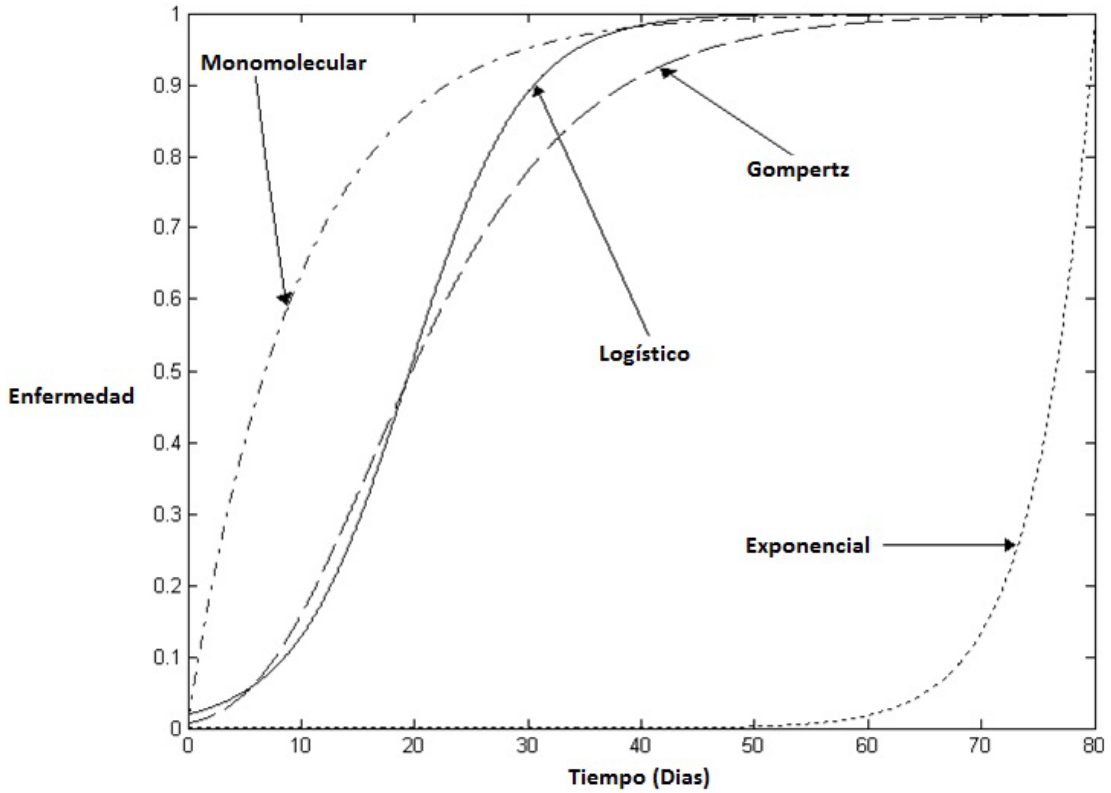

Figura 5. 1. Ejemplos de curvas de progreso de la enfermedad representados por modelos monomoleculares, exponenciales, logísticos y Gompertz.

5.1.2 Ecuaciones diferenciales ligadas (LDE)

Esta herramienta matemática realiza la descripción de epidemias de enfermedades en plantas modelando cada una de las variables consideradas determinantes en el desarrollo de la enfermedad y posteriormente ligando cada una de ellas (ver Figura 5.2). LDE tiene la ventaja de incorporar nuevos términos en el modelo (Madden, 2006), sin embargo, los modelos generados por esta herramienta generalmente no permiten obtener una solución analítica y por tanto se ocupan métodos numéricos para calcular una solución (Xu, 2006; Madden 2006) la cual, con los desarrollos computacionales alcanzados hasta ahora, son fácilmente obtenibles. Un modelo relativamente simple de ecuaciones diferenciales ligadas para enfermedades policícilicas involucra variables como tejido sano, tejido infeccioso, tejido latente e individuos removidos (hojas, raíces y plantas) (Madden, 2006); Zhang *et al.* (2001) utilizó cuatro ecuaciones diferenciales ligadas para ilustrar el efecto de sinergismo entre virus de plantas donde cada ecuación diferencial representa uno de las siguiente cuatro categorías: planta sana, planta infectada con el tipo de virus A

solamente, planta infectada con un virus del tipo B y planta infectada con ambos virus A y B.

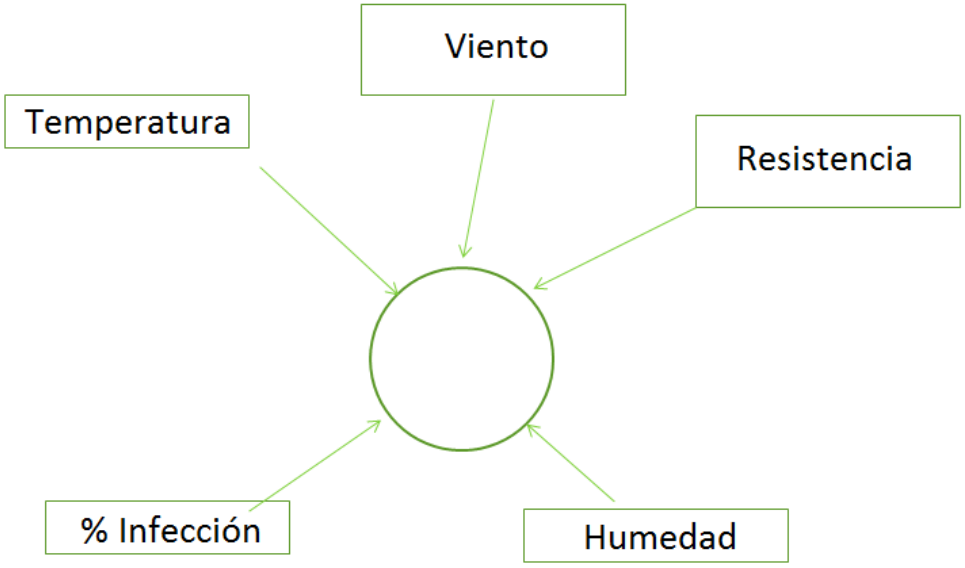

Figura 5. 2. Variables comúnmente utilizadas por el método de ecuaciones diferenciales ligadas.

5.1.3 Área bajo la curva de progreso de la enfermedad (AUDPC)

Esta técnica es muy útil cuando los patrones observados no pueden ajustarse utilizando las curvas de progreso de la enfermedad (Mannen y Xu, 2003; Xu, 2006). El área bajo la curva de progreso de la enfermedad puede ser vista como la cantidad de enfermedad integrada entre dos tiempos de interés y es calculada no importando la forma de la curva (Shanner y Finner, 1977) (ver Figura 5.3). Los datos del progreso de la enfermedad son resumidos en un solo valor utilizando AUDPC; este es adecuado cuando el daño en el hospedero, la cantidad y duración de la enfermedad son proporcionales (Xu, 2006). AUDPC es generalmente utilizado para hacer comparaciones entre tratamientos (Jeger, 2004; Xu, 2006) y para evaluar la resistencia de especies de plantas a los patógenos (Milukova et al., 2008; Irfaq at al., 2009).

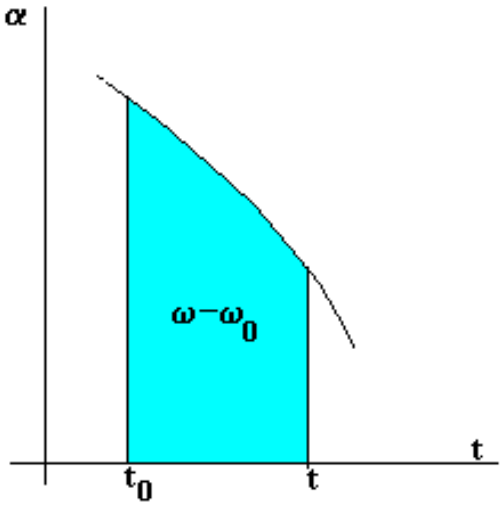

Figura 5. 3. Área bajo la curva entre dos instantes de tiempo.

5.1.4 Simulaciones por computadora

Esta herramienta es utilizada comúnmente en conjunto con LDE para determinar las características clave del sistema patológico. Varios modelos han sido utilizados para simular la dinámica de las enfermedades de plantas con el objetivo de prevenir y controlar la epidemia de la enfermedad. Uno de los primeros programas fue EPIDEM desarrollado por Wagonner y Horsfall (1969) el cual fue diseñado para simular la enfermedad del tizón temprano de tomate y papa provocado por el hongo *Alternaria solani* y esto es resultado de modelar cada etapa de vida del patógeno como una función de variables ambientales. En la actualidad, programas de computadora son utilizados para soportar otras técnicas con el objetivo de predecir enfermedades en plantas y medir el impacto de patologías sobre ciertas especies basándose en variables particulares como humedad de hoja, lluvia, humedad del ambiente, etc. Un ejemplo de esto es el programa PLASMO que es utilizado para medir el impacto en la calidad de *Plasmora vitícola* debido a le duración de la humedad de la hoja (Marta *et al*., 2005; Orlandini *et al*., 2008).

Las herramientas matemáticas antes mencionadas son utilizadas para modelar o describir el desarrollo de enfermedades en plantas a través del tiempo, lo cual sirve como indicador del estado de salud de las plantas. Existen técnicas las cuales nos permitió conocer la salud de una planta basándose en síntomas visibles y no visibles al ojo humano que permiten conocer alguna

alteración en la fisiología o procesos metabólicos de las plantas debido a algún factor biótico o abiótico, entre los métodos más populares se encuentran los siguientes:

1. Métodos inmunoquímicos y microbiológicos.
2. Métodos ópticos.
3. Evaluaciones visuales (EV).
4. Visión por computadora (VC).
5. Compuestos Volátiles Orgánicos (VOC).

5.1.5 Métodos inmunoquímicos y microbiológicos

Lo métodos inmunoquímicos y microbiológicos más populares son el PCR (Polymerase Chain Reaction) y ELISA (Enzyme Linked Immunosorbent Assay) debido a que son capaces de cuantificar de manera precisa la cantidad de virus, bacterias y hongos presentes en el tejido de plantas lo cual sirve como indicador de severidad de la enfermedad. PCR es una técnica la cual permite replicar muy rápidamente cantidades diminutas de ADN y así amplificarlas hasta tal punto en que el ADN se hace fácilmente detectable para ser estudiado o para cualquier otro propósito. ELISA es un ensayo diseñado para detectar y cuantificar sustancias tales como péptidos, proteínas, anticuerpos y hormonas. En una ELISA un antígeno debe ser inmovilizado a una superficie sólida y entonces unirse con un anticuerpo que está ligado a una enzima, la detección es realizada midiendo la enzima conjugada por medio de una incubación con un sustrato para producir un producto medible. Estas técnicas, aunque son muy populares, consumen tiempo e implican la destrucción de la muestra a ser analizada (Heuser and Zimmer, 2003; Maciá-Vicente *et al*., 2009).

5.2 Métodos ópticos

5.2.1 Termografía

Una herramienta importante para detectar enfermedades en plantas en etapas tempranas es la termografía, esta técnica permite la detección de enfermedades virales y fúngicas en plantas antes de que los primeros síntomas puedan ser detectados visualmente por un evaluador (Chaerle *et al*., 2009). No obstante, esta técnica aunque es muy prometedora, requiere equipo costoso ya que el costo de las cámaras infrarrojas más sencillas oscila entre $30,000 y $50,000, además requieren personal capacitado y no realiza análisis *in-situ*.

5.2.2 Reflectancia hyperespectral

La reflectancia hyperespectral es una técnicas que han sido utilizadas para la detección temprana de desordenes bióticos y abióticos en plantas. Se basan en el hecho que la energía luminosa puede ser absorbida por el proceso fotosintético, disipada en forma de calor y reflejada por emisiones de fluorescencia de clorofila. De tal manera que una reducción y/o un incremento en la disipación térmica o vicerversa puede ser detectado por medio de reflectancia hyperespectral, este método permite obtener una firma espectral de la planta al excitarla con una fuente luminosa de varias longitudes de onda del espectro electromagnético el cual puede ir desde el rango visible, infrarrojo cercano y hasta el infrarrojo lejano, este método implica el uso de equipo costoso y personal entrenado y algunas veces necesita destruir la muestra bajo análisis lo cual representa un estrés para la planta (Delalieux *et al*., 2009).

5.2.3 Fluorescencia de clorofila

Fluorescencia es el fenómeno donde una cierta cantidad de energía luminosa es retenida y subsecuentemente expulsada después de exponer a la planta a la luz (Taiz y Zeiger, 2002). La fluorescencia de la clorofila ha sido utilizada de varias formas, y su uso para la detección de enfermedades en plantas no es la excepción. Este método, al igual que el método de reflectancia hyperespectral, permite detectar cambios en la disipación y absorción de la energía luminosa por parte de la planta a través de la fluorescencia de la clorofila. El fenómeno se basa en el principio de Kautsky el cual mide la

relación entre la fluorescencia minima F_o y la fluorescencia máxima F_m además conocida como fluorescencia de saturación, el método consiste en colocar la muestra en un cuarto oscuro, la cual es iluminada a través de pulsos para estimar F_o y posteriormente la muestra se ilumina constantemente para obtener F_m. después la viable F_v es calculada utilizando F_m y F_o (F_m - F_o) lo cual conduce a estimar F_v/F_m que a su vez permite la estimación de fluorescencia de clorofila el cual es un estimador de la tasa de fotosíntesis de la planta (Millan-Almaraz *et al*., 2009; Delalieux *et al*., 2009). Como puede suponerse, al igual que el método de reflectancia hyperespectral, este método es costoso, necesita personal entrenado y en la mayoría de los casos no realiza un análisis *in-situ* de la planta.

5.2.4 Otras técnicas

Existen otras técnicas basadas en métodos ópticos para la detección de infecciones y otros tipos de estrés en plantas y frutos que son menos utilizadas que los métodos anteriores, sin embargo, vale la pena mencionarlas. La primera de estas es la resonancia magnética nuclear y las imágenes obtenidas utilizando rayos X. Goodman et al (1992), utilizó imágenes microscópicas de resonancia magnética nuclear para la identificación del patógeno *Botrytis cinerea* en la frambuesa roja. Narvankar et al (2009) utilizó imágenes obtenidas con rayos X para identificar infecciones provocadas por hongos en trigo. Los autores emplearon modelos discriminantes estadísticos y redes Neuronales Artificiales (ANNs) para clasificar las imágenes de diferentes variedades de trigo.

5.3 Evaluaciones visuales

Las estimaciones visuales implican utilizar personal que emite una evaluación acerca del estado de la planta basado en síntomas visuales de la planta enferma, este método como hace suponer, induce subjetividad y frecuentemente es inexacto e impreciso (Diaz-Lago *et al*., 2003; Bock *et al*., 2008; Bock *et al*., 2009). Varios trabajos cuando miden la resistencia de plantas a ciertos patógenos utilizan escalas para evaluar la severidad de la planta o usualmente hacen la evaluación basada en inspecciones visuales. Anaya-Lopez *et al*. (2003) utilizó una escala de nueve niveles para medir

cualitativamente la severidad de plantas de chile afectadas por geminivirus. Otro tipo de evaluaciones llamadas mediciones pictóricas de enfermedad han sido creadas y se basan en diagramas estándares que ilustran el desarrollo de las etapas en la enfermedad sobre unidades simples (hojas y frutos) o largas compuestas por ramas o plantas completas (Cooke, 2006). Holb *et al*. (2003) investigaron las relaciones entre mediciones de enfermedad, incidencia de enfermedad, severidad de la roya en manzanas y sus implicaciones para el desarrollo de modelos predictivos; las mediciones de enfermedad fueron basados en la severidad de la hoja y fruto utilizando ecuaciones matemáticas las cuales clasifican el fruto y la hoja dentro de escalas de seis y siete niveles de severidad respectivamente.

5.4 Visión por computadora (VC)

La visión por computadora trata de resolver las desventajas que presenta la estimaciones visuales debido a que la VC ofrece mediciones de alta precisión, exactitud y reproducibilidad comparado con las EV. Sin embargo hasta ahora los sistemas basado en VC no son capaces de llevar a cabo análisis *in-situ* y en tiempo real, además, por lo general analizan solo uno o dos síntomas en especifico. Acorde con Bock et al (2009), VC es incapaz de distinguir síntomas particulares de enfermedades en plantas cuando la planta es afectada por varias enfermedades. Martin y Rybicki (1998) realizaron una comparativa entre un sistemas basados en VC desarrollado por ellos y los sistemas basados en VC comerciales para evaluar la clorosis presente en hojas de maíz provocada por el virus de la roya del maíz (MSV). Camargo y Smith (2009) implementaron un sistema de visión por computadora para clasificar los síntomas visuales causados por insectos y bacterias; síntomas tales como manchas y deformaciones fueron identificadas y obtenidas de diferentes regiones de la planta como lo son hoja, fruto y tallo utilizando técnicas como matriz de co-ocurrencia, dimensión fractal y lagunaridad, que en conjunto con una máquina de soporte de vector (SVM) fueron utilizadas para llevar a cabo la clasificación de los síntomas antes mencionados. Camargo y Smith (2008) propusieron una metodología basada en VC para identificar síntomas en hojas enfermas basadas en transformaciones de color H, I3 y I3b

así como máximos locales localizados en el histograma. En el trabajo presentado por Wijekon *et al*. (2008) una cuantificación de enfermedades fúngicas fue hecha, donde diagramas de diferentes enfermedades provocadas por hongos propuesta por James (1977) fueron utilizadas para cuantificar la infección en plantas de nicotina utilizando el software llamado Scion, las imágenes fueron de hojas arrancadas y no arrancadas para ser analizadas utilizando escáner y cámara respectivamente a través de un análisis fuera de sitio. Al-hiary *et al*. (2011) propuso un sistema basado en VC para clasificar hojas afectadas por diferentes patógenos; el algoritmo está basado en el cálculo de valores estadísticos de la textura y redes neuronales artificiales para realizar la clasificación; el algoritmo detecta y clasifica plantas enfermas con una precisión de entre 83% y 94%. Aunque los sistemas descritos anteriormente basados en VC dan mediciones precisas, estos consumen demasiado tiempo para realizar el análisis, necesitan personal capacitado para realizar el análisis y frecuentemente analizan solo un síntoma en específico.

5.5 Compuestos orgánicos volátiles

Los compuestos orgánicos volátiles (VOC) liberados por las plantas son influenciados por factores físico-químicos (humedad, temperatura, luz, condiciones de suelo, crecimiento y etapa de desarrollo de la planta) que afectan las condiciones fisiológicas de la misma, así influenciando el perfil VOC (Sankaran *et al*., 2010). Diferentes tipos de estrés biótico y abiótico puede provocar cambios en los perfiles VOC de las plantas y pueden ser utilizados como un indicador indirecto para la medición de enfermedades de las mismas. Los dos métodos comunes para la medición del perfil de los metabolitos volátiles libreados por las plantas son basados en cromatografía de gases (GC) y narices electrónicas. Laothawornkitkul *et al*. (2008) evaluó el potencial de la firma de compuesto volátiles para monitoreo de enfermedades en plantas de pepino, chile y tomate. Liu *et al*. (2005) inoculó raíces de papa con *Phytophthora infestans, Pythium ultimum, y Botrytis cinerea;* y analizó el resultado de los perfiles VOC usando GC. Los sistemas basados en VOC desarrollados hasta ahora para el monitoreo de enfermedades no son capaces de realizar análisis *in-situ*, en tiempo real; además de que presentan las

desventajas de la variación natural en el perfil VOC dentro de las especies de plantas, además de ser costosos (Sankaran et al., 2010).

VI. **MATERIALES Y MÉTODOS**

6.1 Síntomas

Los síntomas en plantas son definidos como respuestas a las alteraciones en sus funciones fisiológicas y desordenes metabólicos que son causados principalmente por infecciones o deficiencias nutricionales (Agrios, 2005; Taiz y Zeiger, 2006). Los síntomas pueden ser visualizados en hojas, tallos y raíces, de modo que, mediciones precisas de síntomas en plantas pueden ser usados como indicadores indirectos para el monitoreo de enfermedades y desnutrición en plantas, principalmente para estimar perdidas en los campos de cultivo y generación de resistencia contra enfermedades de plantas Bock *et al*. (2008). Existe una gran variedad de síntomas que se presentan en plantas enfermas y en las que presentan deficiencias nutricionales; sin embargo, los que se estudiaran en este trabajo son: clorosis, deformación de hoja, manchas blancas, necrosis y mosaicos. A continuación se describe como se manifiesta cada uno de estos síntomas de manera detallada y que son lo que los provoca.

6.1.1 Clorosis

El síntoma de la clorosis es definido como un amarillamiento del tejido normalmente verde que, en el caso de plantas enfermas, puede deberse debido a la destrucción de la clorofila o anormalidades en la formación de ésta (Agrios, 2005). La clorosis puede ser causada por patógenos de tipo viral, bacteriológico o fúngico. En el caso de deficiencias nutricionales, la clorosis es el síntoma más común y puede ser causado por varias razones, una de ellas es la carencia de minerales que sirven como componente base de muchas células de plantas, enzimas y vitaminas, además como componentes esenciales en los procesos metabólicos; estos minerales son nitrógeno y azufre; otra razón es debido a la deficiencia de los minerales tales como potasio, calcio y magnesio presente en plantas en forma de cationes y iones, los cuales juegan un papel

importante en el proceso fotosintético (Taiz y Zeiger 2006). El síntoma de la clorosis puede ser localizado o generalizado, lo cual significa que la clorosis puede afectar solamente ciertas regiones o la hoja completa. Un ejemplo ideal de hoja sana, hoja con clorosis generalizada y localizada se muestra en la Figura 6.1. La Figura 6.1(a) muestra la imagen de una hoja de calabaza sana que tiene un tejido verde homogéneo idealizado, por otro lado, la Figura 6.1(b) muestra una hoja de calabaza idealizada con el síntoma de clorosis localizada; la hoja presenta una sección con color verde homogéneo y la sección de la hoja faltante es cubierta por un color amarillento. La Figura 6.1(c) muestra una hoja de calabaza idealizada con síntoma de clorosis generalizado, la hoja presenta un color amarillento cubriendo completamente todo el tejido.

Figura 6. 1. a) Hoja de calabaza sana con color verde homogéneo. b) Hoja de calabaza con síntoma de clorosis localizada. c) Hoja de calabaza con clorosis generalizada.

6.1.2 Necrosis

Al tejido muerto en plantas en un área localizada es llamada necrosis y comúnmente resulta en lesiones de color café o negras, generalmente precedidas por un amarillamiento (clorosis). Estos síntomas pueden ser provocados por patógenos de plantas o deficiencias de minerales tales como boro, potasio, calcio, cloro y sodio (Trigiano *et al*., 2004; Taiz y Zeiger, 2006). La Figura 6.2 muestra tres imágenes esquematizadas que presentan como se manifiesta este síntoma sobre las hojas de las plantas, la Figura 6.2(a) presenta una hoja sana la cual tiene un color verde homogéneo cubriendo completamente la hoja, La Figura 6.2(b) muestra una hoja enferma no clorótica con síntomas de necrosis y la Figura 6.2(c) presenta una hoja enferma con síntomas de necrosis y clorosis generalizada. Es importante mencionar que

estas imágenes fueron generadas de manera artificial y tiene la finalidad de ilustrar de manera idealizada como se manifiestan los síntomas sobre las hojas.

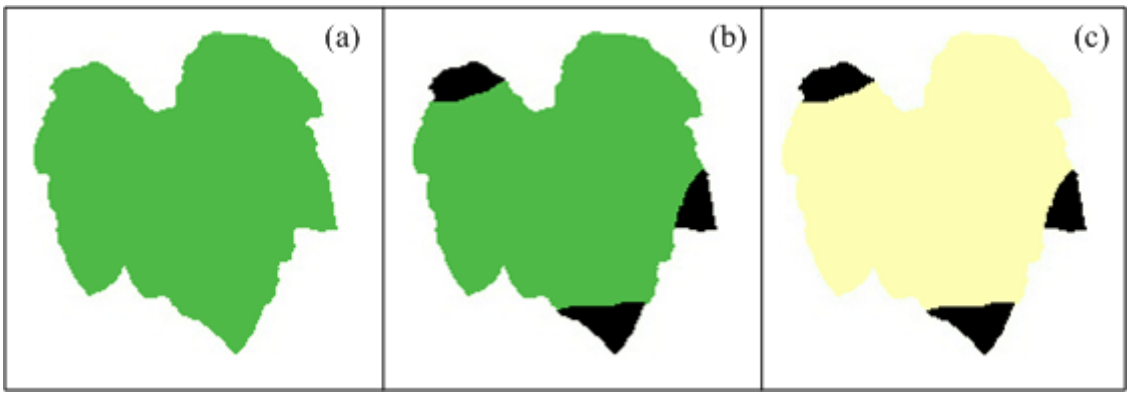

Figura 6. 2. a) Hoja de calabaza con color verde homogéneo. b) Hoja de calabaza no clorótica con áreas neuróticas. c) Hoja de calabaza clorótica con áreas neuróticas.

6.1.3 Deformación de la hoja

Cambios en la superficie de las hojas de la planta resultan en áreas que están retorcidas, deformadas o distorsionadas; estas deformaciones pueden ser descritas como burbujas, rugosidad o curveo (Trigiano *et al*., 2004). Estos síntomas pueden ser causados por patógenos de plantas o deficiencias nutricionales, principalmente por la carencia de potasio (Taiz y Zeiger, 2006); estos tipos de deformaciones implican un cambio en la forma normal de los bordes de la hoja. La Figura 6.3(a) presenta el contorno de una hoja esquematizada sana de planta de chile, la Figura 6.3. (b) y (c) muestran el contorno esquematizado de hojas no sanas que presentan deformaciones debido a la presencia de burbujas y rugosidad. Es claro como la hoja sana (Figura 6.3(a)) presenta una forma más simétrica que las otras dos hojas, un estimador de estas deformaciones puede ser obtenidos a través de las características geométricas de la hoja como se verá más adelante.

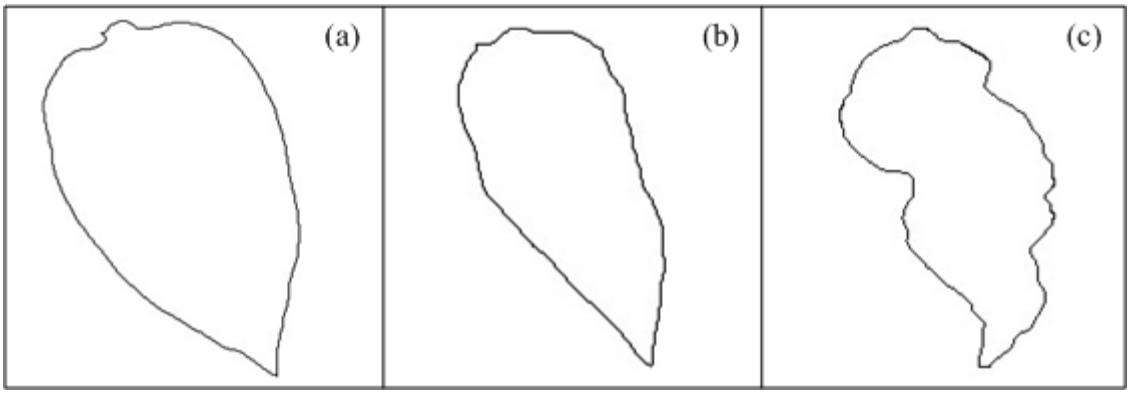

Figura 6. 3. a) Contorno de hoja de hoja de chile. b) Contorno de chile con poca deformación. c) Contorno de hoja de chile con deformación severa.

6.1.4 Manchas blancas

Las manchas blancas son provocadas cuando los patógenos de las plantas o la deficiencia de minerales involucrada en la biosíntesis de clorofila tal como zinc, afectan las funciones de fotosíntesis y respiración; esto provoca inestabilidades de la planta para responder contra el patógeno (Agrios, 2005; Taiz y Zeiger, 2006). La Figura 6.4(a) presenta una hoja de frijol sana esquematizada con color verde generalizado y las Figuras 6.4(b) y (c) muestran hojas de frijol enfermas esquematizadas con síntomas de manchas blancas; es claro que, la presencia de manchas blancas es mayor en las hojas enfermas (Figura 6.4(b) y (c)) en comparación con la hoja sana (Figura 6.4(a)).Las manchas blancas pueden afectar hojas cloróticas y no cloróticas.

6.1.5 Mosaico

El síntoma de mosaico es caracterizado por áreas blancas, amarillas o verdes brillantes mezcladas con el color verde normal de la hoja, también pueden presentarse colores intensos mezclados con áreas de color normal en flores o frutos; estos síntomas son provocados principalmente por patógenos virales (Agrios, 2005). Dependiendo de la intensidad de los patrones o decoloraciones, los tipos de mosaico pueden ser descritos como moteado, patrones de anillo, patrones lineales, aclaramiento de nervadura, entre otras (Agrios, 2005). La Figura 6.5 muestra tres tipos de densidades de mosaico, el cual consiste en un aclaramiento de nervadura. La Figura 6.5(a) muestra un diagrama esquematizado de la nervadura de una hoja sana. La Figura 6.5(b) y

(c) presentan una diagrama esquematizado de hojas de frijol enfermas, las cuales presentan una baja densidad y una alta densidad del síntoma de mosaico (aclaramiento de nervadura), respectivamente. Se puede ver, de la comparación entre hojas sanas y enfermas, como las venas de la hoja se vuelven más claras y por tanto más perceptibles al ojo humano cuando las hojas presentan este tipo de mosaico.

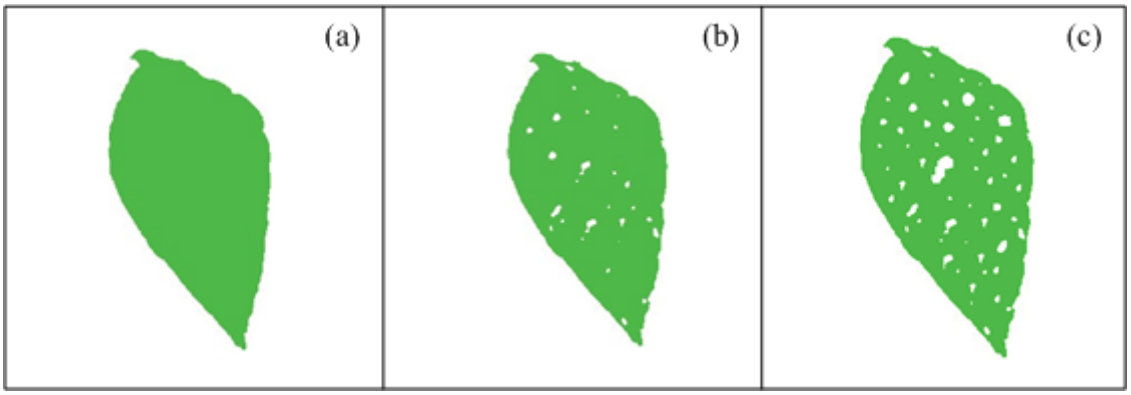

Figura 6. 4. a) Hoja de frijol sana con color verde homogéneo. b) Hoja de frijol enferma con baja densidad de síntoma de manchas blancas. c) Hojas de frijol enferma con alta densidad de síntoma manchas blancas.

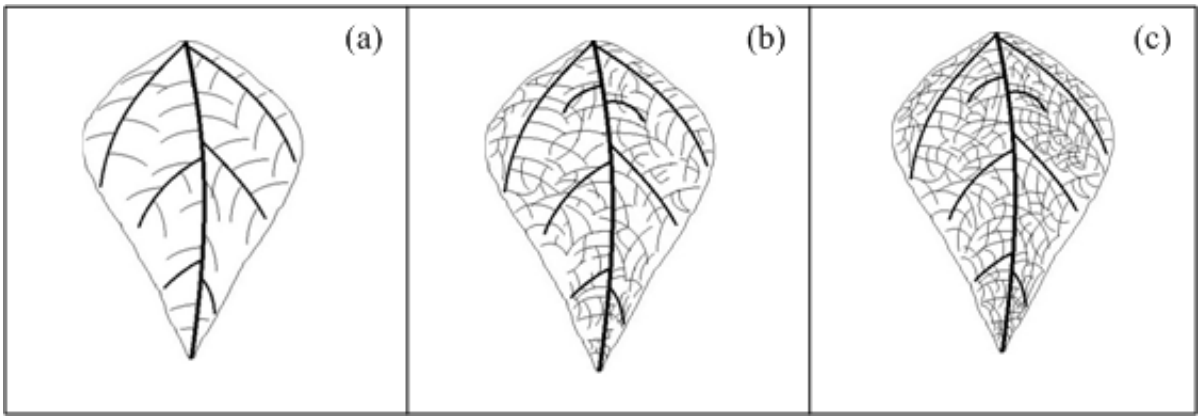

Figura 6. 5. a) Hoja de frijol sana sin síntoma de mosaico. b) Hoja de frijol enferma con baja densidad de síntoma de mosaico. c) Hoja de frijol enferma con alta densidad de síntoma de mosaico.

6.2 Procesamiento de imágenes

En la revisión del estado del arte, se presentaron herramientas matemáticas las cuales han sido utilizadas para tratar de conocer de manera más precisa como se desarrolla un síndrome en una planta, sin embargo, estas herramientas matemáticas generalmente se basan en estimaciones de

variables externas como temperatura, humedad y algunas otras en estimaciones visuales para determinar que tan enferma se encuentra la planta. Para conocer o cuantificar las enfermedades en las plantas las técnicas mostradas en la revisión de literatura han sido las más usadas, sin embargo los trabajos citados para detectar y cuantificar enfermedades en plantas reflejan desventajas tales como análisis destructivo, alto costo, subjetividad y la necesidad de personal capacitado para realizar el análisis. La visión por computadora (VC) es una técnica que trata de resolver estas desventajas, sin embargo, los trabajos hasta ahora realizados basados en VC no realizan análisis *in-situ* y en tiempo-real y analizan de uno o dos síntomas solamente. De modo que es deseable un sistema que permita la cuantificación de síntomas en plantas utilizando visión por computadora que supere las desventajas de los trabajos anteriormente citados. Para esto se necesitan emplear técnicas y algoritmos de procesamiento de imágenes que puedan ayudar a detectar y cuantificar estos síntomas de manera precisa. A continuación se describen los algoritmos de procesamiento de imágenes empleados en este trabajo.

6.2.1 Operaciones morfológicas

La morfología matemática nació en 1964 cuando G. Matheron fue requerido para investigar la relación entre la geometría de medios porosos y sus permeabilidades (Serra, 1982). La noción de estructura geométrica o textura no es puramente objetiva, esto no existe en el fenómeno mismo o en el observador, pero si en algún lugar entre los dos, la morfología matemática cuantifica esta intuición introduciendo el concepto de elementos estructurales. En procesamiento de imágenes, esta metodología se basa en la teoría de conjuntos y gran parte de su éxito se debe a que sus operaciones simplifican la imagen y preservan la forma original de los objetos (Pajares y Cruz, 2002). El procesamiento morfológico de imágenes permite realizar técnicas como segmentación, clasificación de patrones, detección de formas, análisis de textura, etc. Por lo tanto, resulta atractivo y ventajoso la aplicación de esta metodología para la detección de estos síntomas por medio de la combinación de operadores y operaciones morfológicas entre las cuales están la dilatación,

erosión, apertura y cerradura; estas operaciones básicas, así como algunas otras utilizadas en la realización de este trabajo son descritas a continuación.

6.2.1.1 Dilatación⊕

La dilatación de *A* por *B* es el resultado de todos los desplazamientos de la reflexión de *B* sobre *A* en los cuales ambos se traslapan en al menos un elemento (ver ecuación (6.1)) (González y Woods, 2002). En otras palabras, esta operación consiste en que al sobreponer el elemento estructurante *B* reflejado en una imagen *A*, el centro de este contenga a un elemento del conjunto *A*, cuando esto ocurre, el elemento estructurante llena las posiciones adyacentes de sus píxeles vecinos con el valor del píxel más alto, dilatando de esta manera la imagen. Un ejemplo de la operación de dilatación se muestra en la Figura 6.6, donde la Figura 6.6(a) muestra un conjunto *A*, la Figura 366(b) es el elemento estructurante cuadrado reflejado *B* y en la Figura 6.6(d) se observa el resultado de la dilatación de *A* por *B* el cual corresponde a la zona sombreada, donde la línea punteada muestra el conjunto original *A* y la línea sólida muestra el límite del cual cualquier desplazamiento más allá de *B* reflejado dejará de traslapar al conjunto *A*.

$$A \oplus B = \left\{ z \middle| \left[\left(\hat{B} \right)_z \cap A \right] \subseteq A \right\} \tag{6.1}$$

6.2.1.2 Erosión⊗

La erosión se define como el resultado de todos los puntos tal que *B* trasladado por *z*, es contenido en *A* (ver ecuación (6.2)) (González y Woods, 2002). En otras palabras, consiste en colocar el elemento estructurante *B* sobre la imagen *A*, pero a diferencia de la dilatación, esta requiere que todos los píxeles del elemento estructurante *B* contengan un elemento de *A*, cuando esto sucede, se aplica un adelgazamiento de regiones gruesas de la imagen, a esta operación se le llama erosión. Un ejemplo de la operación de erosión se muestra en la Figura 6.6, donde la Figura 6.6(a) muestra un conjunto *A*, la Figura 6.6(c) es el elemento estructurante cuadrado *B* y en la Figura 6.6(e) se observa el resultado de la erosión de *A* por *B* el cual corresponde a la zona sombreada, donde la línea punteada muestra el conjunto original A y la línea

sólida muestra el límite del cual cualquier desplazamiento más allá del origen de *B* provocara que este elemento estructurante deje de estar contenido completamente en A.

$$A \otimes B = \left\{ z \middle| (B)_z \subseteq A \right\} \tag{6.2}$$

6.2.1.3 Apertura (°)

La operación de apertura consiste en aplicar una erosión para simplificar su estructura y posteriormente una dilatación para remarcarla (ver ecuación 6.3), la Figura 6.7 muestra la operación de apertura en una señal unidimensional.

$$\varphi = A \circ B = (A \otimes B) \oplus B \tag{6.3}$$

6.2.1.4 Cerradura (•)

Esta operación es dual a la dilatación, puesto que implica aplicar una dilatación para posteriormente aplicar una erosión, y lo que hace es básicamente cerrar contornos (dilatación) y para posteriormente adelgazarlos (erosión) (ver ecuación 6.4), la Figura 6.8 muestra la operación de cerradura en una señal unidimensional.

$$\gamma = A \bullet B = (A \oplus B) \otimes B \tag{6.4}$$

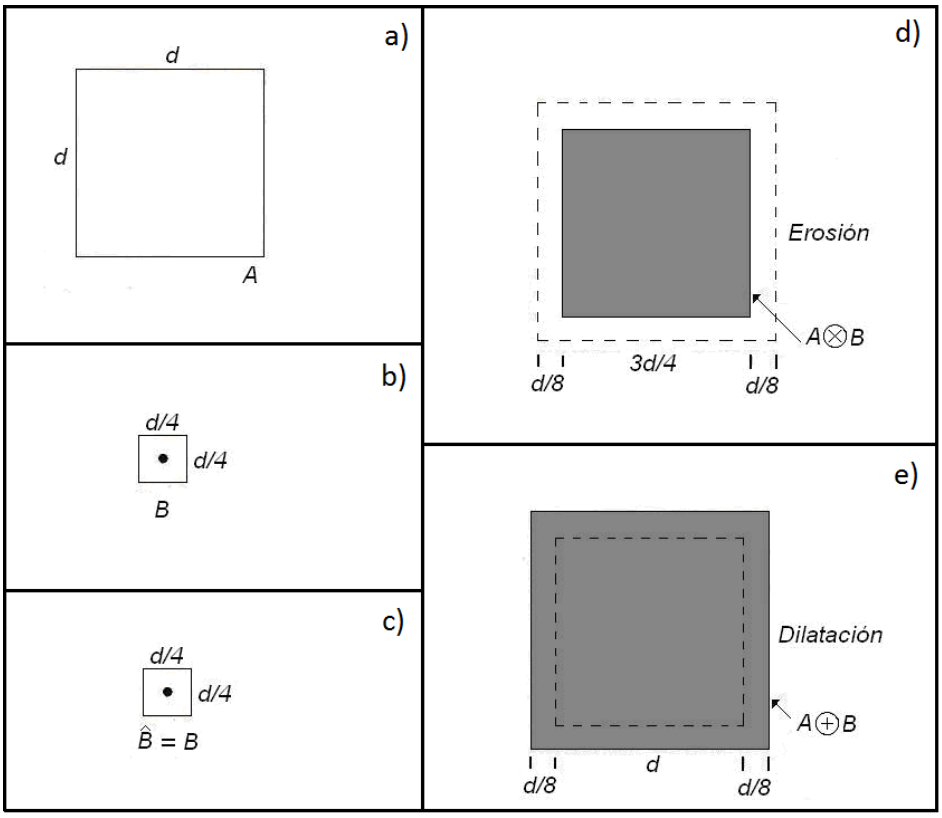

Figura 6. 6. a) Conjunto *A*, b) Elemento estructurante cuadrado (el punto negro representa el centro) usado para operación de dilatación, (c) Elemento estructurante cuadrado usado para operación de erosión, d) Dilatación de *A* por *B* zona oscura, e) Erosión de *A* por *B* zona oscura (González y Woods, 2002).

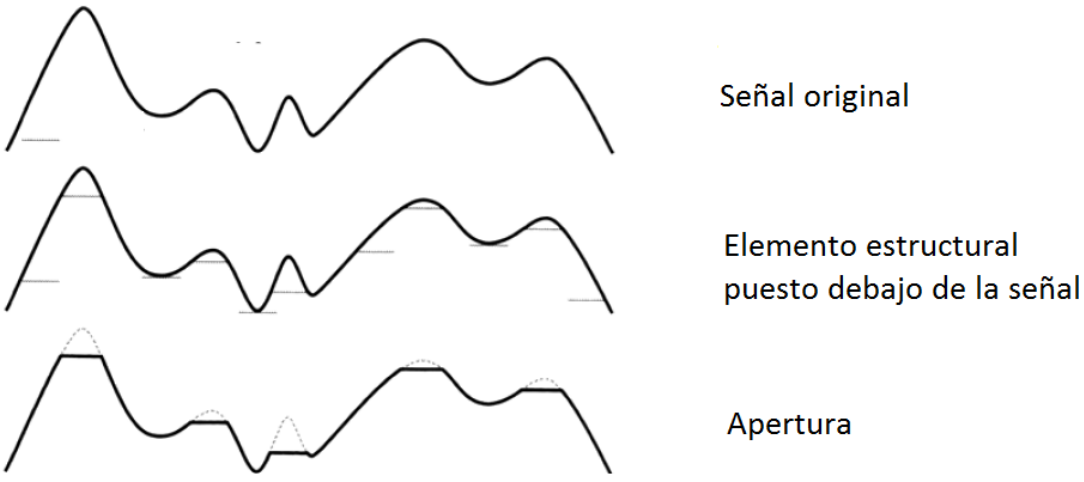

Figura 6. 7. Operación de apertura sobre una señal unidimensional.

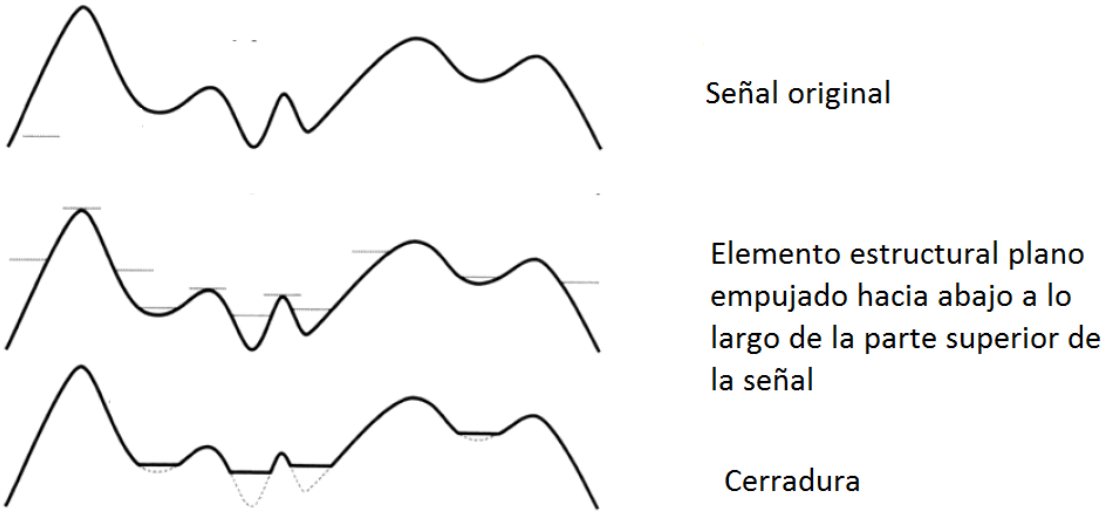

Figura 6. 8. Operación de cerradura sobre una señal unidimensional.

6.2.1.5 Transformación por Top-hat (ThwB) y Bottom-hat (ThbB)

Esta transformación es una de las más importantes en procesamiento morfológico de imágenes y se emplea principalmente para la detección de objetos, mejoramiento de imágenes, y segmentación (Bai y Zhou, 2010), esta transformación está basada en la ecuación (6.5). Esta transformación consiste en trasladar un elemento estructurante de tamaño *M* por dentro de la superficie de la imagen o de la señal según sea el caso, y los puntos en el que el elemento estructurante no sea capaz de llegar son los puntos en los cuales se presenta picos en intensidades de niveles de gris a esta operación se le llama apertura; por lo tanto si a la imagen original se le resta la apertura de la imagen se obtiene puntos máximos de intensidad que pueden servir para mejorar el contraste en la imágenes. La transformación bottom-hat trabaja de manera muy similar a la operación top-hat y se basa en la ecuación (6.6), sin embargo, a diferencia de la transformación top-hat, la operación de bottom-hat resalta los puntos de menores situados entre dos picos de intensidad de la imagen o de la señal, para esto hace uso de la operación cerradura, en la Figura (6.9) y (6.10) se muestra ejemplos de la aplicación de la transformación top-hat y bottom-hat respectivamente.

$$Thw_B = A - \gamma_B(A) \tag{6.5}$$

$$Thb_B = \varphi_B(A) - A \tag{6.6}$$

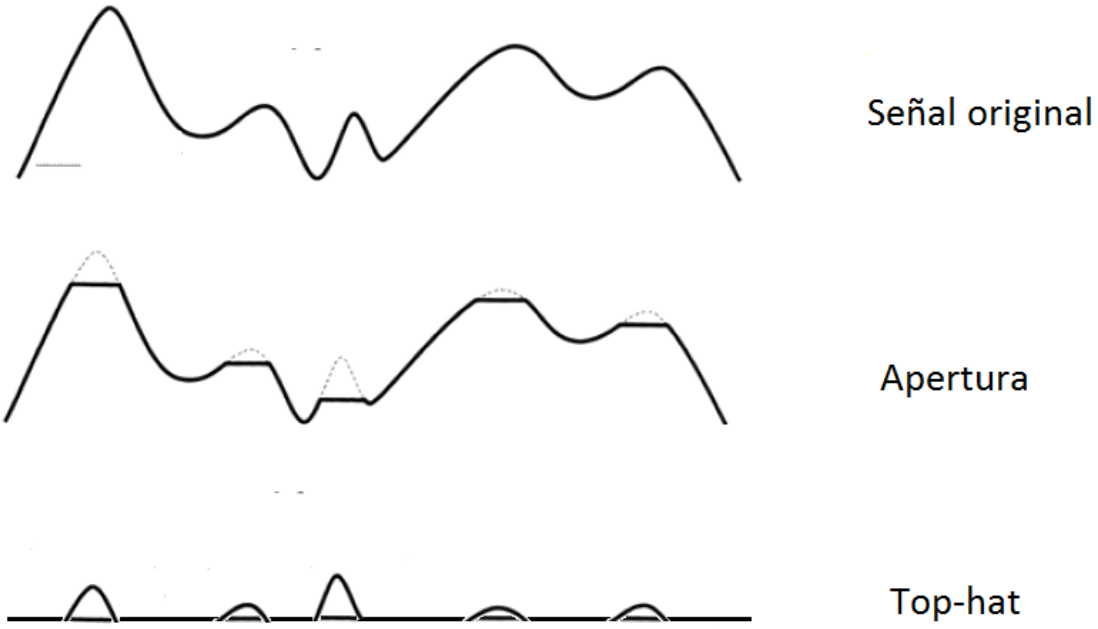

Figura 6. 9. Ejemplificación de la transformación Top-hat.

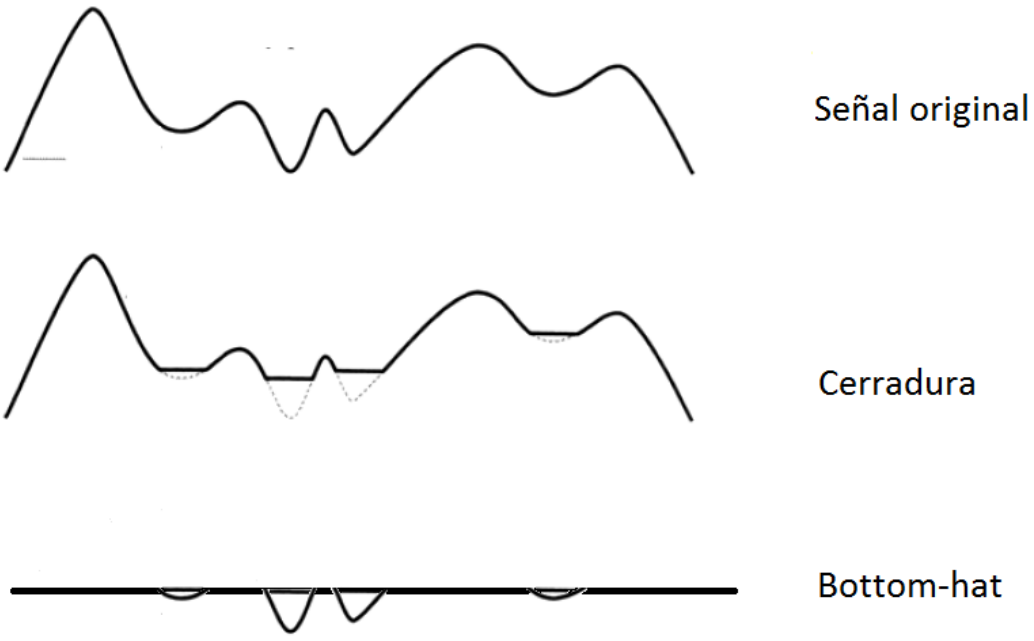

Figura 6. 10. Ejemplificación de la transformación bottom-hat.

6.2.2 Segmentación

La segmentación de imágenes es uno de los pasos más importantes tratándose del análisis de datos, su principal objetivo es dividir una imagen en dos partes que tienen una fuerte correlación con objetos o áreas del mundo

real contenidos en la imagen (Sonka, 2008). Una segmentación completa resulta de una serie de regiones desunidas que corresponden únicamente con objetos en la imagen de entrada, y la segmentación parcial resulta de regiones que no corresponden directamente con objetos de la imagen. Para realizar una segmentación completa muchas veces es necesario un profundo conocimiento de técnicas de procesamiento de imágenes así como un alto conocimiento del fenómeno que se está analizando; sin embargo, muchas veces una segmentación completa puede ser resuelta usando procesamientos simples.

Si la segmentación parcial es necesaria, una imagen es dividida en regiones separadas que son homogéneas con respecto a cierta propiedad tal como brillo, color, reflectividad, textura, etc. Si una imagen de una escena compleja es analizada, por ejemplo, una fotografía aérea de una escena urbana, una serie de posibles traslapes entre regiones no homogéneas puede ocurrir. Por lo tanto, donde existe la posibilidad de un posible traslape entre regiones no homogéneas, es necesario un procesamiento antes o después de la segmentación, esto con el objetivo de que la segmentación de la imagen se pueda realizar de manera satisfactoria con la ayuda de información de alto nivel.

La ambigüedad de los datos de la imagen es uno de los principales problemas de la segmentación, la cual es frecuentemente acompañada de ruido. La segmentación de las imágenes puede ser dividida en tres grupos de acuerdo a las características dominantes que estos emplean. La primera es la que se basa en el conocimiento global, este conocimiento puede ser de toda la imagen o solo una parte; el conocimiento es frecuentemente representado por un histograma de la imagen. La segunda se basa en los bordes de la imagen y la tercera es la segmentación basada en regiones; estos dos últimos métodos quizá utilicen características tales como brillo, textura, velocidad de campo, etc, para la detección de bordes o regiones crecientes. La Figura 6.11 presenta una segmentación basada en bordes de objetos de una imagen, en donde la finalidad es la detección de figuras geométricas.

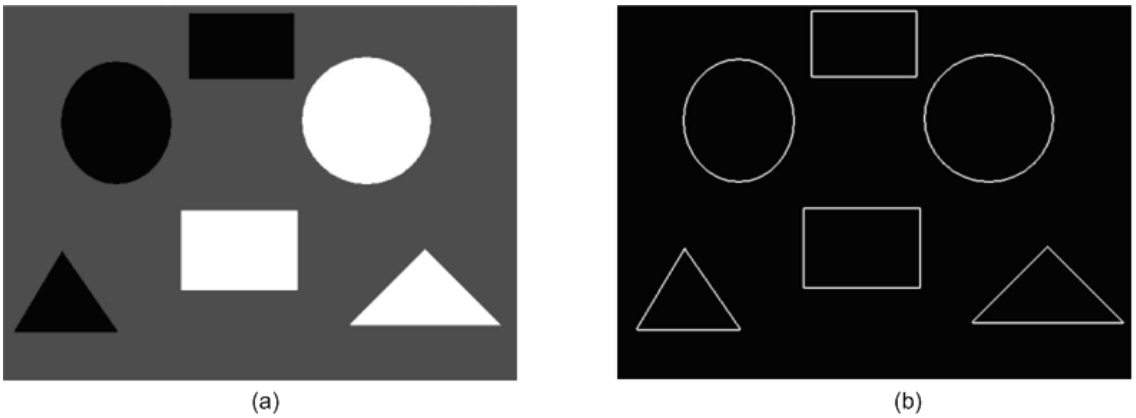

Figura 6. 11. a) Imagen con objetos geométricos. b) segmentación del contorno de los objetos geométricos de la imagen original.

6.2.3 Ecualización del histograma

En el área de procesamiento de imágenes, existen diferentes técnicas importantes, las cuales son utilizadas para extraer información de la imagen, una de estas técnicas es el histograma, el cual es la base de numerosas técnicas de procesamiento de imágenes en el dominio espacial. Existen diversas aplicaciones las cuales hacen uso del histograma, una de ellas es el mejoramiento de la imagen, además de que provee información estadística acerca de la misma; esta información es utilizada para aplicaciones en procesamientos tal como compresión y segmentación (Gonzalez y Woods, 2002). Los histogramas tienen además la ventaja de ser fáciles de calcular y además no se requiere de muchos recursos de memoria, lo cual hace de ésta una técnica muy utilizada. Una de las técnicas de mejoramiento de contraste más sencillas que son utilizadas en diversas aplicaciones es la ecualización del histograma; este procedimiento consiste en transformar la imagen para obtener una imagen de salida con valores en el rango de [O_{min} O_{max}], esta operación se basa en la ecuación (6.7).

$$O(y,x)=\frac{(O_{\max}-O_{\min})}{(I_{\max}-I_{\min})}(In(y,x)-I_{\min})+O_{\min} \tag{6.7}$$

En la Figura 6.12 se pueden observar dos imágenes iguales en contenido, sin embargo una presenta mejor contraste respecto a la otra. La Figura 6.12 (a) muestra una imagen con bajo contraste, esto se puede corroborar en su histograma que se muestra en la Figura 6.12(c), de las misma

manera, la Figura 6.12(b) presenta la misma imagen de la Figura 6.12(a) sin embargo, esta imagen presenta un mayor contraste tal y como se puede corroborar su histograma mostrado en la Figura 6.12(d), el cual, como se puede observar, se encuentra distribuido en todos los niveles de gris posibles, que en este caso es de 0 a 255.

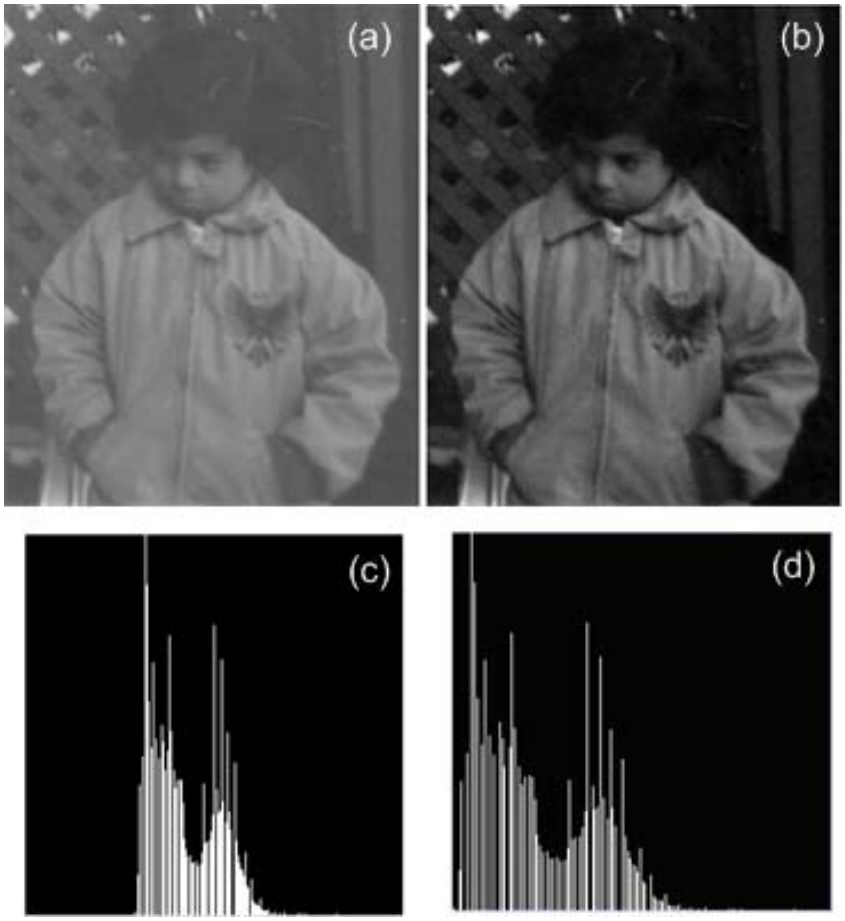

Figura 6. 12. a) Imagen original con bajo contraste. b) imagen con contraste modificado utilizando la ecualización de histograma. c) Histograma de la imagen del inciso a). d) Histograma de la imagen del inciso d).

6.2.4 Algoritmo de Canny

En la actualidad existen varios métodos para la detección de bordes con los cuales se pueden obtener resultados variables. Uno de los algoritmos más poderosos para la detección de bordes es el método de Canny. Jonh Canny definió un conjunto de metas para un detector de bordes y describió un método óptimo para su consecución (Canny, 1988).

- **La tasa de error:** el detector deberá de responder solamente a bordes y deberá encontrarlos todos; ninguno podrá perderse.
- **Localización:** la distancia entre los pixeles de borde encontrados por el detector y el borde deberá ser tan pequeña como sea posible.
- **Respuesta:** El detector no deberá detectar múltiples bordes donde solamente existe un borde.

El algoritmo de Canny puede describirse de la forma siguiente:

Léase la imagen a ser procesada, *I*.
Genérese una máscara Gaussiana de 1D, *G*, para convolucionarla con *I*. La desviación estándar *s* de esta gaussiana es un parámetro para el detector de bordes. Recuérdese que una gaussiana tiene la forma de la ecuación (6.8).

$$G(x) = e^{-\frac{x^2}{2\sigma^2}} \tag{6.8}$$

Genérese una mascara de 1D, *G*, para la primera derivada de la gaussiana en las direcciones *x* e *y*; llámese G_x y G_y a estas máscaras. Úsese el mismo valor de *s* del paso anterior. La derivada con respecto de *x* seria como se muestra en la ecuación (6.9).

$$G'(x) = (-\frac{x}{\sigma^2})e^{-\frac{x^2}{2\sigma^2}} \tag{6.9}$$

Convolucione la imagen *I* con *G* sobre los renglones para obtener la componente de la imagen I_x, y por las columnas, para obtener I_y.

Convolucione I_x con G_x para obtener I'_x, la componente *x* la componente convolucionada con la derivada de la gaussiana, y convolucione I_y con G_y para darnos I'_y.

En este punto pueden verse los resultados parciales combinando las componentes de *x* y de *y*. La magnitud del resultado se calcula en cada pixel *(x,y)* como se muestra en la ecuación (6.10):

$$M(x,y) = \sqrt{\left(I'_x(x,y)^2 + I'_y(x,y)^2\right)} \qquad (6.10)$$

El paso final en el detector de Canny es el paso de supresión de los valores que no son máximos, en donde se remueven los pixeles que no tienen un valor máximo en la vecindad. La Figura 6.13 muestra la utilización del método de Canny para detectar bordes de nervadura en una hoja de frijol.

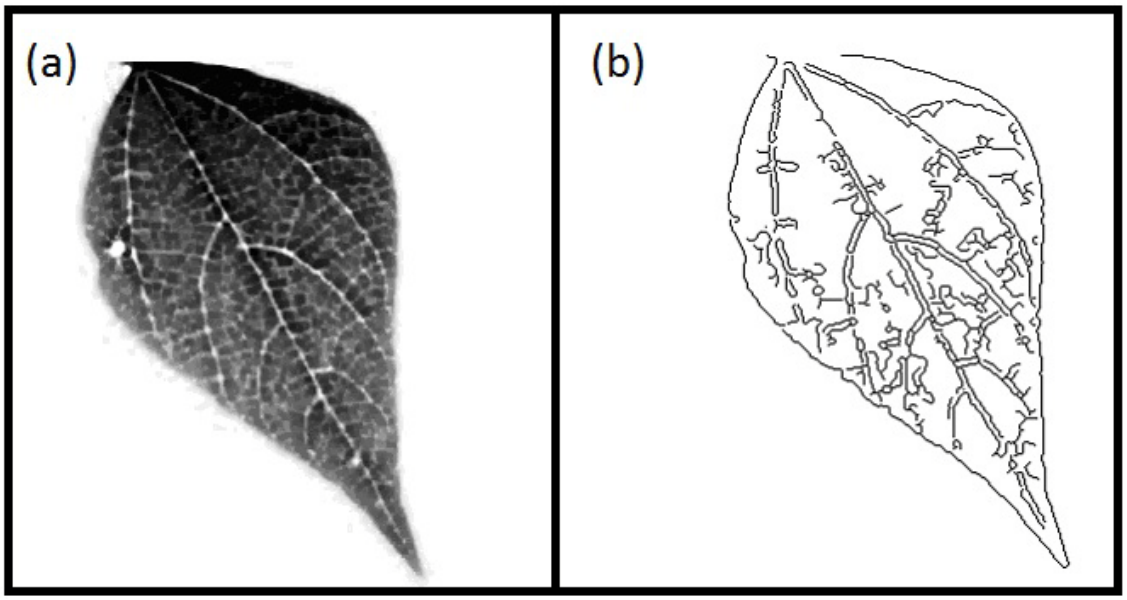

Figura 6. 13. a) Imagen original contrastada. b) Detección de bordes utilizando el algoritmo de Canny y supresión de picos.

6.3 Sensores inteligentes

Frank (2000) definió un sensor inteligente como un sensor que provee funciones mas allá de aquellos necesarios para generar una correcta interpretación de los datos sensados, basados en esto; los sensores inteligentes deben incorporar procesamiento, comunicación e integración de acuerdo a Rivera *et al*. (2008). En concordancia con Mekid (2006), un sensor inteligente utiliza elementos de procesamiento para incorporar capacidades de

procesamiento los cuales realizaran la estimación de ciertas variables y parámetros (posición, velocidad, aceleración, jerk, inclinación, transpiración de plantas, conductancia estomatal) que dependen de los datos provenientes de sensores primarios (encoder, acelerómetro, sensor de temperatura y sensor de humedad). La exactitud y precisión de los sensores inteligentes para estimar variables dependen de metodologías implementadas en los elementos de procesamiento tales como microcontroladores (µC), procesadores digitales de señales (DSP) y computadores personales (PC). En la actualidad las aplicaciones a VC, biología, robótica y mantenimiento industrial requieren metodologías que demandan alta capacidad de computo que los µC, DSP o PC algunas veces no son capaces de satisfacer.

6.4 FPGA (Field Programmable Gate Array)

Los FPGA (Field Programmable Gate Array) son dispositivos que han ganado popularidad, principalmente debido a su alta velocidad de procesamiento, alta reconfigurabilidad, y soluciones tipo SoC (System on a Chip) (Contreras-Medina *et al*., 2010; Contreras-Medina *et al*., 2012). Estas características permiten que los FPGAs sean usados en aplicaciones donde requerimientos de cómputo de alta capacidad sean necesarios y que dispositivos tales PC, DSP y microcontroladores no son capaces de cumplir, en el Cuadro 6.1 se muestra una comparativa de las ventajas y desventajas de estos dispositivos. En VC, las características de alta velocidad de procesamiento que los FPGA ofrecen han sido explotadas para desarrollar sistemas de visión para la clasificación de productos del campo (Pearson, 2009). En robótica, los FPGA han sido empleados para desarrollar sensores inteligentes capaces de obtener estimaciones precisas de parámetros de dinámica, cinemática y vibraciones en robots industriales de una sola unión basados en encoders ópticos incrementales y acelerómetros triaxiales (Rodriguez-Donate *et al*., 2010). En mantenimiento industrial, Rangel-Magdaleno *et al*. (2009) desarrolló un sensor inteligente para el monitoreo de jerk basados en acelerómetros, los cuales actuaban como sensores primarios y una técnica novedosa de sobre muestreo. En el área biológica, Millan-Almaraz *et al*. (2010) utilizó un sensor inteligente basado en FPGA para estimar la dinámica de transpiración de las plantas basado en cinco sensores primarios

para medir la temperatura del aire, la temperatura de la hoja, la humedad relativa del aire, la humedad relativa de salida de la planta y radiación.

Cuadro 6. 1. Ventajas y desventajas de las plataformas tecnológicas para el procesamiento de señales.

Plataforma	**Ventajas**	**Desventajas**
PC	- Utiliza computadoras de propósito general - Diseño en alto nivel - Interfaces estándares	- Velocidad limitada - computo especulativo
Procesadores DSP	- circuito probado funcionalmente - Plataforma de diseño de alto nivel - Puente con C y/0 Matlab - Fácil conexión con memoria - Bajo costo - Buena velocidad	- Requiere circuito de soporte periférico - Obsolescencia general - Arquitectura predefinida
Microcontroladores	- Plataforma de diseño de alto nivel - Memoria interna - Puertos de comunicación - Bajo costo	- Obsolescencia general - Arquitectura predefinida - No permite la optimización de ciertos algoritmos
FPGA (Arreglo de Compuertas Programables en Campo)	- Posibilidad SoC - Libertad de arquitectura - Alta Reconfigurabilidad - Portabilidad - Diseño del sistema por el usuario final	- Desperdicio inherente de recursos - Desarrollo de dependencia tecnológica con los fabricantes - Tiempo de desarrollo - Complejidad

6.5 Algoritmos para procesamiento de imagenes

6.5.1 Algoritmo para la cuantificación de la clorosis

Como se mencionó anteriormente, una área clorótica está definida como un amarillamiento de tejido normalmente verde; por lo tanto, una buena identificación de áreas cloróticas es hecha usando la componente amarilla de la imagen resultando de la combinación de los mapas de colores rojo y verde (ver Figura 6.14(a)). Por lo tanto, se propone un algoritmo basado en análisis de color para cuantificar la clorosis. El algoritmo puede ser dividido en dos etapas, la primera etapa consiste en calcular la componente amarilla de la hoja utilizando la ecuación (6.11); *Red* and *Green* corresponden a los componentes rojo y verde de la imagen original, respectivamente; posteriormente, la hoja es dividida en cuatro secciones como se muestra en la Figura 6.14(b) usando las coordenadas del centroide de la imagen *Cx* y *Cy*, calculados utilizando la ecuación (6.12) (Pratt, 2001) con *N* y *M* siendo el numero de renglones y columnas respectivamente. La segunda etapa está a cargo de calcular los valores promedio del amarillo de las cuatro secciones de la hoja usando la ecuación (6.13), *Yellow (i,j)* es el nivel de intensidad del amarillo en las coordenadas correspondientes *(i,j)*. L_k es el número de pixeles de la sección *k* (donde *k* = 1,2,3,4) y *i* y *j* son el índice de línea y columna respectivamente. R_k es el valor promedio de pixel amarillo de la sección *k*; estos valores permiten calcular el módulo de un vector formado por estos cuatro valores de amarillo R_n mostrados en la ecuación (6.14), y el módulo del vector R_{diff} que representa los valores diferenciales entre los diferentes valores de amarillo que se obtienen restando los valores de amarillo promedio de cada región de las otras regiones como se muestra en la ecuación (6.15); R_n permite cuantitativamente conocer si la hoja está completamente clorótica, mientras que R_{diff} permite conocer cuantitativamente que tan localizada o generalizada es la clorosis. El rango de dentro del cual, los valores de R_n y R_{diff} pueden caer puede variar de acuerdo al tipo de hoja analizada, es difícil establecer un rango máximo y minino debido a que se deben hacer una cantidad de experimentos considerable para estimar este valor.

$$Yellow = 0.5Red + 0.5Green \tag{6.11}$$

$$Cx = \frac{\sum_{i=1}^{N}\sum_{j=1}^{M} i \cdot Yellow(i,j)}{\sum_{i=1}^{N}\sum_{j=1}^{M} Yellow(i,j)} \quad , \quad Cy = \frac{\sum_{i=1}^{N}\sum_{j=1}^{M} j \cdot Yellow(i,j)}{\sum_{i=1}^{N}\sum_{j=1}^{M} Yellow(i,j)} \tag{6.12}$$

$$R_K = \left\{ \frac{1}{L_K} \sum_{i=1}^{N}\sum_{j=1}^{M} Yellow(i,j) \,|\, Yellow(i,j)\, \varepsilon\, R_k \right\} \tag{6.13}$$

$$R_n = \left\| \left[R_1 ; R_2 ; R_3 ; R_4 \right] \right\| \tag{6.14}$$

$$R_{diff} = \left\| \left[R_1 - R_2 ; R_1 - R_3 ; R_1 - R_4 ; R_2 - R_3 ; R_2 - R_4 ; R_3 - R_4 \right] \right\| \tag{6.15}$$

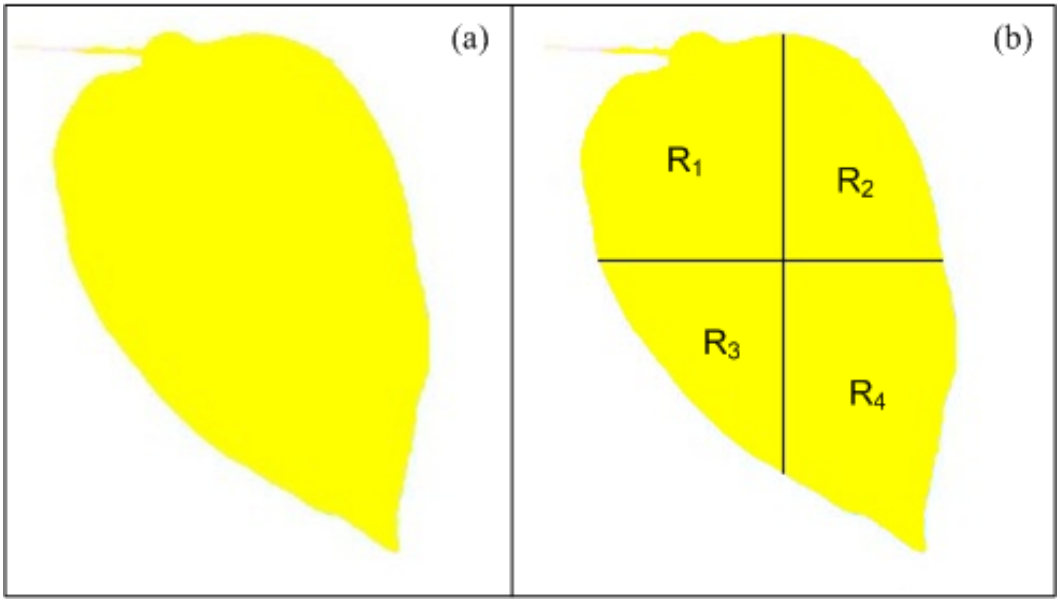

Figura 6. 14. a) Componente amarilla de hoja de planta de chile. b) Hoja de chile sana dividida en cuatro regiones (R1, R2, R3, R4)

6.5.2 Algoritmo para la detección de áreas necróticas

Para cuantificar el área necrótica en hojas, un algoritmo basado en color usando las componentes de verde y azul es propuesto. La Figura 6.15(a) muestra una hoja de frijol en formato RBG (Red, Green, Blue) y sus correspondientes componentes azul y verde son mostrados en la figura 6.15 (b) y (c) respectivamente. El componente del verde es utilizado para aislar las partes necróticas de la hoja (A_{np}) del total de la hoja y el fondo debido a que esta componente ofrece un buen contraste entre las regiones no-necróticas y

necróticas. El componente de azul es utilizado para calcular el total del área de la hoja A_T debido a que esta componente es menos sensible a otros síntomas tales como clorosis y ofrece una mejor diferenciación de la hoja. Antes de aplicar una binarización de la imagen, un filtro de media es utilizado utilizando la operación de apertura con una máscara cuadrática de 5x5; esta permite una mejor diferenciación entre las zonas necróticas y no necróticas. Una vez cuantificada el área necrótica y el total del área de la hoja como se muestra en la Figura 6.15 (d) y (e), la estimación del área necrótica A_n en porcentaje es hecha utilizando la ecuación (6.16). A_n es el porcentaje de área necrótica de la hoja en relación al total de la hoja:

$$A_n = \frac{A_{np}}{A_T} * 100\% \qquad (6.16)$$

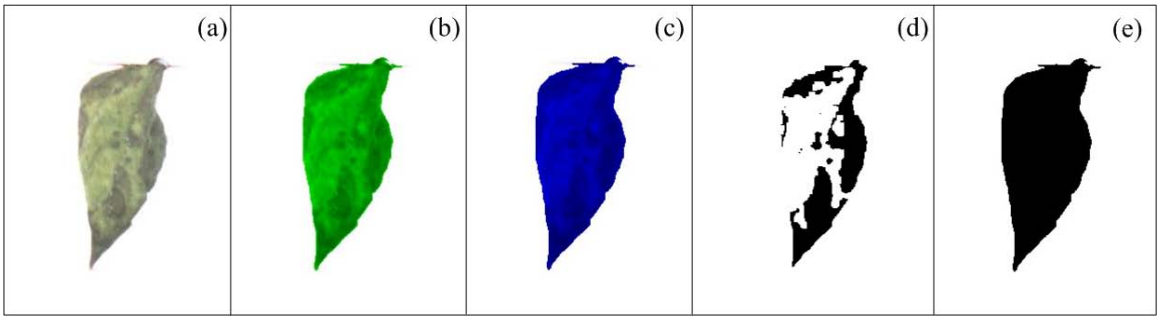

Figura 6. 15. Hoja de frijol con necrosis. a) hoja de frijol necrótica en formato RGB. b) Componente verde de hoja de frijol necrótica. c) componente de azul de hoja de frijol necrótica. d) segmentación del área necrótica del frijol. e) Segmentación del área total de la hoja.

6.5.3 Algoritmo para cuantificar la deformación de la hoja

La metodología propuesta para medir la deformación de la hoja es un algoritmo basado en color que utiliza, de la imagen original (Figura 6.16 (a)), el componente azul (Figura 6.16(b)) debido a que esta componente es menos sensitiva a otros síntomas tales como clorosis, la cual puede provocar errores en las cuantificaciones. Actualmente existen varias técnicas para determinar propiedades geométricas de un objeto; una de las más empleadas es el índice de esfericidad (Pratt, 2001). Este método da una medición cuantitativa acerca de que tan esférico es un objeto. Para

calcular este índice es necesario obtener el área (*A*) y el perímetro (*p*) de un objeto (hoja) que, en el caso de procesamiento de imágenes, son calculados en pixeles; Figuras 6.16 (c) y 6.16 (d) muestran la segmentación del área y el perímetro respectivamente. Cuando *A* y *p* son obtenidas, el índice de esfericidad *I* es calculado utilizando la ecuación (6.17). Después de esto, los valores de *I* de la hoja sana y enferma (deformada) son comparados para cuantitativamente determinar que tan deformada esta la hoja enferma tomando como referencia la hoja sana. En este trabajo, *I* es además llamado índice de deformación debido a que es la variable que es medida para cuantificar la deformación de la hoja.

$$I = \frac{4\pi A}{p^2} \tag{6.17}$$

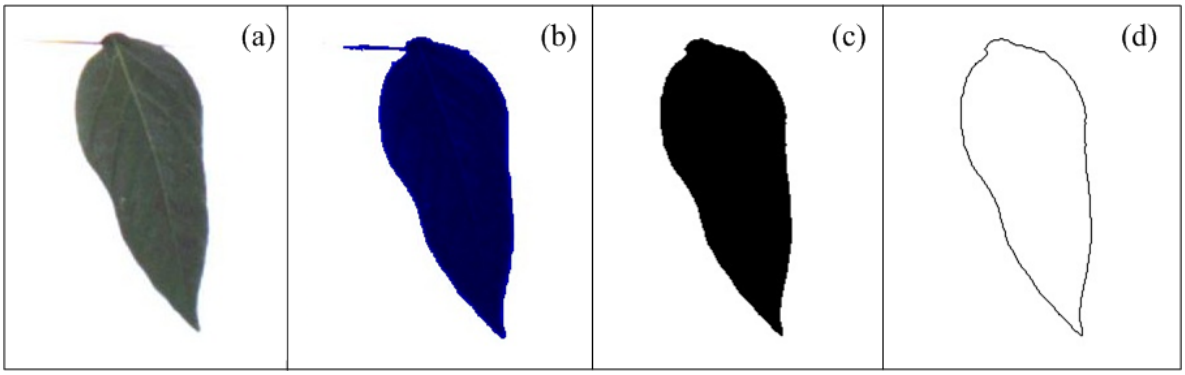

Figura 6. 16 a) Hoja de chile original. b) Componente azul de la hoja de chile. c) Obtención del área de la hoja. d) Segmentación del contorno de la hoja.

6.5.4 Algoritmo para la cuantificación de manchas blancas

El algoritmo para la detección y cuantificación de manchas blancas estima el área ocupada por las manchas blancas en hojas. Las manchas blancas están presentes en los tres componentes (Rojo, Verde y Azul). Por lo tanto, se propone un algoritmo que utiliza el componente de color azul debido a las razones antes mencionadas. La Figura 6.17(a) muestra una hoja de frijol en formato RGB afectado con manchas blancas y la Figura 6.17(b) muestra la componente azul de la imagen original. Como primer paso, la componente del azul es binarizada con un umbral predefinido para aislar la hoja del fondo (Figura 6.17(c)); este umbral para los casos aquí presentado es fijo, pero puede

ser definido por el usuario de acuerdo a las condiciones de iluminación. Después de un proceso de binarización, el número de pixeles en el fondo es calculado usando un algoritmo de conectividad, después, el complemento de la imagen es obtenido y el área de la hoja sin manchas blancas es aislado y cuantificado usando el algoritmo de conectividad (Figura 6.17(d)). Una vez teniendo el área de la hoja sin manchas blancas y el área del fondo de la imagen, es posible obtener el área ocupada por las manchas blancas A_{ws} usando la ecuación (6.18), donde A_{BG} es el área del fondo y A_{TL} es el área de la hoja sin las manchas blancas. El porcentaje del área de la hoja ocupada por las manchas blancas A_{pws} es estimada usando la ecuación (4.9). El valor constante A_{zs} representa el tamaño de la imagen en pixeles.

$$A_{ws} = A_{ZS} - A_{BG} - A_{TL} \tag{6.18}$$

$$A_{pws} = \frac{A_{ws}}{\left(A_{TL} + A_{ws}\right)} * 100\% \tag{6.19}$$

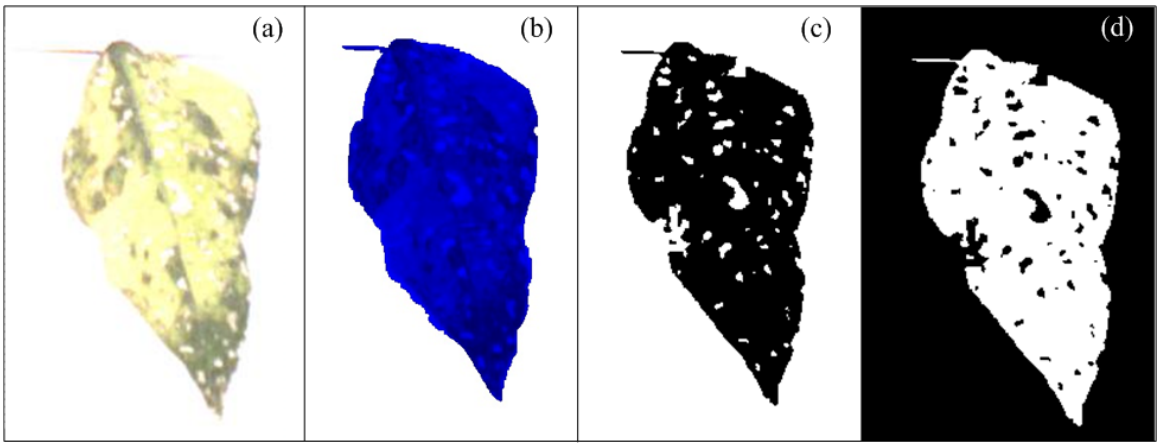

Figura 6. 17. a) Hoja de frijol con manchas blancas. b) Componente azul de hojas de frijol con manchas blancas. c) Segmentación del fondo y las manchas blancas d) Segmentación del área de la hoja sin manchas blancas.

6.5.5 Algoritmo de mosaico

El síntoma del mosaico es caracterizado por la presencia de un alto número de nervadura en hojas enfermas. Este síntoma no es claro cuando es visualizado bajo condiciones naturales y es detectado de mejor manera bajo una luz de alta intensidad trasera como se puede ver en la figura de la puesta

del experimento (Figura 6.19(a)); esta metodología mejora la visibilidad de la nervadura de la hoja y por consecuencia, el síntoma del mosaico puede ser identificado y cuantificado de mejor manera. Debido a las razones antes mencionadas, se propone utilizar el componente azul para cuantificar el síntoma, ya que la marcación de nervadura se presenta prácticamente de la misma manera en los tres componentes, sin embargo, el componente del azul es menos sensible a otros síntomas comunes tales como clorosis. Para realizar una mejor cuantificación del mosaico, la planta es fotografiada bajo condiciones de iluminación trasera de alta intensidad, estas condiciones son generadas por un panel de LEDs; también se utiliza un flash de LED como se puede observar en la Figura 6.19(b). El flash y el panel de LEDs son encendidos por el usuario antes de que la planta sea fotografiada; esto crea mejores condiciones de iluminación para detectar el síntoma del mosaico en hojas. Después de que la hoja ha sido fotografiada, el siguiente paso es procesar la imagen para obtener un mejoramiento de contraste. Para obtener una mejor diferenciación entre la nervadura de la hoja y el tejido. Primeramente, el componente del azul es obtenido de la imagen original y después los valores de gris de este componente fueron distribuidos en el rango de 0 a 1023, esto puesto que los datos que se reciben de la cámara son de 10 bits. El resultado de este procedimiento se puede observar en la Figura 6.18 (b). Posteriormente, se llevan a cabo transformaciones top-hat y bottom-hat de la imagen las cuales son aplicadas secuencialmente, estas transformaciones, junto con la imagen original sirven para obtener un mejoramiento de contraste como se puede observar en la Figura 6.18 (c). Finalmente, el algoritmo de Canny, el cual es unos de los métodos más utilizados para obtener bordes de objetos en una imagen, es aplicado junto con una operación de binarización para obtener los bordes de las nervaduras de la hojas (Canny, 1988) (ver Figura 6.18(d)). La cuantificación de las venas de la hoja es hecha estimando el área cubierta por los bordes de la nervadura de la hoja con respecto a la referencia del total de la hoja de acuerdo a la ecuación (6.20).

$$A_{mosaic} = \frac{A_{map}}{A_{TL}} * 100\% \tag{6.20}$$

A_{map} es el área cubierta con los bordes de las nervaduras, A_{TL} es el área total de la hoja y A_{mosaic} es el porcentaje de la hoja cubierta por los bordes de las nervaduras.

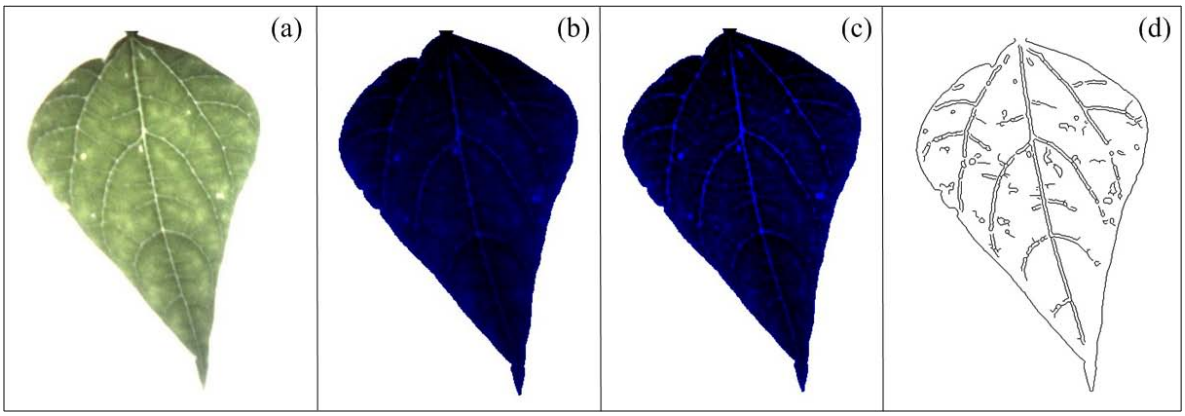

Figura 6. 18. a) Hoja de frijol en formato RGB. b) Componente azul de la hoja del frijol después de aplicar la ecualización de histograma. c) Componente de la hoja de frijol con un mejoramiento de contraste después de aplicar las transformaciones de top-hat y bottom-hat. (d) Identificación de las nervaduras de la hoja.

6.5.6 Sensor inteligente (Smart-sensor)

El sensor inteligente consiste en cuatro componentes principales: cámara como sensor primario, unidad de procesamiento en hardware (unidad HSP) como elemento de procesamiento, periféricos de salida (display LCD, monitor o puertos de comunicación con PC), LEDs de alta intensidad que sirven como luz de flash y LEDs de alta intensidad para generar las condiciones de iluminación trasera necesaria para la detección y cuantificación del síntoma del mosaico. Tres paneles son empleados dependiendo del síntoma bajo análisis. La metodología del sensor inteligente puede ser dividida en tres etapas. En la primera etapa, la imagen de la hoja es adquirida usando un sensor CMOS MT9M011 de 1/3-pulgadas de tamaño y 1.3 Megapíxeles, el cual es fabricado por la compañía micron (MT9M011, 2004). Después de capturar la imagen, ésta es enviada a la unidad HSP, la cual es una tarjeta de desarrollo Altera DE2 que contiene un FPGA EP2C35F672C6N Cyclone II, Memoria dinámica de acceso aleatorio sincronía (SDRAM) de 8 Mbytes y puertos periféricos (Altera, 2010). La segunda etapa es donde la imagen es procesada para la cuantificación del área clorótica, deformación, área con manchas blancas, área necrótica y síntomas de mosaico. Finalmente una

tercera etapa despliega la imagen original o la procesada, según sea el caso, a través de una pantalla LCD o el monitor. Opcionalmente la imagen puede ser enviada a la PC a través del puerto serial utilizando protocolo RS-232 para crear una base de datos de las imágenes adquiridas para un análisis posterior, la metodología donde se encuentran todos los componentes aquí citados se muestra en la Figura 6.19(a). Los tres paneles mencionados anteriormente, consisten en un panel blanco opaco usados para la cuantificación de clorosis, deformación de hoja, cuantificación del área con manchas blancas y necrosis. El panel blanco transparente es usado de manera conjunta con el panel de LEDs para la cuantificación del síntoma de mosaico. El panel de LED genera una luz trasera de alta intensidad que conjuntamente con el panel transparente permite que la luz pase a través de la hoja; esto amplifica la visibilidad de la nervadura de la hoja. Figura 6.19 (b) muestra la puesta del experimento donde todas las partes pueden ser identificadas en el diagrama a bloques del sistema propuesto. El sensor inteligente es montado sobre un mecanismo móvil con la finalidad de mover el sistema para poder realizar análisis *in-situ*.

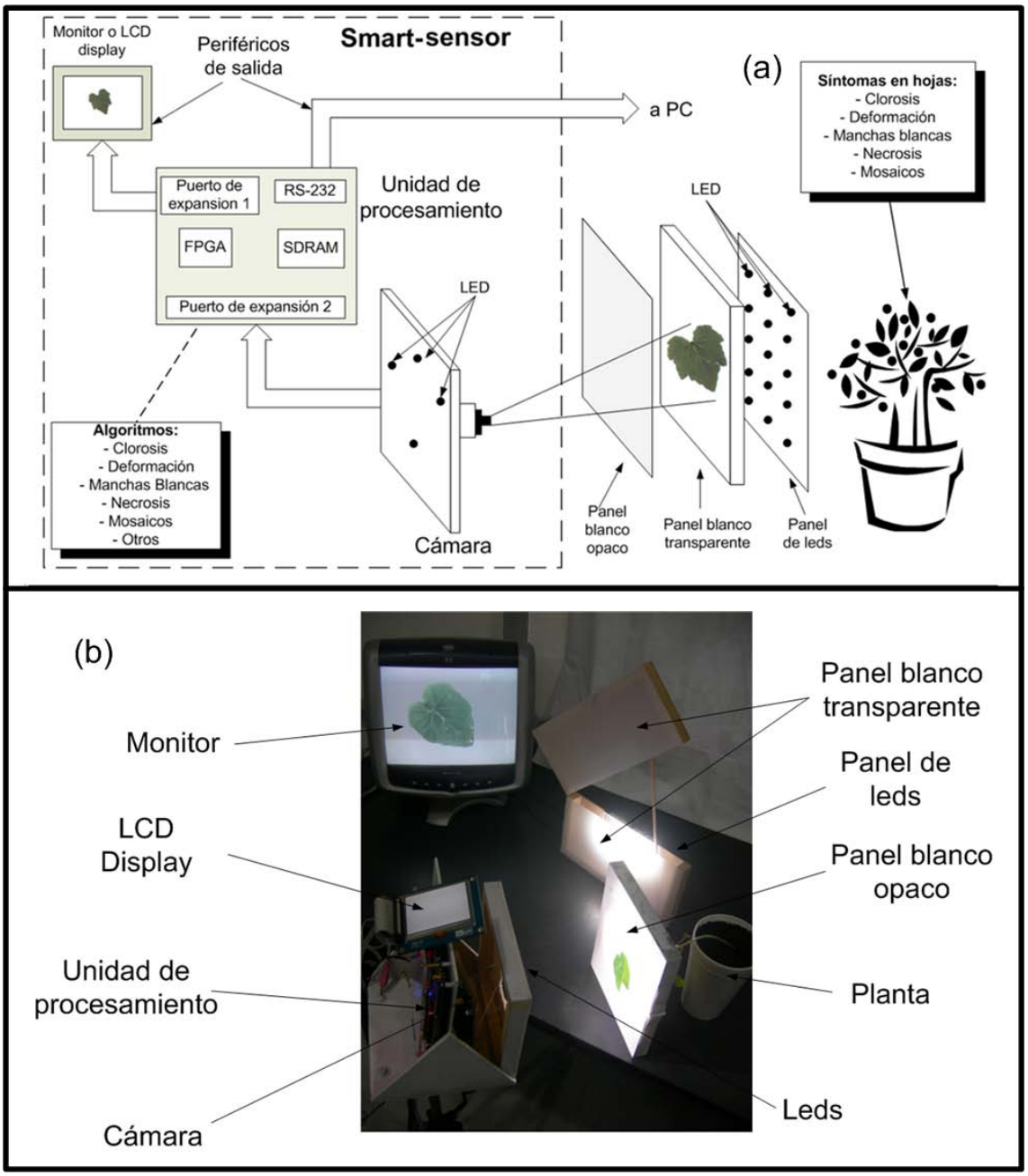

Figura 6. 19. Metodología del sensor inteligente. a) Diagrama a bloques del sistema propuesto. b) Puesta del experimento.

6.6 Unidad HSP

La unidad HSP está a cargo de controlar el flujo de datos provenientes de la cámara y llevar a cabo los procesamientos para las cuantificaciones de síntomas. La unidad HSP está compuesta principalmente de cuatro partes: el FPGA, SDRAM de 8 Mbyte, puertos periféricos (RS-232) y puertos de expansión. El FPGA es el componente clave de la unidad HSP y aquí es donde

los controladores de los dispositivos conectados son embebidos y donde los procesamientos se llevan a cabo como se puede ver en la Figura 6.20. Los controladores y bloques de procesamiento son implementados como se muestra en la Figura 6.20. Los controladores y bloques de procesamiento consisten en IP (Intelectual Property) cores que controlan los dispositivos conectados al FPGA y procesan la imagen; estos bloques trabajan a diferentes frecuencias de reloj con el objetivo de evitar cuellos de botella de transferencias de datos entre la cámara, SDRAM, bloques de procesamiento y puertos periféricos y para cumplir con las especificaciones de los dispositivos periféricos tales como la pantalla LCD que opera usando un reloj de 33.2 MHz, la SDRAM que trabaja a 100 MHz y el reloj de la interface de la cámara que es fijado a 25 MHz. Los bloques de procesamiento trabajan con un reloj de 25 MHz, y comprenden 5 módulos a cargo de cuantificar los síntomas antes mencionados, estos bloques dan como salida, el nivel absoluto de clorosis R_n, las diferencias entre las 4 secciones de la hoja R_{diff}, el índice de deformación I, el porcentaje de área necrótica A_n, el porcentaje de área de la hoja cubierta con manchas blancas A_{pws} y el porcentaje de la hoja afectada por el síntoma de mosaico A_{mosaic}.

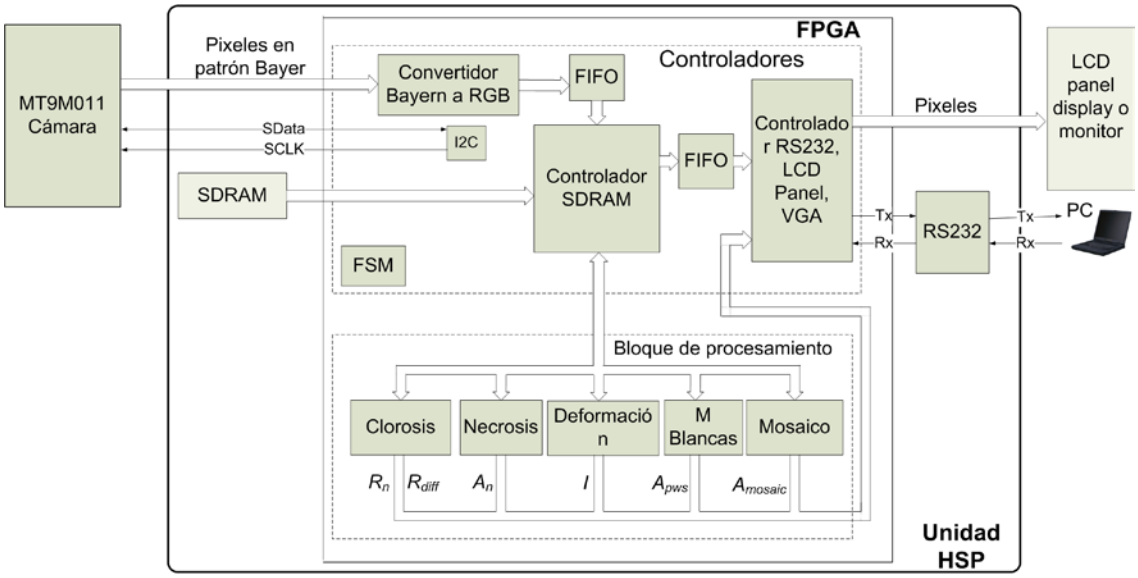

Figura 6. 20. Estructura Hardware de una unidad HSP

VII. **RESULTADOS**

7.1 Clorosis

Para probar la metodología propuesta para la cuantificación de la clorosis, plantas de calabaza y chile fueron utilizadas. Las plantas de calabaza fueron puestas en contenedores con sustrato durante 4 semanas sin agregar solución nutritiva alguna, para que las plantas desarrollaran de áreas cloróticas en hojas. Conjuntamente, las plantas de chile fueron infectadas con el virus común del frijol, el cual provoco síntomas de clorosis en las plantas. La Figura 7.1 muestra hojas de calabaza y chile con diferentes niveles de clorosis. De acuerdo a R_n y R_{diff} (valores mostrados en la parte inferior de cada figura) la hoja de la figura 7.1(a) presenta el valor más bajo de R_n y un bajo valor de R_{diff}, estos valores sugieren que la hoja esta casi completamente cubierta por un color verde homogéneo como se puede ver en la Figura. La hoja de la Figura 7.1(b) aun tiene un valor bajo de R_n pero tiene el valor más alto de R_{diff} lo que significa que la hoja tiene un clorosis localizada alta y una clorosis generalizada baja. Los valores altos y bajos de clorosis siempre se toman en cuenta con referencia a las hojas sanas, los valores obtenidos de las hojas sanas pueden servir como valores de referencia para determinar que tan clorótica están las hojas enfermas. La hoja de la Figura 7.1(c) muestra un alto valor de R_n y un bajo valor de R_{diff}, estos valores indican que la hoja ha sido cubierta casi en su totalidad por zonas cloróticas (clorosis generalizada) como puede ser visto en la Figura. De la misma manera, la hoja de la Figura 7.1(d) muestra el valor más alto de R_n y el valor más bajo de R_{diff}, estos valores indican un alto nivel de clorosis generalizada.

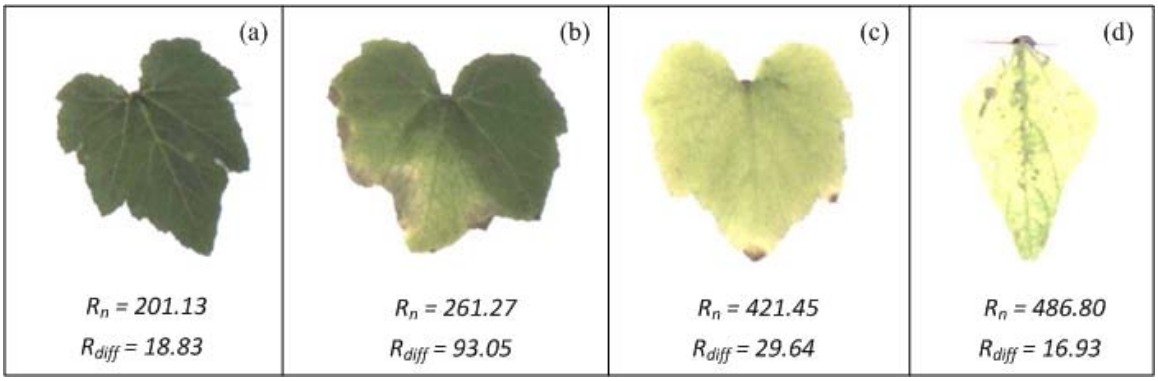

Figura 7. 1. Diferentes niveles de clorosis generalizada y localizada en hojas de calabaza y chile. a) Hoja de calabaza con baja clorosis generalizada y baja clorosis localizada. b) Hoja de calabaza con

clorosis localizada alta. c) Hoja de calabaza con clorosis generalizada alta. d) Hoja de chile con clorosis generalizada alta.

7.2 Necrosis

El algoritmo de necrosis fue probado utilizando plantas de frijol infectadas por el virus común del mosaico del frijol y plantas de chile infectadas con la bacteria *Xanthomonas campestris*. La imagen de la hoja de frijol (Figura 7.2(a) y (b)) y la imagen de las hojas de chile (Figura 7.2(c) y (d)) fueron fotografiadas de acuerdo a la metodología mostrada anteriormente. De acuerdo a los valores mostrados (valores presentados en la parte inferior de cada una de las imágenes), *An* sugiere que la hoja de la figura 7.2(a) presenta la área necrótica mayor y la hoja de la Figura 7.2(c) presenta el menor porcentaje de área necrótica. Estas diferencias entre cada uno de los valores de A_n son difíciles de detectar usando VE.

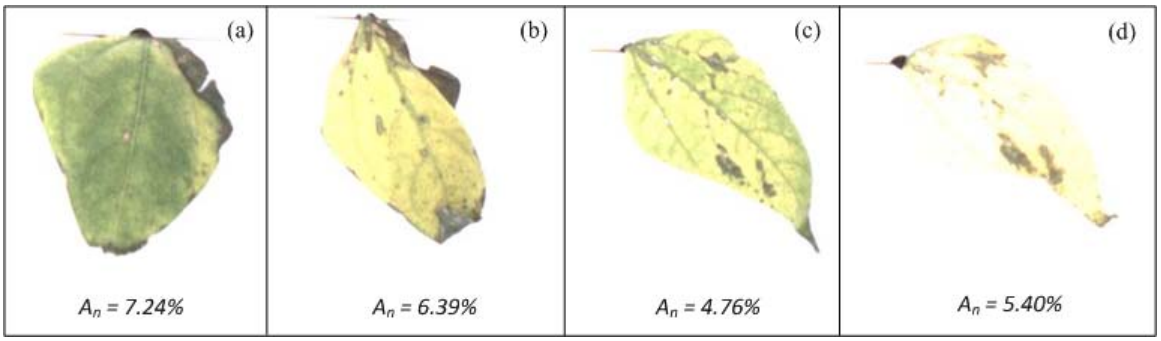

Figura 7. 2. Hojas de frijol y chile con diferentes niveles de necrosis. a) Hoja de frijol con necrosis y bajo porcentaje de clorosis localizada. b) Hoja de frijol con necrosis y alta clorosis generalizada. c) y d) Hojas de chile con necrosis y alta clorosis generalizada.

7.3 Deformación de la hoja

El algoritmo de la deformación de la hoja fue probado utilizando hojas de plantas de chile infectadas con la bacteria *Xanthomonas campestris*. Las imágenes de estas plantas fueron procesadas de acuerdo a la metodología presentada anteriormente. La Figura 7.3 muestra la forma de contorno de hojas de chile remarcadas en negro. De acuerdo a la estimación de índice de deformación (Mostrado al pie de cada figura) la hoja de la Figura 5.3(a) tiene un índice de deformación de 0.98, el cual es más alto comparándolo con los

valores mostrados de las figuras restantes (Figuras 7.3(a), (b) y (c)), de manera similar, la hoja de la Figura 7.3(d) presenta el más bajo índice de deformación (*I* = 0.86), mientras que la Figura 7.3(b) y 7.3(c) presentan el mismo índice de deformación (*I* = 0.90), estos valores sugieren que ambas hojas tiene deformaciones similares. La diferencia entre el valor de *I* entre las hojas sanas y no sanas indican que las hojas de la Figura 7.3 (a), (b) y (c) están más deformadas que la hoja de la figura 7.3(a). Es fácil notar las diferencias entre la Figura 7.3(a) y las otras figuras tal y como se obtiene con el índice de deformación de la hoja. Sin embargo, esto se complica cuando se quiere observar las diferencias entre las hojas enfermas (Figura 7.3(b), (c) y (d)).

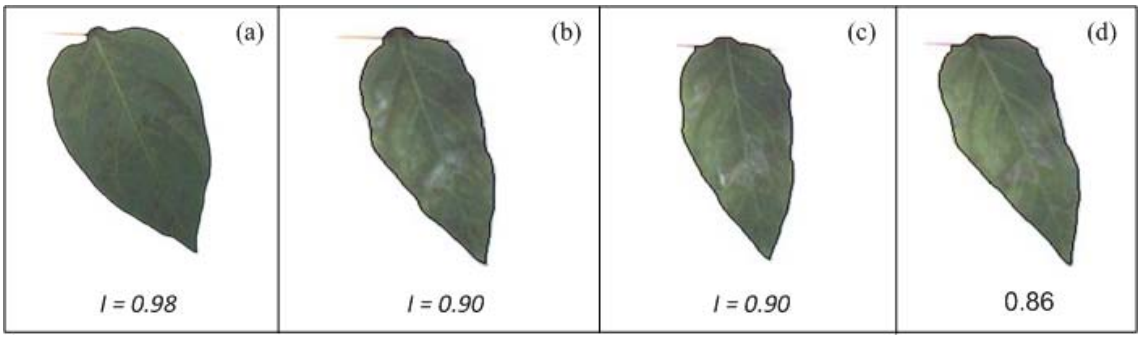

Figura 7. 3. Hojas de chile con diferentes índices de deformación. a) Hoja de chile con el más alto índice de deformación. b) y c) Hojas con índice de deformación intermedio. d) Hoja de chile con el más bajo índice de deformación.

7.4 Manchas blancas

El algoritmo para evaluar el área de manchas blancas fue probado utilizando plantas infectadas con el virus de mosaico común del frijol. La Figura 5.4 muestra hojas de frijol con el síntoma de manchas blancas. Los valores de manchas blancas $A_{pws,}$ mostrados en el pie de cada figura, sugieren una tendencia incremental de manchas blancas en las hojas. La hoja de la Figura 7.4(a) es la hoja con menos porcentaje de manchas blancas de acuerdo con el valor de A_{pws} y la hoja de la figura 7.4 (d) es la hoja con el más alto porcentaje de manchas blancas. Las hojas mostradas en la Figura 7.4 (b) y (c) tienen valores intermedios de A_{pws}. Las diferencias entre las Figuras 7.4 (a) y las Figuras 7.4(a), (b) y (c) son fácilmente identificadas mediante VE; sin embargo, VE no puede ser una herramienta fiable para indicar diferencias entre las Figuras 7.4(b), (c) y (d).

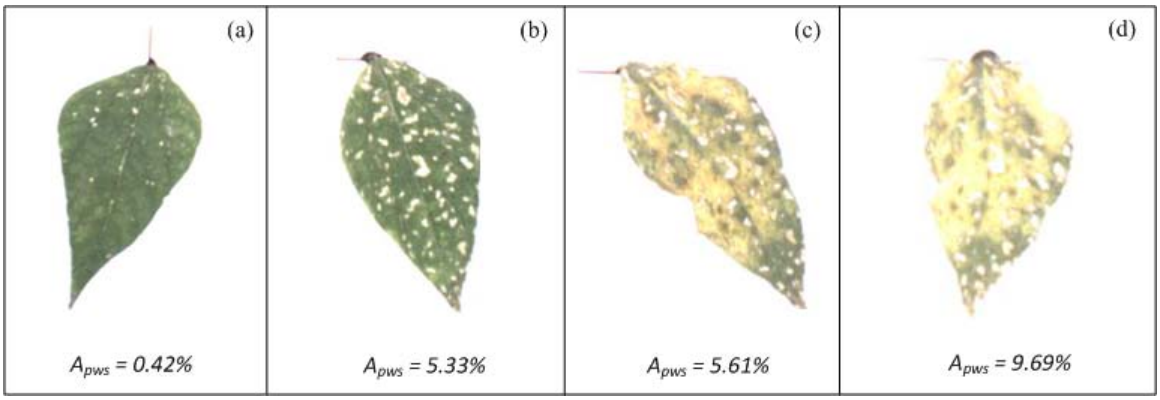

Figura 7. 4. Hoja de frijol con diferentes porcentajes de tejido de la hoja ocupados por manchas blancas. a) Hoja de frijol con el más bajo porcentaje de hoja ocupado por las manchas blancas. b) Hoja de frijol con porcentaje intermedio de área ocupada por manchas blancas. c) Hoja de frijol clorótica con porcentaje intermedio ocupado por manchas blancas. d) Hoja de frijol clorótica con el más alto porcentaje de área ocupada por manchas blancas.

7.5 Mosaicos

El algoritmo del virus del mosaico fue probado utilizando plantas de frijol infectadas con el virus del mosaico común, el cual provoca el síntoma del mosaico de aclaramiento de nervadura. La Figura 7.5 muestra hojas con y sin síntoma de mosaico; los valores de A_{mosaic} mostrados en la Figura 7.5 sugieren que las hojas de la Figura 7.5(a) y (b), los cuales son hojas sanas, tienen un menor porcentaje de área cubierta por el síntoma del mosaico que las hojas enfermas de las Figuras 7.5(c) y (d). Estas diferencias entre las hojas sanas y las hojas enfermas son cuantificables a través del procedimiento descrito anteriormente al obtener A_{mosaic}, lo que para las estimaciones visuales sería muy complicado.

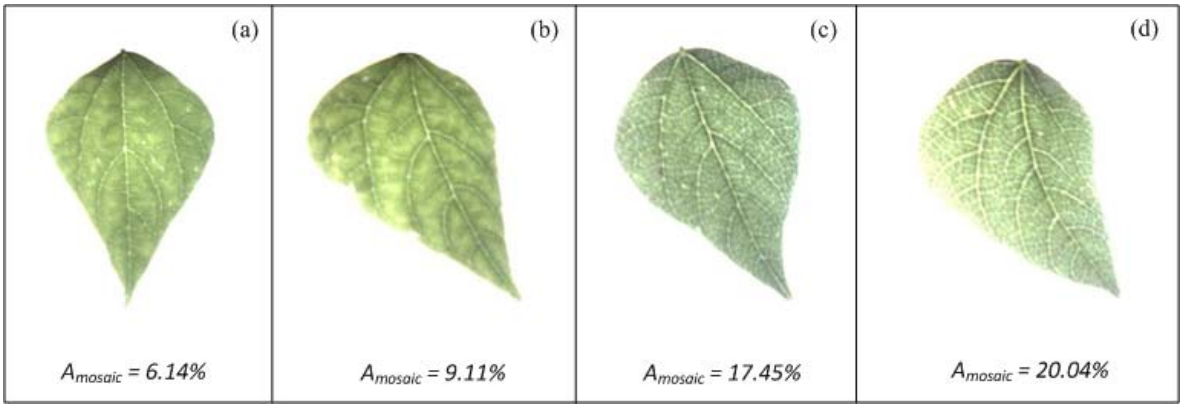

Figura 7. 5. Hojas de frijol con diferentes porcentajes de hoja cubierta por el síntoma del mosaico. a) y b) Hojas de frijol sanas con el más bajo porcentaje de área cubierta por el síntoma del

mosaico. c) y d) Hojas de frijol no sanas con el más alto porcentaje de área cubierta por el síntoma del mosaico.

7.6 Implementación en el FPGA

Los bloques de procesamiento en el FPGA de la unidad HSP usan un reloj de 25 MHz; los tiempos de procesamiento empleados por cada bloque para realizar su función correspondiente son mostrados en el Cuadro 5.1.

Cuadro 7. 1. Tiempos de procesamiento de los bloques implementados en el FPGA.

Bloques de procesamiento	Tiempo de procesamiento (ms)
Chlorosis	123.398
Necrosis	12.289
Deformacion	48.490
Manchas blancas	264.192
Mosaico	354.080

La implementación utiliza 7403 elementos lógicos, 34 multiplicadores de 9 bits y 235616 bits de memoria del FPGA, lo que corresponde a 22.29%, 48.57% y 48.70% de uso del chip respectivamente. Se puede notar que todos los algoritmos de procesamiento tiene un tiempo de ejecución menor a 1 s, lo cual garantiza las capacidades de procesamiento *in-situ* y en tiempo real. Por otro lado, hay más del 50% de los recursos del FPGA disponibles para incorporar futuros algoritmos de procesamiento.

VIII. **CONCLUSIONES**

El presente trabajo describe un sensor inteligente capaz de proveer cuantificaciones precisas, confiables y robustas de síntomas comunes en hojas de plantas enfermas y con deficiencias nutricionales; estos síntomas son; clorosis, necrosis, deformación, manchas blancas y mosaicos. El sensor inteligente emplea un sensor CMOS de 1/3-pulgada de 1.3 Megapíxeles que actúa como sensor primario y una tarjeta de desarrollo Altera-DE2 que contiene un FPGA Cyclone II EP2C35F672C6N que sirve como elemento de procesamiento debido a que este contiene los suficientes recursos para satisfacer la alta demanda computacional de los algoritmos propuestos. Las metodologías novedosas y las características del FPGA son explotadas por el sensor inteligente para obtener mediciones de síntomas de plantas de manera cuantitativa, *in-situ*, precisa, no destructiva y en tiempo-real. La funcionalidad del sensor inteligente fue exitosamente probada analizando los cinco síntomas antes mencionados presentes en hojas de plantas enfermas y con deficiencias nutricionales. Un análisis comparativo de los resultados muestran que los valores cuantitativos de las Figuras 7.1, 7.2, 7.3, 7.4 y 7.5 están en concordancia con las EV hechas sobre estas mismas hojas; en consecuencia, el sistema que se propone puede ser empleado en futuros trabajos como una herramienta poderosa y practica para dar, a través de la cuantificación de síntomas en las hojas de las plantas, descripciones precisas y confiables del desarrollo del síndrome en plantas o para determinar cuantitativamente las deficiencias nutricionales de las plantas. Este trabajo puede además servir como una herramienta para conocer la resistencia de variedades especificas de plantas a ciertos patógenos y por consecuencia, ayudar a desarrollar variedades más resistentes. Para un futuro desarrollo, las capacidades de reconfigurabilidad del FPGA permiten la incorporación de diferentes algoritmos capaces de estimar otros síntomas que no fueron considerados para este trabajo.

REFERENCIAS BIBLIOGRÁFICAS

Agrios, G.N. 2005. *Plant Pathology* (5th ed.). Elsevier Academic Press: London, UK.

Al-Hiary, H., Bani-Hamad, S., Reyelat, M., Braik, M., Alrahamneh, Z. Fast and accurate detection and classification of plant diseases. 2011. Int. J. Comput. Appl. 17, 31–38.

Altera Section I. 2010. Cyclone II Device Family Datasheet; Altera Corp.: San Jose, CA, USA.

Anaya-Lopez, J.L., Torres-Pacheco, I., Gonzalez-Chavira, M., Garzon-Tiznado, J.A., Pons-Hernandez, J.L., Guevara-Gonzalez, R.G., Muñoz-Sánchez, C.J., Guevara-Olvera, L., Rivera-Bustamante, B.F., Hernandez-Verdugo, S. 2008. Resistence to geminivirus mixed infections in Mexican wild peppers. Hort. Sci. 38, 251–255.

Bai, X., Zhou, F. 2010. Analysis of different modified top-hat transformation based on structuring element construction. Signal Processing. 90:2999-3003.

Bock, C.H., Cook, A.Z., Parker, P.E., Gootwald, T.R. 2008. Characteristics of the perception of different severity measures of citrus canker and the relationships between the various symptom types. Plant. Dis. 92, 927–939.

Bock, C.H., Parker, P.E., Cook, A.Z. 2008. Visual rating and the use of image analysis for assessing different symptoms of citrus canker of grapefruit leaves. Plant. Dis. 92:530-541.

Bock, C.H.; Cook, A.Z.; Parker, P.E.;Gootwald, T.R. 2009. Automated image analysis of the severity of foliar citrus canker symptoms. Plant. Dis. 93:660-695.

Camargo, A., Smith, J.S. 2008. An image-processing algorithm to automatically

identify plant disease visual symptoms. Biosyst. Eng. 102:9-21.

Camargo, A., Smith, J.S. 2009. Image pattern classification for the identification of disease causing agents in plants. Comput. Electron. Agr. 66:121-125.

Chaerle, L., Hagenbeek, D., Bruyne, E.D., Valcke, R., Van Der Straeten, D. 2004. Thermal and chlorophyll-fluorescence imaging distinguish plant-pathogen interactions at early stage. Plant. Cell. Physiol. 45: 887-896.

Contreras-Medina, L. M., Torres-Pacheco, I., Guevara-González, R.G., Romero-Troncoso, R.J., Terol-Villalobos, I.T., Osornio-Rios, R.A. 2009. Mathematical modelling tendencies in plant pathology. Afr. J. Biotechnol. 8: 7399-7408.

Contreras-Medina, L.M., Romero-Troncoso, R.J., Cabal-Yepez, E., Rangel-Magdaleno, J.J., Millan-Almaraz, J.R. 2010. FPGA based multiple-

channel vibration analyzer for industrial application in induction motor failure detection. IEEE Trans. Instrum. Meas. 59, 63–72.

Contreras-Medina, L. M., Osornio-Rios, R.A., Torres-Pacheco, I., Romero-Troncoso, R.J., Guevara-González, R.G., Millan-Almaraz, J.R. 2012. Smart Sensor for Real-Time Quantification of Common Symptoms Present in unhealthy Plants. Sensors. 12, 784-805.

Cooke, B.M. 2006. Disease assessment and yield loss, In: The epidemiology of plant disease. Kaye (eds). Springer, Dordrech, The Netherlands.

De Wolf, E.D., Isard, S.A. 2007. Disease cycle approach to plant disease prediction. Annu. Rev. Phytopathol. 45:203-220.

Delaieux, S., Auwerkerken, A., Verstraeten, W., Somers, B., Valcke, R., Lhermitte, S., Keulemans, J., Coppin, P. 2009. Hyperspectral reflectance and fluorescence imaging to detect scab induced stress in apple leaves. Remote. Sens. 27, 858-874.

Díaz-Lago, J.E., Stuthman, .D.D., Leonard, .K.J. 2003. Evaluation of component partial resistance to oat crown rust using digital image analysis. Plant. Dis. 87: 667-674.

FAO. Global hunger declining but still unacceptably high international targets difficult to reach. <http://www.fao.org/docrep/012/al390e/al390e00.pdf>.

Frank, R. 2000. Understanding Smart Sensors. (2nd ed.). Artech House: Norwood, Massachusetts.

Gonzalez. R.C., and Woods. R.E. 2001. Digital Image Processing. (2nd Ed). Prentice Hall, New Jersey, USA.

Goodman, B.A., Williamson, B., Chudek, J.A. 1992. Non-invasive observation of the development of fungal infection in fruit. Protoplasma. 166, 107–109.

Heuser, T., Zimmer, W. 2003. Genus- and isolate-specific real-time PCR quantification of Erwinia on leaf surface of English oaks (Quercus robur L.). Curr. Microbiol. 47, 214–219.

Holb, I.J., Heijne, B., Jeger, M.J. (2003. Summer epidemic of apple scab: The relationship between measurements and their implications for the development of predictive models and threshold levels under different disease control levels. J. Phytopathol. 151: 335-343.

INIFAP (Instituto Nacional de Investigaciones Forestales Agrícolas y Pecuarias). Reporte anual 2009: Ciencia y Tecnología para el campo Mexicano.<http://www.inifap.gob.mx/investigacion/reportes/reporte_anual2009.pdf>.

Irfaq, M., Ajab, M., Hongxiang, M., Khattak, G.S.S. 2009. Assessment of genes controlling area under disease progress curve (AUDPC) for stripe rust (P. Striiformis F. Sp. Tritici) in two wheat (Triticum Aestivum L.) crosses. Cytol. Genet. 43: 241-252.

Jeger, M.J. 2004. Analysis of disease progress as a basis for evaluating

disease management practices. Annu. Rev. Phytopatol. 42: 61-82.

Laothawornkitkul, J., Moore, J.P., Taylor, J.E., Possel, M., Gibson, T.D., Hewitt, C.N., Paul, N.D. 2008. Discrimination of plant volatile signatures by an electronic nose: A potential technology for plant pest and disease monitoring. Environ. Sci. Technol. 42, 8433–8439.

Liu, L., Vikram, A., Hamzehzarghani, H., Kushalappa, A.C. 2005. Discrimination of three fungal disease of potato tubers based on volatile metabolic profiles developed using GC/MS. Potato Res. 48, 85–96..

Maciá-Vicente, J.G., Jansson, H., Talbot, N.J., Lopez-Llorca, L.V. 2009. Real-time quantification and live-cell imaging of endophytic colonization of barley (Hordeum vulgare) roots by Fusarium equiseti and Pochinia chlamydosporia. New. Phytol.182, 213-228.

Marta, A.D., Magarey, R.D., Orlandini, S. 2005. Modelling leaf wetness duration and downy mildew simulation on grapevine in Italy. Agric. For. Meteorol. 132: 84-95.

Martin, D.P., Rybicki. E.P. 1998. Microcomputer-based quantification of maize streak virus symptoms in Zea mays. Phytopathology. 88, 422–427.

Mekid, J. 2006. Futher structural intelligence for sensors cluster technology in manufacturing. Sensors. 6:557-577.

Mikulova, K., Bojnanska, K., Cervená, V. 2008. Assessment of parcial resistance to powdery mildew in hexaploid wheat genotypes. Biologia. 63:477-481.

Millan-Almaraz, J.R., Guevara-Gonzalez, R.G., Romero-Troncoso, R.J., Osornio-Rios, R.A., Torres-Pacheco, I., 2009. Advantages and disadvantages on photosynthesis measurement techniques: A review. Afr. J. Biotechnol. 8,7340-7349.

Millan-Almaraz, J.R., Romero-Troncoso, R.J., Guevara-Gonzalez, R.G., Contreras-Medina, L.M., Carrillo-Serrano, R.V., Osornio-Rios, R.A., DuarteGalvan, C., Rios-Alcaraz M.A., Torres-Pacheco, I. 2010. FPGA-based Fused Smart Sensor for Real-Time Plant-Transpiration Dynamic Estimation. Sensor. 10:8316-8331.

MT9M011 Data Sheet. 2004. Micron Technology Inc.: Boise, ID, USA.

Navakar, D.S., Singh, C.B., Jayas, D.S., White, N.D.G. 2009. Assessment of soft X-ray imaging for detection of fungal infection in wheat. Byosist. Eng. 103, 49–56.

Orlandini, S., Masseti, L., Marta, D.A. 2008. An agrometeorological approach for the simulation of Plasmora viticola. Computers and electronics in agriculture, 64: 149-161.

Pajares G., J. de la Cruz. 2002. Visión por Computador: Imágenes Digitales y Aplicaciones, Ed. Alfaomega.

Pearson, T. 2009. Hardware-based image processing for high-speed inspection of grains. Comput. Electron. Agr. 69:12–18.

Pratt, W.K. 2001. Digital Image Processing. (3rd ed.); John Wiley & Sons: New York, NY, USA.

Rangel-Magdaleno, J.J., Romero-Troncoso, R.J., Osornio-Rios, R.A., Cabal-Yepez, E. 2009. Novel oversampling technique for improving signal-to-quantization Boise ratio on accelerometer-based smart jerk sensor in CNC applications. Sensors. 9:3767-3789.

Rivera, J., Herrera, G., Chacón, M., Acosta, P., Carrillo, M. 2008. Improved progressive polynomial algorithm for self-adjustment and optimal response in intelligent sensors. Sensors. 8: 7410-7427.

Rodriguez-Donate, C., Morales-Velazquez, L., Osornio-Rios, R.A., Herrera-Ruiz, G., Romero-Troncoso, R.J. 2010. FPGA-Based fused smart sensor for dynamic and vibration parameter extraction in industrial robot links. Sensors 10:4114-4129.

Sankaran, S., Mishra, A., Ehsani, R., Davis, C. 2010. A review of advanced techniques for detecting plant diseases. Comput. Electron. 72, 1–13.

Segarra, J., Jeger, MJ., Van den Bosch, F. 2001. Epidemic dynamics and

patterns of plant diseases. Phytopathol. 91:1001-1010.

Serra. J. 1982. Image analysis and mathematical morphology. (1st Ed). Academic Press, Inc. Orlando, Florida, USA.

Shaner, G., Finney, R.E. 1977. The effect of nitrogen fertilization on the expression of slow-mildewing resistance in Knox wheat. Phytopathology, 67: 1051-1056.

Sonka, M.; Hlavac, V.; Roger, Boyle. 2008. Image Processing, Analysis and Machine Vision (3rd ed.). Thomson: Toronto, ON, Canada.

Taiz, L., Zeiger, E. 2006. Plant Physiology (4th ed.). Sinauer Associates: Sunderland, MA, USA.

Trigiano, R.N., Windham, M.T., Windham, A.S. 2004. Plant Pathology: Concepts and Laboratory Exercises. (5th ed.). CRC Press: Los Angeles, FL, USA.

Van der Plank, J.E. 1960. Analysis of epidemias. In: Plant Pathology. Horsfall JG and Cowling EB (eds). Academic Press, New York, USA.

Van Maanen, A., Xu., X.M. 2003. Modelling plant disease epidemics. European J. Plant Pathol. 109: 669-682.

Waggoner, P.E., Horsfall, J.G. 1969. EPIDEM a simulator of plant disease

written for a computer. Conn. Agric. Exp. Stn. Bull. No. 698.

Ware, J.O., Young, V.H. 1934. Control of cotton and ‘rust’. University of Arkansas Agricultural Experimental station Bulletin 308, Fayetteville, AR.

Ware, J.O., Young, V.H., Janssen, G. 1932. Cotton wilt studies. III. The behavior of certain cotton varieties grown on soil artificially infested with the cotton wilt organism. University of Arkansas Agricultural Experimental Station Buletin 269, Fayetteville, AR.

Wijekoon, C.P., Goodwin, P.H., Hsiang, T. 2008. Quantifying fungal infection of plant leaves by digital image analysis using Scion Image software. J. Microbiol. Methods. 74:94-101.

Xu, X. 2006. Modelling and interpreting disease progress in time. In: The epidemiology of plant disease. Cooke BM, Gareth Jones D and Kaye (eds) Springer, Dordrecht, The Netherlands.

IX. APENDICE A. PRODUCTOS GENERADOS DURANTE LA TESIS DOCTORAL

- **Artículos derivados de tesis Doctoral.**

ARTICULO 1. "Mathematical modeling tendencies in plant pathology"

Journal: African Journal of Biotechnology

ISSN: ISSN 1684-5315

ARTICULO 2. "Smart Sensor for Real-Time Quantification of Common Symptoms Present in Unhealthy Plants"

Journal: Sensors MDPI

ISSN: 1424-8220

- **Artículos generados durante los estudios doctorales**

ARTICULO 3. "FPGA-Based Multiple-Channel Vibration Analyzer for Industrial Applications in Induction Motor Failure Detection"

Journal: IEEE Transactions on Instrumentation and Measurement

ISSN: 0018-9456

ARTICULO 4. "FPGA-based Fused Smart Sensor for Real-Time Plant-Transpiration Dynamic Estimation"

Journal: Sensors MDPI

ISSN: 1424-8220

ARTICULO 5. "Estimating the response of tomato (Solanum lycopersicum) leaf area to changes in climate and salicylic acid applications by means of artificial neural networks"

Journal: Biosystems Engineering

ISSN: 1537-5110

ARTICULO 6. "Novel Methodology for Online Half-Broken-Bar Detection on Induction Motors"

Journal: IEEE Transactions on Instrumentation and Measurement

ISSN: 0018-9456

- **CAPITULOS DE LIBRO:**

NOMBRE DE CAPITULO DE LIBRO: "Methods for Detection and Quantification of Aflatoxins"

Nombre del libro: Aflatoxins – Detection, Measurement and Control

Editorial: InTech

ISSN: 978-953-307-711-6

NOMBRE DE CAPITULO DE LIBRO: "Characteristics of mycotoxin analysis tools for tomorrow"

Nombre del libro: Aflatoxins - Recent Advances and Future Prospects

Editorial: InTech

Capítulo de libro aceptado para publicarse

African Journal of Biotechnology Vol. 8 (25), pp. 7399-7408, 29 December, 2009
Available online at http://www.academicjournals.org/AJB
ISSN 1684–5315 © 2009 Academic Journals

Review

Mathematical modeling tendencies in plant pathology

L. M. Contreras-Medina[1,2], I. Torres-Pacheco[1], R. G. Guevara-González[1], R. J. Romero-Troncoso[2], I. R. Terol-Villalobos[3] and R. A. Osornio-Rios[2]*

[1]Laboratorio de Biosistemas, División de Estudios de Posgrado, Facultad de Ingeniería, Universidad Autónoma de Querétaro, Cerro de las Campanas s/n, C.P. 76010, Querétaro, Qro., México.
[2]HSPdigital CA Mecatrónica, Facultad de Ingeniería, Campus San Juan del Río, Universidad Autónoma de Querétaro, Querétaro, Qro. México.
[3]Centro de Investigación Desarrollo Tecnológico en Electroquímica, Parque Tecnológico Querétaro, Sanfandila-Pedro Escobedo, C.P. 76700-APDO 064, Querétaro, Qro. México.

Accepted 11 December, 2009

Nowadays plant diseases represent one of the major threats for crops around the world, because they carry healthy, economical, environmental and social problems. Considering this, it is necessary to have a description of the dynamics of plant disease in order to have sustainable strategies to prevent and diminish the impact of the diseases in crops. Mathematical tools have been employed to create models which give a description of epidemic dynamics; the commonly mathematical tools used are: Disease progress curves, Linked Differential Equation (LDE), Area Under disease Progress Curve (AUDPC) and computer simulation. Nevertheless, there are other tools that have been employed in epidemiology of plant disease like: statistical tools, visual evaluations and pictorial assessment. Each tool has its own advantages and disadvantages. The nature of the problem and the epidemiologist necessities determine the mathematical tool to be used and the variables to be included into the model. This paper presents review of the tools used in epidemiology of plant disease remarking their advantages and disadvantages and mathematical modeling tendencies in plant pathology.

Key words: Plant disease epidemics, mathematical modeling, disease progress curves, area under disease progress curve, linked differential equation.

INTRODUCTION

Currently plant diseases, weeds and environmental factors are the major threats to agricultural production, mainly in less developed countries because they provoke between 31 to 42 percent of worldwide crop losses (Van den Bosch et al., 2006). Taking into account that 14.1% of crops are lost to plant disease alone, the total world-wide crop loss from plant disease is about $220 billion dollars, this implies several problems in other important sectors (e.g. health, environmental, social) (Agrios, 2005); these losses are in part responsible for the suffering of 800 million people who lack adequate food (Strange and Scott, 2005). Due to the aforementioned problems it is necessary to have adequate, economic and environmentally acceptable strategies to manage the epidemic development of plant diseases in order to decrease the crop losses and reduce their consequences (Van Maanen and Xu, 2003; De Wolf and Isard, 2007). Most current practices have been used in order to control epidemics, like the use of chemical control (Blaise et al., 1999) having a direct environmental impact due to its chemical residues (Orlandini et al., 2008). Then, in order to obtain sustainable practices for strategic and tactical management of diseases and also to decrease its environmental impact, it is necessary to understand the determining factors of epidemics (Royle and Ostry, 1995; Jeger, 2004). Mathematical, statistical and other tools have been used to understand these factors by modeling the epidemic dynamics; the objective in modeling is to simplify the reality in order to summarize the process of the epidemic (Van Maanen and Xu, 2003). Mathematical tools have been gaining popularity because they allow knowing a description of the epidemic dynamics and by consequence, to develop optimal forecasting and con-

*Corresponding author. E-mail: raosornio@hspdigital.org. Tel: +52-427-274-12-44. Fax: +52-427-274-12-44.

trolling mechanisms. Descriptions of temporal disease progress were used prior to 1960s when Ware et al. (1932) and Ware and Young (1934) presented curves to illustrate the effects of crop resistance and fertilizer treatment for the dynamics of cotton, Wilt and Large (1945, 1952) proposed disease progress curves to demonstrate the benefits of fungicide applications on the development of potato late blight. Nevertheless, the first temporal development model of plant disease epidemic was proposed by Van der Plank (1960, 1963), which has been the base of many epidemiological models created so far. The mathematical tools employed in plant disease epidemiology use several variable values as inputs; these variables are considered according to the nature of the problem and the questions to be answered (Van der Plank, 1982). Schoeny et al. (2007) proposed a predictive model of Ascochyta blight where an important variable in the model was the airborne inoculums. The variables used by the mathematical tools summarize the key characteristics in the epidemic dynamics. The most common mathematical tools used in plant disease epidemiology are: disease progress curves, linked differential equations, area under disease progress curve and computer simulations. Nevertheless, there are other tools to evaluate the disease progress. This paper presents an updated review about mathematical tools used in plant disease epidemiology. The paper is divided in five sections, the first one presents the mathematical tools used for modeling plant disease epidemics, the second section shows an analysis of variables commonly utilized by mathematical tools, the third section presents an analysis about the advantages and disadvantages of mathematical tools used in plant disease epidemiology, the fourth section shows tendencies in epidemiology of plant disease and finally the fifth section presents conclusions.

MATHEMATICAL TOOLS USED IN PLANT DISEASE EPIDEMIOLOGY

Plant diseases epidemics are investigated according to variables of interest which are formulated as functions of external factors, for instance temperature and rain (Van Maanen and Xu, 2003). The problem nature and epidemiologist specific questions determine the mathematical tool to be used for modeling plant disease epidemics (Kranz and Royle, 1978; Sutherst, 1993; Van Maanen and Xu, 2003; Xu, 2006). Next, the most common mathematical tools to describe epidemic dynamics are presented.

Disease progress curves

Disease progress curves show the epidemic dynamics over time (Agrios, 2005). This mathematical tool can be used to obtain information about the appearance and amount of inoculum, changes in host susceptibility during growing period, weather events and the effectiveness of cultural and control measures. Growth models provide a range of curves that are often similar to disease progress curves (Van Maanen and Xu, 2003) and represent one of the most common mathematical tools to describe temporal disease epidemics (Xu, 2006). The growth models commonly used are: Monomolecular, Exponential, Logistic and Gompertz (Zadok and Schein, 1979; Nutter, 1997; Nutter and Parker, 1997; Xu, 2006). A brief description of each growth model is presented as follows:

Monomolecular

This growth model is appropriate for modeling epidemics where there is not secondary spread within a growing season, meaning that the plant disease has a single cycle during growing season (Forrest, 2007). This model is also called negative exponential model (Campbell and Madden, 1990).

Exponential

This model is also known as the logarithmic, geometric or Malthusian model. This growth model is appropriate when newly diseased (infected) individuals lead to more diseased (infected) individuals and has been used to model changes in disease prevalence on a geographic scale, it can be applied to describe the very early stages of most polycyclic epidemics (Forrest, 2007).

Logistic

Was proposed firstly by Veshulst in 1838 to represent human population growth. A second type of logistic model was proposed by Van der Plank (1963), being more appropriate for most polycyclic diseases, meaning that there is a secondary spread within a growing season (Forrest, 2007). This growth model is the most widely used for describing epidemics of plant disease (Segarra et al., 2001; Jeger, 2004).

Gompertz

This growth model is appropriate for polycyclic diseases as an alternative to logistic models. Gompertz model has an absolute rate curve that reaches a maximum more quickly and declines more gradually than the logistic models (Forrest, 2007).

Figure 1 shows examples of disease progress curves represented by growth models, where it can be seen that Gompertz and logistic models have a characteristic sigmoid form and an inflection point meaning secondary

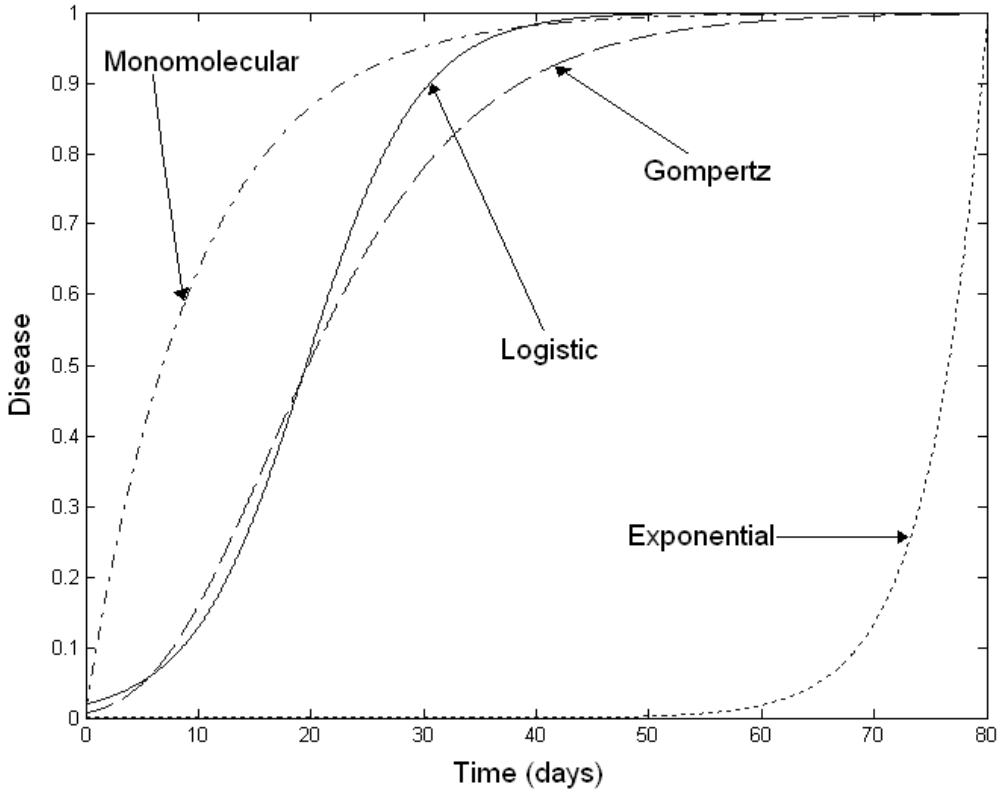

Figure 1. Examples of disease progress curves represented by monomolecular, exponential, logistic and Gompertz models.

inoculation or plant-to-plant spread within the crop in contrast to monomolecular model, which does not have inflection point. The exponential model presents a very small value at the beginning comparing with the other models and latter it increases exponentially.

In general, growth models that incorporate few variables to describe temporal disease dynamics have a good performance; however, this kind of models sometimes do not satisfy the acquiring process of key characteristics because they frequently ignore relevant variables that affect the epidemic development (Xu, 2006), e. g. host growth, fluctuating environmental condition, length of latent and infectious period, etc. Nevertheless, advances in statistical and computing technologies have allowed incorporating several of these kinds of characteristics in order to obtain a more reliable model. It is important to mention that the researchers should be aware of some violations presented in these models by checking if some assumptions about the epidemic are not met and if there are some inevitable violations; they must try to find means to reduce such violations in order to diminish the bias and to correctly interpret results (Xu, 2006). Van der Plank (1960) used exponential, monomolecular and logistic models to describe the development of epidemics. Xu (1999) used a logistic model to forecast and model the apple powdery mildew provoked by *Podosphaera leucotricha*. The work presented by Mersha and Hau (2008) uses logistic and Gompertz models to study the effects of rust bean on host dynamics of common bean in controlled greenhouse experiments with and without fungicide sprays. A deep description of these growth models can be found in the book written by Campbell and Madden (1990).

Linked differential equations (LDE)

This mathematical tool achieves the description of plant disease epidemics by modeling each of the variables considered to be determinant in epidemic development and latter making the link between them. LDE allows the inclusion of new terms into the model as needed (Madden, 2006). When this technique cannot be easily integrated to obtain an analytical solution, it needs numerical methods to provide a numerical solution (Xu, 2006; Madden, 2006); nowadays, the advances in computational technology have permitted that numerical solutions could be easily obtained through mathematically-oriented software like MATHCAD or MATHEMATICA (Madden, 2006).

Usually LDE is employed to investigate relationships of the plant disease dynamics in relation to the host, environment and human intervention (Mannen and Xu, 2003). A relatively simple linked differential equations for

polycyclic disease involve variables like healthy tissue, latently infected, infectious and removed individuals (leaves, roots, plants) (Madden, 2006). Zhang et al. (2001) used four linked differential equations to illustrate the effect of synergism between plant viruses where each differential equation represents one of the following four categories: healthy host plant, infected host plant with a virus kind A alone, infected with a virus kind B alone, and infected with both viruses A and B, the obtained results were used to understand an epidemic that has been ongoing in Uganda since the late 1980s and the information about the development of Cassava Mosaic Disease (CMD) epidemic in Uganda and neighboring countries supports model results.

Area under disease progress curve (AUDPC)

This technique is very useful when the observed patterns cannot be fitted by progress disease curves (Van Maanen and Xu, 2003; Xu, 2006). AUDPC is the amount of disease integrated between two times of interest and it is calculated regardless the curve shape (Shaner and Finney, 1977). Disease progress data is summarized into one value by AUDPC; it is suited when host damage and the amount and duration of the disease are proportional (Xu, 2006).

If a model fits satisfactorily the disease patterns, AUD PC can be obtained from the model by integrating over certain interval of time (Jeger and Viljanen-Robinson, 2001). AUDPC, percentage disease index (PDI) and apparent infectious rate (r) were used to measure the resistance to early blight of tomato with respect to several variables of disease epidemics; these variables were: tomato variety, plant age, artificial and natural inoculation; the obtained values served as indicators to classify the tomato variety into one of the six scales of resistance (highly resistant, resistant, moderately resistant, moderately susceptible, susceptible and highly susceptible) (Pandey et al., 2003). AUDPC is generally used to make comparison between treatments (Jeger, 2004; Xu, 2006) and to evaluate the resistance of plant species to the pathogens (Jeger and Viljanen-Rollinson, 2001; Pandey et al., 2003; Mikulova et al., 2008; Irfaq et al., 2009).

Computer simulation

This tool, jointly with LDE, is used to determine the key dynamic features of the pathosystem. Several models have been used to simulate dynamics of plant diseases in order to prevent and control disease epidemics. One of the first programs was the EPIDEM written by Wagonner and Horsfall (1969) and it was designed to simulate epidemics of early blight of tomato and potato caused by the fungus *Alternaria solani* and it resulted from modeling each stage of the life cycle of the pathogen as a function of the environment. Subsequently, several kinds of computer programs were created like MYCOS for *Mycospaherella* blight of chrysantemus (McCoy, 1976), EPIMAY for southern corn leaf blight (Waggoner et al., 1969), EPIVEN for apple scab caused by *Venturia inaequalis* (Kranz et al., 1973) and a more general and flexible plant simulator called EPIDEMIC (Shrum, 1975) because it could be easily modified for another plant-pathogen system. Improvements of previously developed computer models continue being made and used for new applications (Jeger, 2004), for instance epidemic model EPIMUL has been used to simulate the efficacy of various mixtures in relation to a range of different pathogen characteristics (Lannou et al., 1994). Nowadays, computer programs are used to support other techniques for predicting plant disease and to measure the impact of pathology over certain plant species based on particular variables like leaf wetness, duration of leaf wetness, primary inoculums, temperature, rainfall and moisture. One example of this is PLASMO which is used to measure the impact on the quality of *Plasmora viticola* due to leaf wetness duration (Marta et al., 2005; Orlandini et al., 2008).

Visual evaluation, pictorial assessment and statistical tools

All the previously mentioned mathematical tools display descriptions of the disease dynamics and also give important characteristics about the epidemics as output (e.g length of different infectious event, severity and infection intensity during growing season, etc). Several works, when measuring plant resistance to certain kind of pathogens use scales to evaluate the severity of the plant or usually make the evaluation based on visual inspecttion. Anaya-Lopez et al. (2003) used a nine-level scale to measure qualitatively the severity of pepper disease provoked by geminiviruses, this scale has been previously used in other works (Hernandez-Verdugo et al., 1998; Godinez-Hernandez et al., 2001). Another kind of evaluation, called pictorial disease assessment, has also been created based on standard diagrams that illustrate the development of the stages in the disease on small simple units (leaves, fruits) or on large composite units such as branches or whole plants (Cooke, 2006); for instance, the modified Cobb scale, which is used to determine the percentage of possible rusted tissue (Roelfs et al., 1992). Holb et al. (2003) investigated the relationship between disease measurement, disease incidence, severity of apple scabs and their implications for the development of predictive models and thresholds levels; the disease assessment based on leave severity and fruit severity are made using a mathematical equation which classifies the fruit and leave severity into a six- and seven-level scale, respectively. Recently, certain works determine visually the severity of infections by evaluating

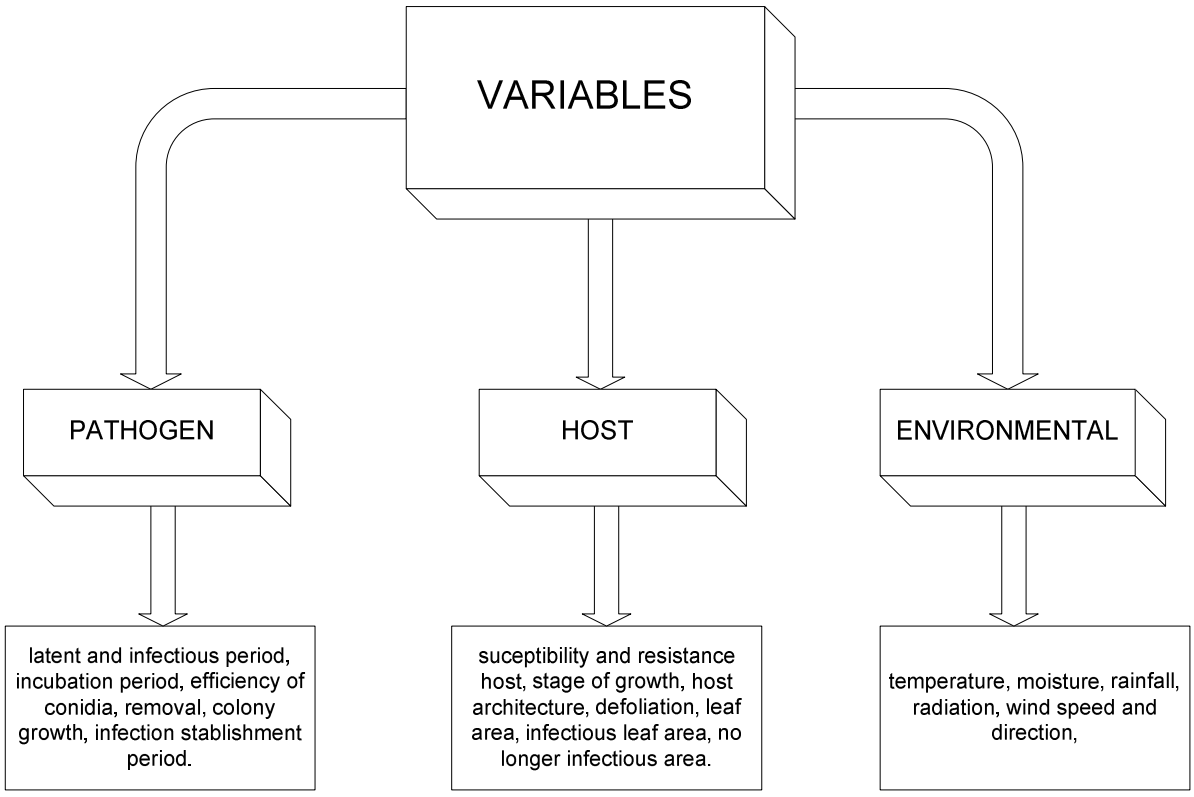

Figure 2. Classification of variables according to pathogen, host and environment.

the leaf area that presents oil spots (Orlandini et al., 2008), where the ability of the surveyors was standardized firstly by mean of cross-tests (Kranz, 1988) and also the severity was classified into a five-level scale.

It is important to mention that there are other tools used in plant pathology, these are the statistical tools such as: including survival analysis, nonparametric analysis of disease association, multivariate statistical methods, neural networks, meta-analysis, Bayesian statistics, generalized linear models, linear mixed models, decision theory, etc (Garret et al., 2004; Scherm et al., 2006;). These tools use normally distributed ordinal and discrete data, for instance, the linear mixed model, whereas the generalized linear mixed model works with discrete data (Garret et al., 2004). The statistical tools are employed depending on the necessity. For example, Multivariate statistical tools are used to reduce the space of *n* variables into a low-dimensional space, to assess group differences and variable contribution and to describe and predict the relationship between two sets of variables (Sanogo and Yang, 2004). Survival analysis is a technique for analyzing data sets in which the time until an event occurs is the dependent variable containing censored observations (Scherm and Ojiambo, 2004). Bayesian statistician make use of probability theory to reflect uncertainty; within the Bayesian framework, parameters are treated as if they were random variables and described with probability distributions rather than point estimates (Mila and Carriquiry, 2004).

USING VARIABLES

A proposed model that uses mathematical tools should include the variables that represent the key features in the development of epidemics according with the objective of the investigation; for instance, temperature, moisture, susceptibility and resistance of host, initial inoculum, latent and infectious period and efficiency of conidia are examples of commonly included variables in used models to describe plant disease epidemics (Van der Plank, 1982; Maneen and Xu, 2003; De Wolf and Isard, 2007). The variables that the epidemiologists include depend on the pathosystems, the nature of the problem and the answers to be found (Xu, 2006). The central principle of plant pathology is the disease triangle, where the development of plant disease requires these three equally-relevant components (Parker and Gilbert, 2004).

1. A susceptible host.
2. A virulent pathogen.
3. A favorable environmental condition.

The Figure 2 shows a classification of the variables according to each component of the disease triangle, it mentions some common variables used for modeling

Table 1. Examples of variables included into different kinds of models.

Main variables included	Name of paper	Reference
Initial inoculum, host growth characteristics, and temperature.	Effect of growth stage and initial inoculum level on leaf rust development and yield loss caused by *Puccinia recondita f. sp. tritici*.	Subba Rao et al., 1989
Rate of lesion increase, conversion rate of infectious into post-infectious tissue, initial proportion of infectious area, initial proportion of disease free-area.	Fungal foliar plant pathogen epidemics: modeling and qualitative analysis.	Kosman and Levy, 1994
Latent infection, visible leaf area, infectious leaf area, no infectious leaf area, infection efficiency of conidia, incubation progress, latency progress, removal, colony growth.	A dynamic simulation model for powdery mildew epidemics on winter wheat.	Rossi and Giosué, 1999
Air temperature, rainfall, relative humidity, leaf wetness duration, initial inoculum, leaf area, spot area, sporulation area, viable spores and incubation.	An agrometeorological approach for the simulation of *Plasmora viticola*.	Orlandini et al., 2008
Temperature, leaf wetness, rainfall, relative humidity.	Modelling of leaf wetness duration and downy mildew simulation on grapevine in Italy.	Marta et al., 2005
Leaf wetness duration, radiation, rainfall, rainfall amount, temperature, wind speed.	Quantifying and modelling the mobilisation of inoculum from diseases leaves and infected defoliated tissues in epidemics of angular leaf spot of bean.	Allorent et al., 2005
Temperature, relative humidity, vapor pressure deficit, total duration rainfall. Low growth rate, disease carrying capacity, infectious period.	Modelling and forecasting epidemics of apple powdery mildew (*Podosphaera leucotricha*).	Xu, 1999
Temperature, wind speed and direction, location and onset of primary infection.	A host-pathogen simulation model: powdery mildew of grapevine.	Calonnec et al., 2008
Temperature, humidity, precipitation leaf wetness duration, wind speed and direction.	Assessment of airborn primary inoculum availability and modeling of disease onset of ascochyta blight in field peas	Schoeny et al., 2007
Temperature, rainfall, plant characteristics (stem density, plant geometry, mean distance between nodes, and leaf area).	Effect of pea plant architecture on spatio-temporal epidemic development of ascochyta blight (*Mycosphaerella pinodes*) in the field.	Le May et al., 2009

plant disease dynamics (Rossi and Giosué, 1999; Xu; 1999; Maanen and Xu, 2003; Orlandini et al., 2008; Le May et al., 2009). Several kinds of variables have been included into certain models which are related in the development of plant diseases. The Table 1 presents some examples of proposed models using mathematical tools here presented and the variables included into the models.

As it can be seen, the variables are chosen according to the studied pathosystem and the objectives of the epidemiologist. It is generally assumed that the environment is the driven force for disease (Hardwick, 2006). Several works use as driving variables those concerning weather; temperature, rainfall, moisture, leaf wetness, wind direction, radiation, among others (Marta et al., 2005; Orlandini et al., 2008). From this, pathogen variables that are involved directly with epidemic development can be formulated as a function of driving variables (van Maanen and Xu, 2003) e.g. latent and infectious period, initial inoculation, oil spoil survival (Calonnec et al., 2008). Also, variables relating to host dynamics should be included in order to know how the pathogen dynamics are linked to the host dynamics and how pathogen affects the growth and reproduction of the host (Anderson and May, 1979; Van Maanen and Xu, 2003) e.g. intrinsic and age-related host dynamics (Shtienberg, 2000; Van Maanen and Xu, 2003).

MATHEMATICAL TOOLS USED IN EPIDEMIOLOGY OF PLANT DISEASE: ADVANTAGES AND DISADVANTAGES

The primary objectives of a mathematical tool is to help to understand how the main factors affect the plant disease development in order to prevent disease appearing and

the development of sustainable strategies for disease management. Models have been created using mathematical tools since the apparition of the first model (Van der Plank, 1960; Van der Plank, 1963). Next, some advantages and disadvantaged of common mathematical tools are presented:

Disease progress curves that use growth models have the advantage of generally describing the disease progress in a good way by adding few variables (Xu, 2006), but sometimes it is not adequate to describe certain kind of pathologies because it needs to incorporate extra-variables that are determinant in the pathosystem. The disadvantages of these models are the assumptions that the epidemiologist needs to make about the variables used by this mathematical tool. The resulting bias depends on the assumptions made and if a violation of the assumptions is presented, it needs to be reinterpreted in order to obtain a correct result. An example of these disadvantages is presented by Rotem et al. (1988) when disease intensity was masked by the loss of infected leaves and the appearance of new healthy leaves. Kushalappa and Ludwing (1982) showed that ignoring the growth-host effects could conduct to underestimate or even to obtain negative rate values because, may be, the rate of host growth is faster than the disease development rate. If disease increase is not as rapid as plant growth, the proportion of diseased tissue on the plant will appear to decrease (Mersha and Hau, 2008). Analogously, if defoliation occurs as a result of disease, the severity of infected plant will appear to decrease (Waggoner and Berger, 1987; Ojiambo and Scherm, 2005).

LDE is one of the most commonly used mathematical tools in modeling epidemics because it allows that new terms be easily included as needed in order to answer the question about the details of the pathosystem (Madden, 2006). In general, it is too difficult to obtain analytical solutions for this mathematical tool, but numerical solutions can be obtained. An advantage of this mathematical tool is the intrinsic relationship with other tools here mentioned like disease progress curves and computer simulations because important components of disease dynamics can be modeled by using growth models that latter could be linked and simulated using computer programs (Mersha and Hau, 2008). A disadvantage of LDE is that the formulated equations using this tool are extremely troublesome for mathematical analysis, which makes difficult the exploration of different biological properties of host and pathogens or to know the results of different control strategies, on long-term disease development (Madden, 2006).

AUDPC is extensively used in analyzing disease progress curves to make comparisons between treatments, to know the relationship between yield losses and disease, to make a genetic analysis, to evaluate the effectiveness of chemical, biological and cultural controls over disease progress and also for knowing the resistance of certain species to plant pathogens (Jeger, 2004). A disadvantage of AUDPC is that it depends on a good fitted disease progress curve to obtain correct results; this approach also can yield misleading results when it is summarized over a particular period instead of over a complete period (Xu, 2006).

The computer simulation is a general natural extension of LDE because it depends on computations to obtain a numerical solution. In computer simulation, some model variables in LDE are often assumed to be functions of external factors like temperature, humidity, radiation, wind direction, etc. This mathematical tool can be used to study theoretical and practical problems of certain kinds of pathologies (Agrios, 2005). One disadvantage of computer simulation is that generally each simulator just incorporates one disease to be simulated, restricting its functionality and also, a computer is required to achieve the task, having an intrinsic economical cost.

Disease evaluation based on visual estimation has a clear disadvantage, because of the variation between different points of view, given by different evaluators; yet, several works have been developed where visual evaluation of host severity is made and classified into a multilevel scale according to the kind of damage that is presented in the host due to the disease evolution (Anaya-Lopez et al., 2003; Hernandez-Verdugo et al., 1998; Godinez-Hernandez et al., 2001). This also provokes unsuitable strategies to forecast and prevent disease due to the subjectivity of the estimation. Similarly, pictorial assessment presents the disadvantage of subjectivity because it is a tool based on visual evaluation that decreases the reliability of an evaluation.

Statistical tools are attractive because they allow to obtain a model where some drawbacks exist, such as when little is known about the structural form of complex relationships between response variables, when theoretical data presented by other investigation needs to be used or when the calculation probabilities for the parameter of interest needs to be calculated based on empirically derived prior probabilities in conjunction with the conditional probability of each possible outcome (Scherm et al., 2006). The statistical tools have the disadvantage of supposing that the data are normally distributed (Garret et al., 2004) and also the theoretical models proposed by using this tool sometimes have non expected results in practice (Scherm et al., 2006). Table 2 summarizes the advantages and disadvantages of the common tools used to describe the dynamics of plant disease.

TRENDS IN EPIDEMIOLOGY OF PLANT DISEASE

The Mathematical tools used to describe disease dynamics of plants have been and continue being the mainstream of theoretical epidemiology (Scherm et al., 2006). Current works use a combination of the mathematical

Table 2. Advantages and disadvantages of common tools used to describe dynamics of plant disease.

Tool	Advantages	Disadvantages
Disease progress curves.	Often with two or three variables describe satisfactorily the disease.	Needs to make assumption to correct interpretation of results, sometimes ignore key components that affect disease development.
Linked Differential Equation.	New terms can be easily included into the model as needed.	Equation generated are extremely troublesome for mathematical analysis.
AUDPC	Is a very useful alternative to fitting growth models, it can work with growth models.	Needs that the amount and duration of disease be proportional to damage, it may give misleading results when AUDPC is summarized over other period than just over a particular period.
Visual evaluation.	Practical evaluation, does not need a PC, only evaluators are needed.	Subjectivity.
Pictorial assessment.	Practical evaluation, does not need a PC, only evaluators is needed.	Subjectivity.
Statistical tools.	Probability calculation based on empirical knowledge, allows using theoretical data.	Supposes that data are normally distributed, the proposed models are mainly based on theory.

PC: Personal computer.
AUDPC: Area under disease progress curve.

tools here presented in order to obtain a better description of plant disease (Mersha and Hau, 2008), which allows developing better strategies for disease management. Trends in mathematical modeling may continue combining the mathematical tools to model the determinant factors of plant disease. Mathematical and statistical tools employ environmental, pathogenic and host variables, whereas other tools use pictorial assessment and visual estimations. It can be suggested the combination of disciplines to join these tools in order to obtain better fitness than the models so far proposed. The support disciplines can be mathematics to obtain a model to fit the data, image processing to obtain a better visual estimation of variables that can be added to the model, and computer technology to process data coming from sensors and subsequently give a better description about the disease development. Then, by combining the disciplines jointly with an accurate measurement of the variables it is possible to improve the disadvantages of the mathematical and statistical tools and the models so far proposed to describe plant disease epidemic and consequently to obtain a model that better describes the plant disease dynamics.

CONCLUDING REMARKS

The most common mathematical tools used to model plant disease epidemics are: Disease progress curve, LDE, AUDPC and Computer simulations. Nonetheless, there are also other ways to give an evaluation about disease dynamics based on visual, pictorial assessment and statistical tools. The variables used by mathematical tools are chosen by relevance, pathosystem features, and epidemiologist necessities, which according to the model objective, the epidemiologist can chose the mathematical tool which solely or jointly with other different mathematical tools gives a better description of the reality in order to obtain a more accurate evaluation of the plant disease epidemics. The possible combination of the tools here presented can be made by the conjunction of several disciplines like image processing which could serve to obtain a better objective estimation of variables that can feed to the model allowing obtain a better fitness.

ACKNOWLEDGEMENTS

i.) I. Torres-Pacheco acknowledge the financing to the projects Fomix Querétaro 101490 and FIFI 2009.
ii.) R. G. Guevara-González acknowledge the financing to the projects Laboratory Equipment of Biosistemas 2008 and PROMEP/103.5/08/3320.
iii.) The National Council of Science and Technology (CONACyT), scholarship 33780.

REFERENCES

Agrios GN (2005). Plant Pathology. Fifth Edition, Elsevier Academic Press, London, UK.

Allorent D, Willocquet L, Sartorato A, Saravy S (2005). Quantifying and modelling the mobilisation of inoculum from diseases leaves and infected defoliated tissues in epidemics of angular leaf spot of bean. Eur. J. Plant Pathol. 113: 377-394.

Anaya-Lopez JL, Torres-Pacheco I, Gonzalez-Chavira M, Garzon-Tiznado JA, Pons-Hernandez JL, Guevara-Gonzalez RG, Muñoz-Sánchez CJ, Guevara-Olvera L, Rivera-Bustamante RF, Hernandez-Verdugo S (2003). Resistance to Geminivirus Mixed Infections in Mexican Wild Peppers. Hortscience. 38: 251-255.

Blaise P, Dietrich R, Gessler G (1999). Vinemild: an application-oriented model of *plasmora viticola* epidemics on *vitis vinifera*. Acta Hortic. 499: 187-192.
Campbell CL, Madden LV (1990). Introduction to plant disease epidemiology. John Wiley & Sons, NY., USA.
Cooke BM (2006). Disease assessment and yield loss, In: The epidemiology of plant disease. BM Cooke, D Gareth Jones and B Kaye (eds). Springer, Dordrecht, The Netherlands, pp. 43-80.
Calonnec A, Cartolaro P, Naulin JM, Bailey D, Langlais M (2008). A host-pathogen simulation model: powdery mildew of grapevine. Plant pathol. 57: 493-508.
De Wolf ED, Isard SA (2007). Disease cycle approach to plant disease prediction. Annu. Rev. Phytopathol. 45: 203-220.
Nutter Jr. FW (2007). The role of plant disease epidemiology in developing successful integrated disease management programs, In: General concepts in integrated pest and disease management. Ciancio A & Mukerji G (eds) Springer, Dordrecht, The Netherlands, pp. 45-79.
Garret KA, Madden LV, Hughes G, Pfender WF (2004). New applications of statistical tools in plant pathology. Phytopathology, 94: 999-1003.
Godinez-Hernandez Y, Anaya-López JL, Diáz-Plaza R, Gonzalez-Chavira M, Rivera-Bustamante RF, Torres-Pacheco I, Guevara-Gonzalez RG (2001). Characterization of resistance to peper huasteco geminivirus in chili peppers (*Capsicum chinese*) from Yucatan, Mexico. Hortscience. 36: 139-142.
Hardwick NV (2006). Disease Forecasting. In: BM The epidemiology of plant disease. Cooke BM, Gareth Jones D and Kaye B (eds). Springer, Dordrecht, The Netherlands, pp. 239-267.
Hernandez-Verdugo S, Guevara-Gonzalez RG, Rivera-Bustamante RF, Oyama K (1998). Los parientes silvestres del chile (*Capsicum* spp.) como recursos genéticos. Biol. Soc. Bot. Mexico. 62: 171-181.
Holb IJ, Heijne B, Jeger MJ (2003). Summer epidemic of apple scab: The relationship between measurements and their implications for the development of predictive models and threshold levels under different disease control levels. J. Phytopathol. 151: 335-343.
Irfaq M, Ajab M, Hongxiang M, Khattak GSS (2009). Assessment of genes controlling area under disease progress curve (AUDPC) for stripe rust (P. *Striiformis* F. Sp. *Tritici*) in two wheat (*Triticum Aestivum* L.) crosses. Cytol. Genet. 43: 241-252.
Jeger MJ, Viljanen-Rollinson SLH (2001). The use of the area under disease-progress curve (AUDPC) to assess quantitative disease resistance in crop cultivars. Theor. Appl. Genet. 102: 32-40.
Jeger MJ (2004). Analysis of disease progress as a basis for evaluating disease management practices. Annu. Rev. Phytopatol. 42: 61-82.
Kosman E, Levy Y (1994). Fungal foliar plant pathogen epidemics: modelling and qualitative analysis. Plant Pathol. 44: 328-337.
Kranz J, Royle DJ (1978). Perspectives in mathematical modeling of plant diseases epidemics, In: Plant Disease Epidemiology. Scott PR and Bainbridge A (eds). Blackwell Scientific Publications, Oxford, London, Edinburgh, Melbourne. pp. 111-120.
Kranz J, Mogk M, Stumpf A (1973). EPIVEN: ein Simulator fur Apfelschorf. Z Pflanzenkr 80: 181-187.
Kranz J (1988). Measuring plant disease, In: Experimental Techniques in Plant disease Epidemiology. Kranz J, Rotem J (eds). Springer-Verlag, Berlin, pp. 35-50.
Kushalappa AC, Ludwig A (1982). Calculation of apparent infection rate in plant disease: development of a method to correct for host growth. Phytopathology, 72: 1373-1377.
Lannou C, Davallaviellepope C, Goyeau H (1994). Host mixture efficacy in disease control- effects of lesion growth analyzed through computer-simulated epidemics. Plant Pathol. 43: 651-662.
Large EC (1945). Field trials of copper fungicides for the control of potato blight I. Foliage protection and yield. Ann. Appl. Biol. 32: 319-329.
Large EC (1952). The interpretation of progress curves for potato blight and other plants diseases. Plant Pathol. 1: 109-117.
Le May C, Ney B, Lemarchand E, Schoeny A, Tivoli B (2009). Effect of pea plant architecture on spatiotemporal epidemic development of ascochyta blight (*Mycosphaerella pinodes*) in the field. Plant Pathol. 58: 332-343.
Van Maanen A, Xu XM (2003). Modelling plant disease epidemics. European J. Plant Pathol. 109: 669-682.
Madden LV (2006). Botanical epidemiology: some key advances and its continuing role in disease management. Eur. J. Plant pathol. 115: 3-23.
Marta AD, Magarey RD, Orlandini S (2005). Modelling leaf wetness duration and downy mildew simulation on grapevine in Italy. Agric. For. Meteorol. 132: 84-95.
McCoy RE (1976). MYCOS, a computer simulator of Ascochyta blight of Chrysanthemum. Proc. Fla. State. Hortic. Soc. 89: 296-299.
Mersha Z, Hau B (2008). Effect of bean rust (*Uromyces appendiculatus*) epidemics of host dynamics of common beans (*Phaseolus bulgaris*). Plant Pathol. 57: 674-686.
Mikulova K, Bojnanska K, Červená V (2008). Assessment of partial resistance to powdery mildew in hexaploid wheat genotypes. Biologia 63: 477-481.
Mila AL, Carriquiry AL (2004). Bayesian analysis in plant pathology. Phytopathology, 94: 1027-1030.
Nutter FW, Parker SK (1997). Fitting disease progress curves EPIMODEL. In: Exercises in plant disease epidemiology. Francl, LJ and Neher DA (eds). APS Press, St. Paul, MN, USA, pp. 24-28.
Ojiambo PS, Scherm H (2005). Temporal progress of *Septoria* leaf spot on rabbiteye blueberry (*Vaccinum ashei*). Plant Dis. 89: 1090-1096.
Orlandini S, Masseti L, Marta DA (2008). An agrometeorological approach for the simulation of *Plasmora viticola*. Computers and electronics in agriculture, 64: 149-161.
Pandey KK, Pandey PK, Kallo G, Benerje MK (2003). Resistance to early blight of tomato with respect to various parameters of disease epidemics. J. Gen. Plant Pathol. 69: 364-371.
Parker IM, Gilbert GS (2004). The evolutionary ecology of novel plant-pathogen interactions. Annu. Rev. Ecol. Evol. Syst. 35: 675-700.
Rossi V, Giosué S (1999). A dynamic simulation model for powdery mildew epidemics on winter wheat. OEPP/EPPO Bulletin, 33: 389-396.
Royle DJ, Ostry ME (1995). Disease and pest control in the bioenergy crops poplar and willow. Biomass Bioenergy, 9: 69-79.
Rotem J, Eidt J, Wendt U, Kranz J (1988). Relative effects of *Alternaria alternate* and A. *macrospora* on cotton. Plant Pathol. 37: 16-19.
Sanogo S, Yang XB (2004). Overview of selected multivariate statistical methods and their use in phytopathological research. Phytopathology, 94: 1004-1006.
Scherm H, Ngugi HK, Ojiambo PS (2006). Trends in theoretical plant epidemiology. Eur. J. Plant Pathol. 115: 61-73.
Scherm H, Ojiambo PS (2004). Applications of survival analysis in botanical epidemiology. Phytopatology, 94: 1022-1026.
Segarra J, Jeger MJ, Van den Bosch F (2001). Epidemic dynamics and patterns of plant diseases. Phytopathology, 91: 1001-1010.
Schoeny A, Jumel S, Rouault F, May Le C, Tivoli B (2007). Assessment of airborne primary inoculum availability and modelling of disease onset of ascochyta blight in field peas. Eur. J. Plant Pathol. 119: 87-97.
Shaner G, Finney RE (1977). The effect of nitrogen fertilization on the expression of slow-mildewing resistance in Knox wheat. Phytopathology, 67: 1051-1056.
Shrum RD (1975). Simulation of wheat stripe rust (Puccinia Striiformis West.) Using EPIDEMIC, a flexible plant disease simulator. Prog. Rep. Pa. Agric. Exp. Stn. p. 347.
Shtienberg D (2000). Modelling: the basis for rationale disease management. Crop Prot. 19: 747-752.
Strange RN, Scott PR (2005). Plant disease: a threat to global food security. Annu. Rev. Phytopatol. 43: 83-116.
Subba Rao KV, Snow JP, Berggren GT (1989). Effect of growth stage and initial inoculum level on leaf rust development and yield loss caused by Puccinia recondita f. sp. tritici. J. Phytopathol. 27: 200-210.
Sutherst RW (1993). Role of modelling in sustainable pest management. In: Pest Control and Sustainable Agriculture. Corey S, Dall D and Milne W (eds) CSIRO, Australia, pp. 66-71.
Van den Bosch F, Akudibilah G, Seal S, Jeger M (2006). Host resistance and the evolutionary response of plant viruses. J. Ecol. 43: 506-516.
Van der Plank JE (1960). Analysis of epidemics. In: Plant Pathology. Horsfall JG and Cowling EB (eds). Academic Press, New York, USA.

pp. 230-287.
Van der Plank JE (1963). Plant disease: epidemics and control. Academic Press, NY., USA.
Van der plank JE (1982). Host-pathogen interaction in plant disease. Academic Press, New York, USA.
Waggoner PE, Berger RD (1987). Defoliation, disease and growth. Phytopathology, 77: 393-398.
Waggoner PE, Horfsall JG, Lukens RJ (1969). Epimay a simulator of Southern corn leaf blight. Conn. Agric. Exp. Atn. Bull. No. 729, 1972.
Ware JO, Young VH, Janssen G (1932). Cotton wilt studies. III. The behavior of certain cotton varieties grown on soil artificially infested with the cotton wilt organism. University of Arkansas Agricultural Experimental Station Bulletin 269, Fayetteville, AR.
Ware JO, Young VH (1934). Control of cotton and 'rust'. University of Arkansas Agricultural Experimental station Bulletin 308, Fayetteville, AR, p. 23.
Xu X (2006). Modelling and interpreting disease progress in time. In: The epidemiology of plant disease. Cooke BM, Gareth Jones D and Kaye B (eds) Springer, Dordrecht, The Netherlands, pp. 215-238.
Xu XM (1999). Modelling and forecasting epidemics of apple powdery mildew (*Podosphaera leucotricha*). Plant Pathol. 48: 462-471.
Zhang XS, Holt J, Colvin J (2001). Synergism between plant virus: a mathematical analysis of the epidemiological implications. Plant Pathol. 50: 732-746.

Sensors **2012**, *12*, 784-805; doi:10.3390/s120100784

OPEN ACCESS

sensors

ISSN 1424-8220

www.mdpi.com/journal/sensors

Article

Smart Sensor for Real-Time Quantification of Common Symptoms Present in Unhealthy Plants

Luis M. Contreras-Medina [1,2], Roque A. Osornio-Rios [1,*], Irineo Torres-Pacheco [2], Rene de J. Romero-Troncoso [1], Ramon G. Guevara-González [2] and Jesus R. Millan-Almaraz [3]

[1] HSPdigital-CA Mecatrónica, Facultad de Ingeniería, Universidad Autónoma de Querétaro, Campus San Juan del Rio, Rio Moctezuma 249, 76807 San Juan del Rio, Qro., México; E-Mails: mcontreras@hspdigital.org (L.M.C.-M.); troncoso@hspdigital.org (R.J.R.-T.)

[2] Ingeniería de Biosistemas CA, División de Estudios de Posgrado, Facultad de Ingeniería, Universidad Autónoma de Querétaro, Cerro de las Campanas S/N, 76010 Querétaro, Qro., México; E-Mails: irineo.torres@uaq.mx (I.T.-P.); ramon.guevara@uaq.mx (R.G.G.-G.)

[3] Facultad de Ciencias Físico-Matemáticas, Universidad Autónoma de Sinaloa, Av. De las Américas y Blvd., Universitarios, Cd. Universitaria, 80000 Culiacán, Sin., México; E-Mail: jrmillan@uas.edu.mx

* Author to whom correspondence should be addressed; E-Mail: raosornio@hspdigital.org; Tel.: +52-427-274-1244; Fax: +52-427-274-1244.

Received: 16 November 2011; in revised form: 7 January 2012 / Accepted: 10 January 2012 / Published: 11 January 2012

Abstract: Plant responses to physiological function disorders are called symptoms and they are caused principally by pathogens and nutritional deficiencies. Plant symptoms are commonly used as indicators of the health and nutrition status of plants. Nowadays, the most popular method to quantify plant symptoms is based on visual estimations, consisting on evaluations that raters give based on their observation of plant symptoms; however, this method is inaccurate and imprecise because of its obvious subjectivity. Computational Vision has been employed in plant symptom quantification because of its accuracy and precision. Nevertheless, the systems developed so far lack *in-situ*, real-time and multi-symptom analysis. There exist methods to obtain information about the health and nutritional status of plants based on reflectance and chlorophyll fluorescence, but they use expensive equipment and are frequently destructive. Therefore, systems able of quantifying plant symptoms overcoming the aforementioned disadvantages that can serve as indicators of health and nutrition in plants are desirable. This paper reports an FPGA-based smart sensor able to perform non-destructive, real-time and *in-situ* analysis of leaf images to

quantify multiple symptoms presented by diseased and malnourished plants; this system can serve as indicator of the health and nutrition in plants. The effectiveness of the proposed smart-sensor was successfully tested by analyzing diseased and malnourished plants.

Keywords: smart sensors; symptoms in plants; computer vision; image processing; plant diseases; FPGA

1. Introduction

In [1,2], symptoms in plants are defined as responses to alterations of their physiological functions and metabolic disorders that are caused principally by infections or nutritional deficiencies. The symptoms can be frequently visualized in leaves, stem and roots, so that precise assessments of plant symptoms can be used as indirect indicators for monitoring disease and malnutrition in plants, estimating yield loss and breeding for resistance against plant diseases [3].

In plant pathology, a pathogen is defined as the agent that causes the disease and a diseased plant is described as visible and invisible responses (symptoms) of cells and tissues to pathogens or environmental factors that can produce alterations in the morphology, physiological functions and integrity of the plant that may cause partial or complete damage [1]. In [1,4] it is mentioned that plant diseases cause up to 14.1% of the worldwide agricultural production losses; this fact results in environmental, economical and health problems. Therefore, disease assessment is critical to various aspect of the study of plant pathogens [5]. Good quality disease assessment data is needed to make appropriate decisions in disease management, to compare treatments, monitor plant diseases and gauge cultivar resistance in plant breeding [5,6].

The study of how the plants obtain and use mineral nutrients is called mineral nutrition; this is central research in modern agriculture because high agricultural yields strongly depend on fertilization with mineral nutrients and before saturation the yields of most crops increase proportionally with the amount of fertilizer that the plants absorb; therefore, mineral nutrition research is necessary to meet the incremental worldwide demand for food [2]. Nutrient deficiency symptoms are the expressions of metabolic disorders resulting from insufficient supply of essential elements; in consequence, precise assessments of these symptoms can be used as reliable nutritional deficiency indicators in order to compare treatments and for fertilizer management.

Nowadays researchers have developed techniques to measure the symptoms presented in plants, and the visual estimation (VE), which implies the use of trained personnel that evaluate the health and nutrition in plants based on visual symptoms, is the most popular [7]. According to Bock *et al*. [7] VE can be used as disease assessment method, as can be seen in [8,9], where individual plants were rated for symptoms using a four-level and nine-level based disease severity index, respectively, in order to know the resistance of common bean to bean dwarf-mosaic virus and resistance of pepper to geminiviruses. Nevertheless, VE is not able to give quantitative evaluations because it introduces subjectivity, inaccuracy and imprecision [3,5,10]. To overcome these drawbacks, computer vision (CV), which is based on Image Analysis (IA), can be used as a disease assessment method [7]; CV is based on plant symptom quantification and compared to VE, offers higher precision, accuracy and

reproducibility assessments, however, according to Bock *et al*. [5], it is incapable of distinguishing particular symptoms of a diseased plant when the plant is affected by various diseases. Martin and Rybicki [11] realized a comparative between commercial CV-based system and custom CV-based system evaluations of chlorotic lesion areas occurring on leaves of *Zea mays* provoked by maize streak virus (MSV). In [12] a CV-based system was used to classify visual symptoms caused by angular bacteria, *Ascochyta blight*, and green stink bug through analysis of coloured images and by using techniques such as co-occurrence matrix, fractal dimension, lacunarity and a support vector machine (SVM). Camargo and Smith [13] proposed a CV-based methodology to identify disease symptoms of photographed leaves based on H, I3a and I3b colour transformation and local maximums localized in the histogram. Wijekoon *et al*. [14] realize a quantification of fungal infections on leaves of *N. benthamiana* infected with anthracnose pathogen, using diagrams of different diseases proposed by James [15], the images were captured using a flat scanner and camera to later being analyzed in the laboratory using CV. Al-Hiary *et al*. [16], proposed an CV-based algorithm to classify diseased leaves affected by different pathogens; the algorithm is based on the computation of texture statistics and neural networks to accomplish the classification; the algorithm detects and classifies the examined plant diseases with a precision between of 83% and 94%. Even thought the aforementioned CV-based systems give precise and accurate assessments, they are time-consuming, not-easy to use and frequently analyze just one specific plant symptom.

Optically-based methods commonly used to detect symptoms provoked by viral, bacterial and fungal disease are thermography, hyperspectral reflectance, chlorophyll fluorescence-based techniques, nuclear magnetic resonance (NMR) spectroscopy and X-ray imaging [17]. According to Chaerle *et al*. [18], thermography allows one to detect symptoms in plants before they can be detected by an evaluator, so that, local temperature changes due to plant defence mechanism against disease can be monitored employing this method [17]. The hyperspectral reflectance technique allows obtaining a signature at varying wavelengths in the visible, near-infrared, and shortwave-infrared range of the electromagnetic spectrum. Delaieaux *et al*. [19] used hyperspectral reflectance to detect apple scab caused by *Venturia inaequalis*; to accomplish that, it was necessary to select the wavelengths best suited for classifying infected leaves from those of the healthy leaves. Chlorophyll fluorescence-based techniques involve fluorescence spectroscopy and fluorescence imaging; both can be used to monitor nutrient deficiencies, environmental-condition-based stress levels and diseases in plants [17,18]. Belasque *et al*. [20] employed fluorescence spectroscopy to detect stress caused by citrus canker and mechanical injury and Bravo *et al*. [21] utilized fluorescence imaging for detecting yellow rust in winter wheat. Similarly, nuclear magnetic resonance and X-ray imaging techniques can be used for detecting infections, different types of stress and health conditions in plants [17,22]. Goodman *et al*. [23] used NMR microscopic imaging for identification of the fungal pathogen *Botrytis cinerea* in red raspberry and Navakar *et al*. [24] applied X-ray imaging to identify fungal infections in wheat. Those optical-based techniques present the disadvantages of needing expensive equipment, trained personnel and time-consuming.

Volatile organic compounds (VOC) released by plants are influenced by physico-chemical factors (humidity, temperature, light, soil condition, growth and developmental stage) that affect the physiological condition of the plant, thereby influencing the VOC profile [17]. Abiotic and biotic stresses can provoke changes in the VOC profiles of the plants; this can be utilized as an indirect indicator for

plant disease assessment. The two common methods for assessing the profile of volatile metabolites released by plants are gas chromatography (GC)-based and electronic-nose-based system techniques. Laothawornkitkul *et al.* [25] evaluated the potential of plant volatile signatures for pest and disease monitoring in cucumber, pepper and tomato plants. Liu *et al*. [26] inoculated potato tubers with *Phytophthora infestans, Pythium ultimum*, or *Botrytis cinerea* and analyzed the resulting VOC profiles using GC. The VOC-based systems developed so far for monitoring plant disease are not able to achieve *in-situ* and time-consuming monitoring and also present the disadvantage of the natural variation in the VOC profile within plant species [17] and expensiveness.

The most popular molecular techniques for plant disease assessment are Polymerase Chain Reaction (PCR) and Enzyme-Linked ImmunoSorbent Assay (ELISA); they have the robustness and capacity to provide plant disease assessments by quantifying the amount of virus, bacteria and fungi in plant tissue as can be seen in [27], where the PCR technique was used to quantify the degree of colonization of English oak (*Quercus robur L.*) leaves by the bacteria *Erwinia*; in the same way, Gutiérrez-Aguirre *et al*. [28] use PCR and ELISA techniques to detect cucumber mosaic virus in tomato plants. Although the molecular techniques offer high precision and accuracy, they present the disadvantage of being destructive, time-consuming and labor-intensive methods; also, they require an elaborate procedure to obtain reliable and accurate results [17].

The aforementioned techniques and works are used for monitoring different kinds of plant symptoms and they can be used as plant disease assessment; in the case of the molecular methods, these assessments are obtained by quantifying directly the amount of pathogens. CV is based on IA and it is a technique that tries to solve the drawbacks of the aforementioned methods; however, greater automation is needed to make this practical [7]. Bock *et al*. [5] mention that where a large number of samples need to be assessed, automation is particularly advantageous to conserve time while ensuring accuracy and precision of measurement. Some commercial and custom image analysis have automated functions; yet, these systems have not been widely applied in measuring plant disease, perhaps due to their complexity and/or expense [5,11,29]. Therefore, a smart-sensors able to accomplish precise and accurate symptoms quantification that could serve to assess diseases and malnutrition in plants and incorporate characteristics such as: low-cost, real-time, non-destructive, and friendly using are desirable.

Frank [30] defined a smart sensor as a sensor that provides functions beyond those necessary for generating a correct interpretation of a sensed or controlled quantity, based on this; smart sensors must incorporate processing, communication and integration according to Rivera *et al*. [31]. Field Programmable Gate Arrays (FPGAs) are devices that have been gaining popularity principally because of their high-speed processing, high reconfigurability and System on a Chip (SoC) solutions [32]; these characteristics permit that the FPGAs be used in applications where high-performance computational capabilities are needed. In CV, the FPGA high-speed processing characteristic has been exploited to develop vision systems to classify crop products [33]. In biology Millan-Almaraz *et al.* [34] used an FPGA-based smart sensor to estimate the plant-transpiration dynamics based on five primary sensors that measure air and leaf temperature, air relative humidity, plant out relative humidity and ambient light.

Because of the aforementioned reasons, this work proposes a low-cost and FPGA-based smart sensor for the quantification of common symptoms presented in diseased and malnourished plants by using CV-based, real-time, non-destructive and *in-situ* analysis of plant-leaf images. The proposed system employs a camera (1/3-inch Megapixel CMOS Active-Pixel Digital Image Sensor MT9M011

manufactured by Micron) [35] as primary sensor and an Altera DE2 development kit containing an EP2C35F672C6N Cyclone II FPGA as processing element or Hardware Signal Processing (HSP) unit. The smart sensor uses several novel colour-based methodologies that make use of morphological image processing and different colour components; these methodologies permit one to choose the appropriate colour component according to the symptom under analysis, always trying to diminish the noise introduced by other symptoms (not under analysis at that moment) that are present in a sample. In this work, the studied symptoms are: chlorosis, leaf deformation, white spots, necrosis, and mosaics because they are common symptoms present in diseased and malnourished plants. The smart-sensor functionality was successfully tested by analyzing quantitatively the aforementioned symptoms present in diseased bean and pepper plants, and malnourished pumpkin plants; the system gives numerical values, by using CV, that objectively describe the degree of the symptom present in the plant leaves. Because the plant symptoms are responses to the alteration of plant physiological functions provoked principally by infections or nutritional deficiencies, the system could be employed, in future works, as a powerful tool to give quantitative descriptions of plant symptoms development; this quantitative descriptions could serve to assess disease and malnourishment in plants.

2. Symptoms in Plants

Symptoms in plants are commonly present in diseased and malnourished plants, and are caused principally by pathogens and mineral deficiencies. Five common symptoms in plants are: chlorosis, leaf deformation, white spots, necrosis, and mosaics. In this work, bean plants (*Phaseolus vulgaris*), pepper plants (*Capsicum annum*), and pumpkin plants (*Curcubita pepo*) were analyzed. Bean plants were infected with the common bean mosaic virus; pepper plants were infected by the bacteria *Xanthomonas campestris* and pumpkin plants were affected just by nutritional deficiencies.

2.1. Chlorosis

Chlorosis is defined as a yellowing of normally green leaf tissue that, in the case of plant diseases, could be due to chlorophyll destruction or failure in chlorophyll formation [1]. It could be caused by a variety of viral, bacterial and fungal pathogens. In the case of nutritional deficiencies, chlorosis is the most common symptom and it can be caused by several reasons, one of them is the lack of minerals that serve as constituent of many plant cells, coenzymes and vitamins and as essential components in the metabolism; these minerals are nitrogen and sulphur; other reason is due to the deficiencies of minerals such as potassium, calcium, and magnesium present within the plants as cations and ions playing an important role in the photosynthetic process [2]. Chlorosis symptoms can be localized or generalized, meaning that chlorosis can affect only certain leaf regions or the complete leaf. An ideal example of healthy leaf and localized and generalized chlorotic leaf can be seen in Figure 1, which shows schematized leaves with idealized symptoms. Figure 1(a) shows a healthy pumpkin leaf that has an idealized homogeneous green colour tissue; aside, Figure 1(b) shows a pumpkin leaf with idealized localized chlorosis; the leaf presents a section with homogeneous green colour tissue and the missing leaf section are covered by a yellowing colour. Figure 1(c) shows a pumpkin leaf with an idealized generalized chlorosis, the leaf presents a yellowing colour completely covering the leaf tissue.

Figure 1. (**a**) Pumpkin leaf with healthy green colour. (**b**) Pumpkin leaf with localized chlorosis. (**c**) Pumpkin leaf with generalized chlorosis.

2.2. Necrosis

Death in plant tissue in a localized area is called necrosis and commonly results in brown or black lesions often preceded by yellowing (chlorosis, or a breakdown in chlorophyll). This symptom can be provoked by plant pathogens or deficiencies of minerals such as boron, potassium, calcium, chlorine and sodium [2,36]. Figure 2 shows three schematized images that present how this symptom manifests over the plant leaves, Figure 2(a) presents a healthy pumpkin leaf with idealized green colour tissue, Figure 2(b) shows an unhealthy pumpkin leaf with idealized necrotic symptoms, and Figure 2(c) presents unhealthy pumpkin leaf with idealized necrotic and generalized chlorotic symptom. These three images show examples of how necrosis symptoms could appear in healthy and chlorotic leaves.

Figure 2. (**a**) Pumpkin leaf with homogeneous green colour. (**b**) Non-chlorotic pumpkin leaf with necrotic areas. (**c**) Chlorotic pumpkin leaf with necrotic areas.

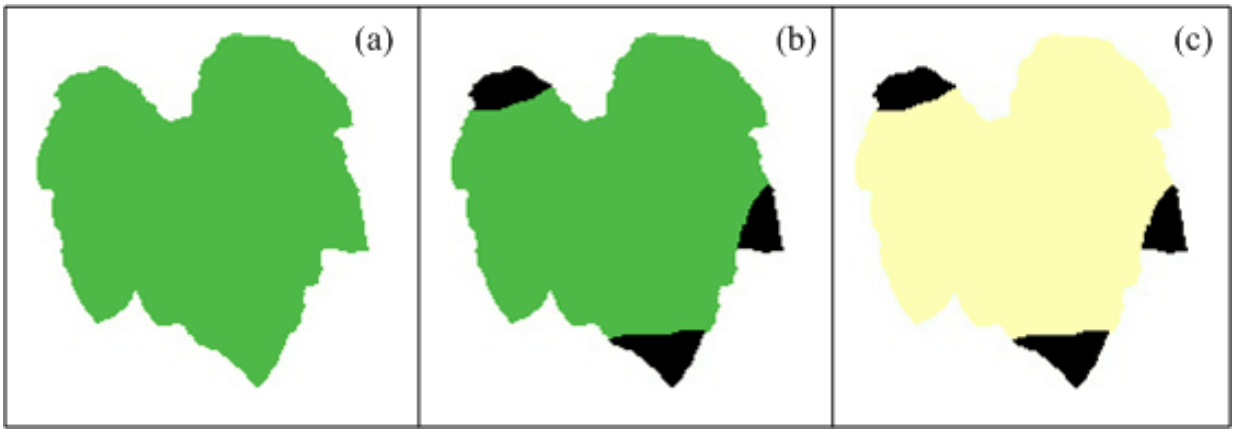

2.3. Leaf Deformation

Changes in the lamina of the host leaf result in areas that are twisted, deformed, or distorted; these deformations can be described as bubbles, rugosity or curls [36]; they can be caused by plant pathogens or mineral nutrition deficiencies, principally by absence of potassium [2]; these kinds of deformations imply a change in the normal shape of the leaf edge. Figure 3(a) presents the outline of a schematized

healthy pepper leaf shape, Figure 3(b,c) shows the contour of schematized non-healthy leaves that present a deformation due to the presence of bubbles and roughness. The three figures show visually the presence of the leaf deformation symptom. It is clear how the healthy leaf presents a more symmetric shape than the other two leaves, these contours can be measured by obtaining leaf geometric characteristics.

Figure 3. (**a**) Contour of healthy pepper leaf. (**b**) Contour of pepper leaf with low deformation. (**c**) Contour of pepper leaf with severe deformation.

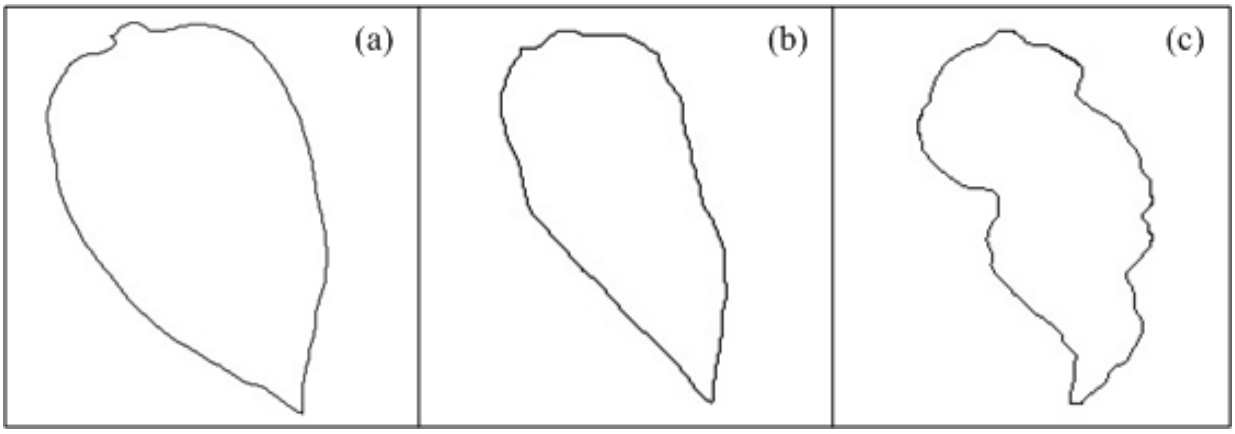

2.4. White Spots

White spots are provoked when plant pathogens or the deficiency of minerals involved in chlorophyll biosynthesis such as zinc, affect the photosynthesis and respiration functions; this leads to inability of the plant to respond to the pathogen [1,2]. Figure 4(a) presents a schematized healthy bean leaf with idealized green colour tissue and Figure 4(b,c) shows schematized unhealthy bean leaves with idealized white-spots symptom; as can be seen, the presence of white spots is clear in unhealthy leaf comparing with a healthy leaf. White spots can affect both chlorotic and non-chlorotic leaves.

Figure 4. (**a**) Healthy bean leaf with green colour tissue. (**b**) Unhealthy bean leaf with low density of white-spot symptom. (**c**) Unhealthy bean leaf with high density of white-spot symptom.

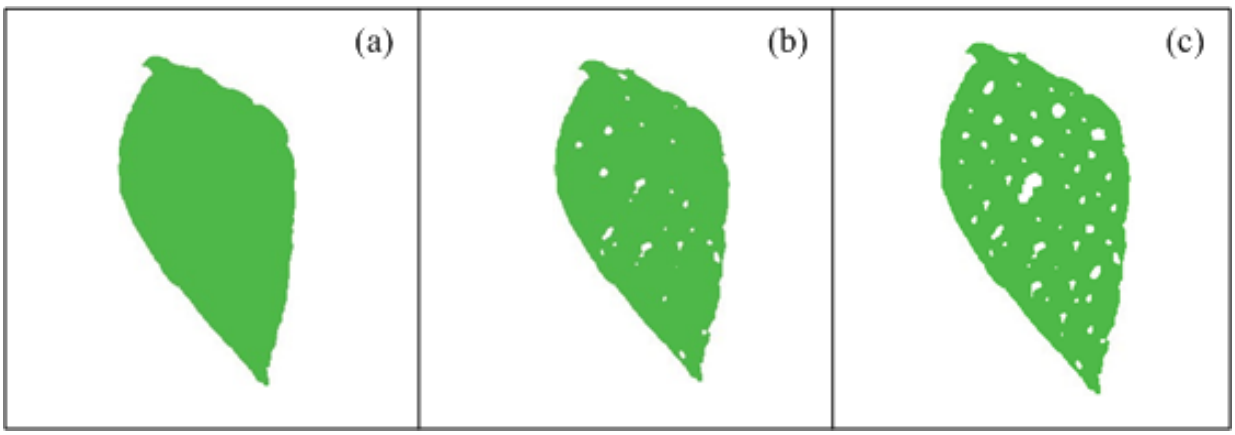

2.5. Mosaics

Mosaics are characterized by light-green, yellow, or white-areas intermingled with the normal green of the leaves or of lighter-coloured areas intermingled with areas of normal colour on flowers or fruits; this symptom is mainly provoked by viral pathogens [1]. Depending on the intensity or pattern of discolorations, mosaic-type symptoms may be variously described as mottling, steaks, ring patterns, line patterns, veinclearing, veinbanding, or chlorotic spotting [1]. Figure 5 shows three idealized veinclearing mosaic-type densities in leaves that are characterized by a clearing of the venation leaf. Figure 5(a) shows a venation diagram of schematized healthy bean leaf. Figure 5(b,c) presents a venation diagram of schematized unhealthy bean leaf with low-density and high-density mosaic symptom (veinclearing), respectively. It can be seen from the comparison between healthy and unhealthy leaves, how leaf venation becomes clearer in unhealthy leaves when it has the mosaic symptom.

Figure 5. (**a**) Healthy bean leaf without mosaic symptom. (**b**) Unhealthy bean leaf with low-density mosaic symptom. (**c**) Unhealthy bean leaf with high-density mosaic symptom.

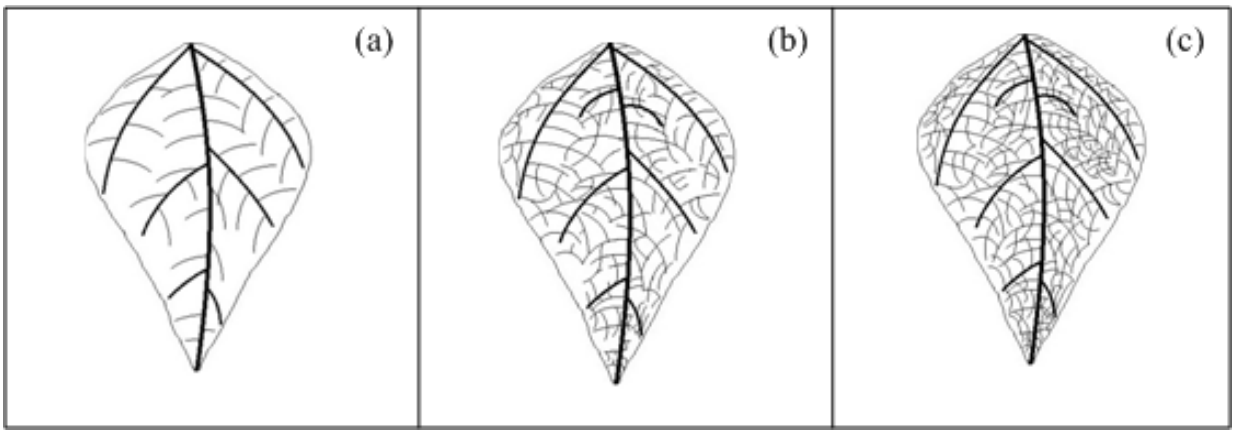

3. Proposed Image Processing Algorithms

3.1. Chlorotic-Area Algorithm

As aforementioned, a chlorotic area can be defined as a yellowing of normally green-leaf tissue; therefore, a good identification of chlorotic areas is done by using the yellow component of the image, resulting from a combination of red and green colormaps (Figure 6(a)). An algorithm based on colour analysis to quantify chlorotic level is proposed; it allows knowing if the chlorosis is generalized or localized. The algorithm can be divided in two stages, the first stage being in charge of calculating the yellow component of the leaf using the Equation (1); *Red* and *Green* correspond to red and green components of the original image, respectively. Then the leaf is divided into four sections as shown in Figure 6(b) using the centroid coordinates of the image *Cx* and *Cy*, depicted by Equation (2) [37] with *N* and *M* being the image row and column, respectively. The second stage is in charge of calculating the average yellow-level values of the four sections of the leaf by using Equation (3). *Yellow*(*i,j*) is the intensity level of the yellow component at the corresponding *(i,j)* index, L_k is the number of pixels of the k section (where k = 1,2,3,4), and i and j are the line and column index, respectively. R_k is the average yellow pixel value of k section; these values permit to calculate the modulus of a vector

formed by these four average yellow level values R_n as shown in Equation (4), and the modulus of the differential yellow level values vector R_{diff} formed by subtracting the yellow level average value of each region from the other ones as shown in Equation (5); R_n allow to quantitatively know how chlorotic is the leaf as a whole, whereas R_{diff} permits to determine whether the chlorosis is localized or generalized:

$$Yellow = 0.5Red + 0.5Green \tag{1}$$

$$Cx = \frac{\sum_{i=1}^{N}\sum_{j=1}^{M} i \cdot Yellow(i,j)}{\sum_{i=1}^{N}\sum_{j=1}^{M} Yellow(i,j)}, \; Cy = \frac{\sum_{i=1}^{N}\sum_{j=1}^{M} j \cdot Yellow(i,j)}{\sum_{i=1}^{N}\sum_{j=1}^{M} Yellow(i,j)} \tag{2}$$

$$R_K = \left\{ \frac{1}{L_K} \sum_{i=1}^{N}\sum_{j=1}^{M} Yellow(i,j) \,|\, Yellow(i,j) \,\varepsilon\, R_k \right\} \tag{3}$$

$$R_n = \left\| [R_1; R_2; R_3; R_4] \right\| \tag{4}$$

$$R_{diff} = \left\| [R_1 - R_2; R_1 - R_3; R_1 - R_4; R_2 - R_3; R_2 - R_4; R_3 - R_4] \right\| \tag{5}$$

Figure 6. (**a**) Yellow component of healthy pepper leaf. (**b**) Sectioned healthy pepper leaf in four regions (R_1, R_2, R_3, R_4).

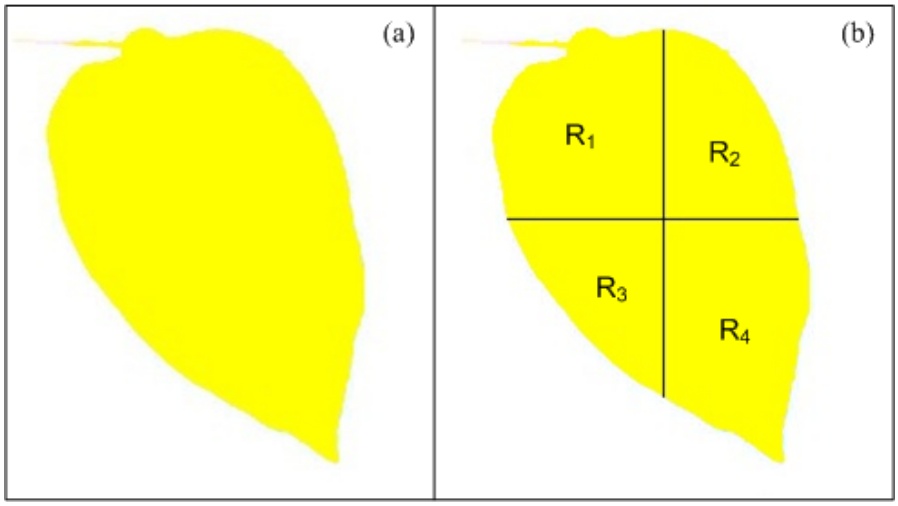

3.2. Necrotic-Area Algorithm

To quantify the necrotic area in leaves, a colour-based algorithm using the green and blue components is proposed. Figure 7(a) shows a bean leaf in RGB (Red, Green, Blue) format and its corresponding blue and green components are shown in Figure 7(b,c), respectively. Green component is used to isolate the necrotic area of the leaf (A_{np}) from the total leaf and background because it offers a better contrast between necrotic and non-necrotic regions. The blue component is utilized to calculate the total leaf area A_T because it is less sensitive to other symptoms such as chlorosis and it offers a better differentiation of leaf from the background. Before applying an image binarization, a median filter based on morphological opening γ_B is accomplished; this operation is based on Equation (6) which in turn is based on morphological dilation δ_B and erosion ε_B (Equations (7) and (8)) [38]; this

permits a better differentiation between necrotic and non-necrotic zones. Once quantified the necrotic and total leaf area in pixels as shown in Figure 7(d,e), necrotic area assessment A_n is estimated by using the Equation (9). A_n is the percentage of necrotic area covering the leaf relative to total leaf area:

$$\gamma_B = A \circ B = (A \Theta B) \oplus B \tag{6}$$

$$\delta_B = A \oplus B = \{z \mid [(C)_z \cap A] \subseteq A\} \tag{7}$$

$$\varepsilon_B = A \Theta B = \{z \mid (B)_z \subseteq A\} \tag{8}$$

$$A_n = \frac{A_{np}}{A_T} * 100\% \tag{9}$$

where A is the image and B is the structuring element. In Equation (7) z represents the set of displacements such that C (which is B reflected) and A overlap by at least one element and in Equation (8) z represents all points such that B translated in A is contained in A.

Figure 7. Bean leaves with necrosis. (**a**) Necrotic bean leaf in RGB format. (**b**) Green component of the necrotic bean leaf. (**c**) Blue component of the necrotic bean leaf. (**d**) Necrotic leaf area segmentation. (**e**) Total leaf area segmentation.

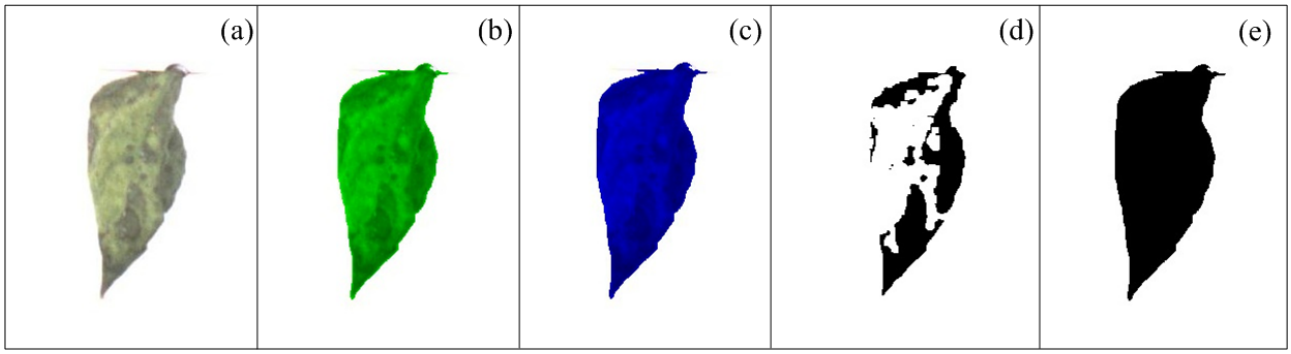

3.3. Leaf-Deformation Algorithm

The methodology proposed for leaf-deformation assessment is a colour-based algorithm that uses, from the original image (Figure 8(a)), the blue component (Figure 8(b)) because it is less sensitive to other symptoms such as chlorosis that can provoke errors in the quantifications. Nowadays, there are several techniques to determine the geometric properties of an object; one of the most employed is the sphericity index [37]. This method gives a quantitative measurement about the sphericity of an object. To calculate this index it is necessary to obtain the area (A) and the perimeter (p) of the object (leaf) that, in the case of image processing, are calculated in pixels; Figure 8(c,d) shows the segmentation of the area and perimeter of the leaf respectively. When A and p are obtained, the sphericity index I is calculated using Equation (10) [37]; after this, I values of healthy and unhealthy (deformed) leaf are compared to quantitatively determine how the unhealthy leaf is deformed taking as reference the healthy leaf. In this work, I is also called deformation index because it is the variable that is measured to quantify the leaf deformation:

$$I = \frac{p^2}{4\pi A} \tag{10}$$

Figure 8. (**a**) Original pepper leaf. (**b**) Blue component of pepper leaf. (**c**) Leaf area segmentation (**d**) Leaf perimeter segmentation.

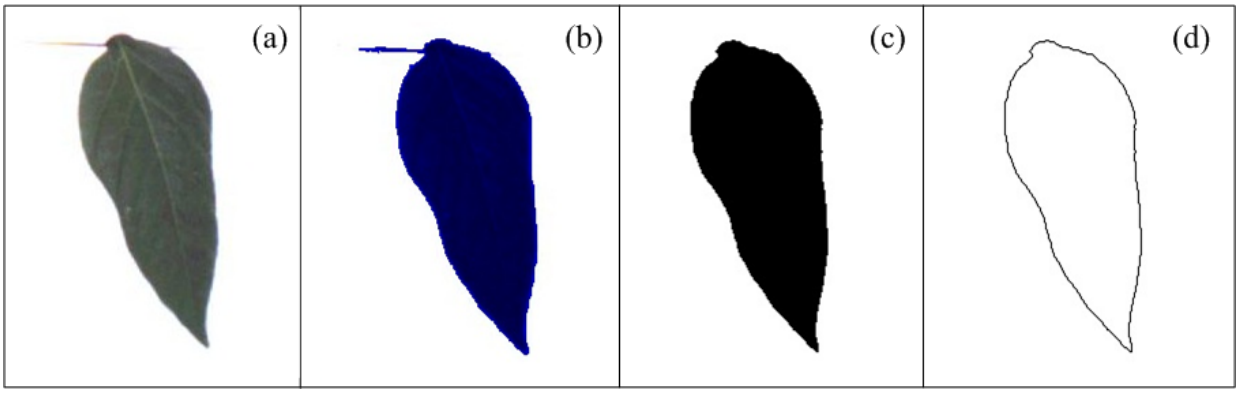

3.4. White-Spots Algorithm

The white-spots algorithm estimates the area occupied by white spots in leaves. They are present in the three components (Red, Green and Blue). Nonetheless, a colour-based algorithm is proposed using the blue component again because of the aforementioned reasons; Figure 9(a) shows a bean leaf in RGB format affected with white spots and Figure 9(b) shows the blue component of the original image.

Figure 9. (**a**) Bean leaf with white spots. (**b**) Blue component of bean leaf with white spots. (**c**) Background and white spots segmentation. (**d**) Segmentation of leaf area without white spots.

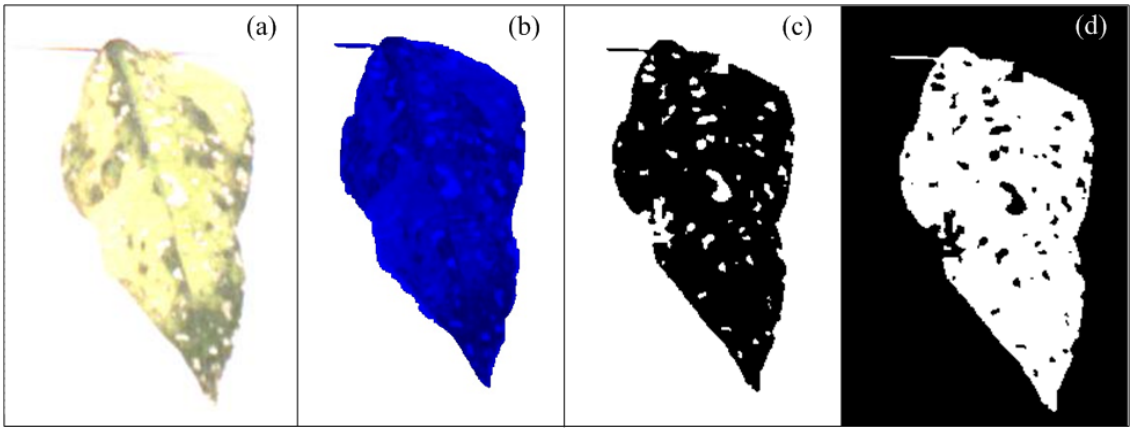

First, the blue component is binarized with a predefined threshold level to isolate the leaf area from background (Figure 9(c)); this threshold level in this case was fixed but can be varied by the user according to the light conditions. After the binarization process, the number of pixels in the background is calculated by using the connectivity algorithm, later, the complement of the image is obtained and leaf area without white spots is isolated and quantified by using the connectivity algorithm (Figure 9(d)). Once we have the leaf area without white spots and the background area it is possible to obtain the area occupied by white spots A_{ws} using Equation (11), where A_{BG} is background area and A_{TL} is leaf area without the white spots. The percentage of leaf area occupied by white spots A_{pws} is estimated using Equation (12). The constant value A_{ZS} represents the size of the image in pixels:

$$A_{ws} = A_{ZS} - A_{BG} - A_{TL} \tag{11}$$

$$A_{pws} = \frac{A_{ws}}{(A_{TL} + A_{ws})} * 100\% \tag{12}$$

3.5. Mosaic Algorithm

The mosaic symptom is characterized by the presence of a high number of leaf venations in diseased leaves. This symptom is not clear when it is visualized under natural conditions, it is better detected under high-intensity and back-light conditions, as can be seen in Figure 10(a); this methodology improves the leaf venation visibility, and consequently, the mosaic symptoms can be better identified and quantified. Because of the aforementioned reasons, the blue component was used to quantify mosaic symptoms. To perform a better mosaic quantification, the plant leaf is photographed under high-intensity and back-light conditions using flash LEDs and a panel LED as can be seen in the picture of the experimental setup shown in Figure 11(b); the flash LED and LEDs of the panel LED are turned on by the user before that the plant leaf be photographed; this creates better light conditions to detect the mosaic symptoms on leaves. After the leaf has been photographed, the next step is to process the image to improve its quality in order to obtain a better differentiation between leaf venation and the leaf tissue. First, the blue component is obtained from the original image and later the gray values of blue component were distributed in the used total gray scale range (from 0 to 1,023) to enhance its contrast (Figure 10(b)), later top-hat Thw_B and bottom-hat Thb_B transformations are sequentially applied in already contrasted image to continue enhance its contrast according to Equations (13) and (14), and as the Figure 10(c) shows, this transformation is based on morphological opening and closing φ_B, respectively, as can be seen in Equations (6) and (15) [38,39]. Finally, Canny algorithm jointly with binarization operation is applied to detect the edges of leaf venation [40] (Figure 10(d)). The quantification of the detected leaf venation is done by estimating the area covered by leaf-venation edges taking as reference the total leaf image according to Equation (16).

Figure 10. (**a**) Bean leaf in RGB format. (**b**) Blue component of bean leaf with histogram equalization. (**c**) Blue component of bean leaf with contrast enhancement after applying the top-hat and bottom-hat algorithms. (**d**) Identification of bean-leaf venation.

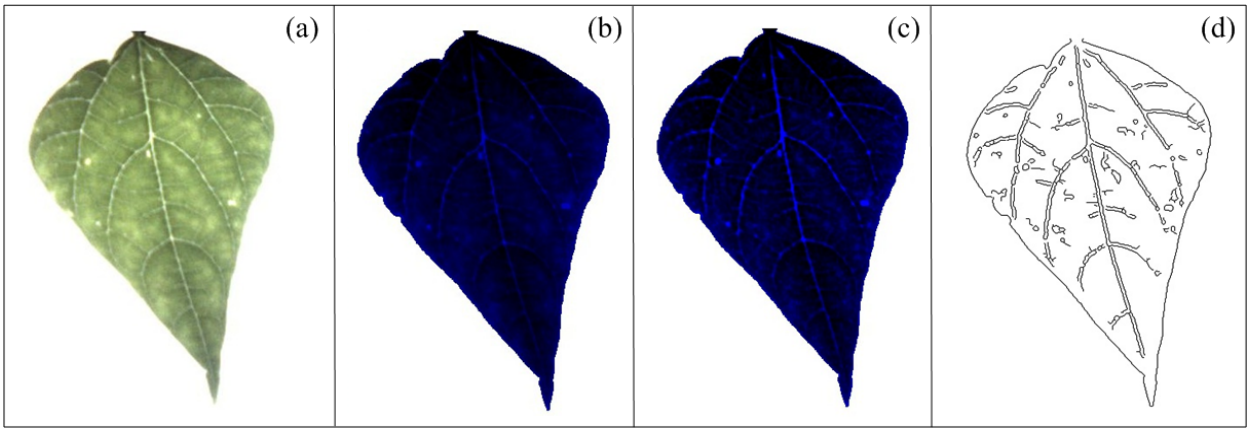

$$Thw_B = A - \gamma_B(A) \tag{13}$$

$$Thb_B = \varphi_B(A) - A \tag{14}$$

$$\varphi_B = A \bullet B = (A \oplus B)\Theta B \tag{15}$$

$$A_{mosaic} = \frac{A_{map}}{A_{TL}} * 100\% \tag{16}$$

where B is the structural element and A is the blue component image. A_{map} is the leaf area covered with the mosaic edges, A_{TL} is the total leaf area and A_{mosaic} is the percentage of the area covered by mosaic edges.

4. Smart Sensor

The smart sensor consists of four major components: a camera as primary sensor, a Hardware Signal Processing (HSP) unit as processing element, output peripherals (LCD display panel or monitor, and an optional PC), high intensity LEDs that serve as flash lights and light sources to generate back-light conditions and three panels that are employed depending on the symptom under analysis (Figure 11). The methodology of smart-sensing cycle could be divided into three stages. In the first stage, leaf-image acquisition is done using a 1/3-inch and 1.3-megapixel CMOS active-pixel digital image sensor MT9M011 manufactured by micron [19], after this, the captured image is sent to the HSP unit, which is an Altera DE2 development kit containing an EP2C35F672C6N Cyclone II FPGA, Synchronous dynamic random-access memory (SDRAM) and peripheral ports [41].

Figure 11. Smart-sensing methodology. (**a**) Block diagram of the proposed system. (**b**) Experimental setup.

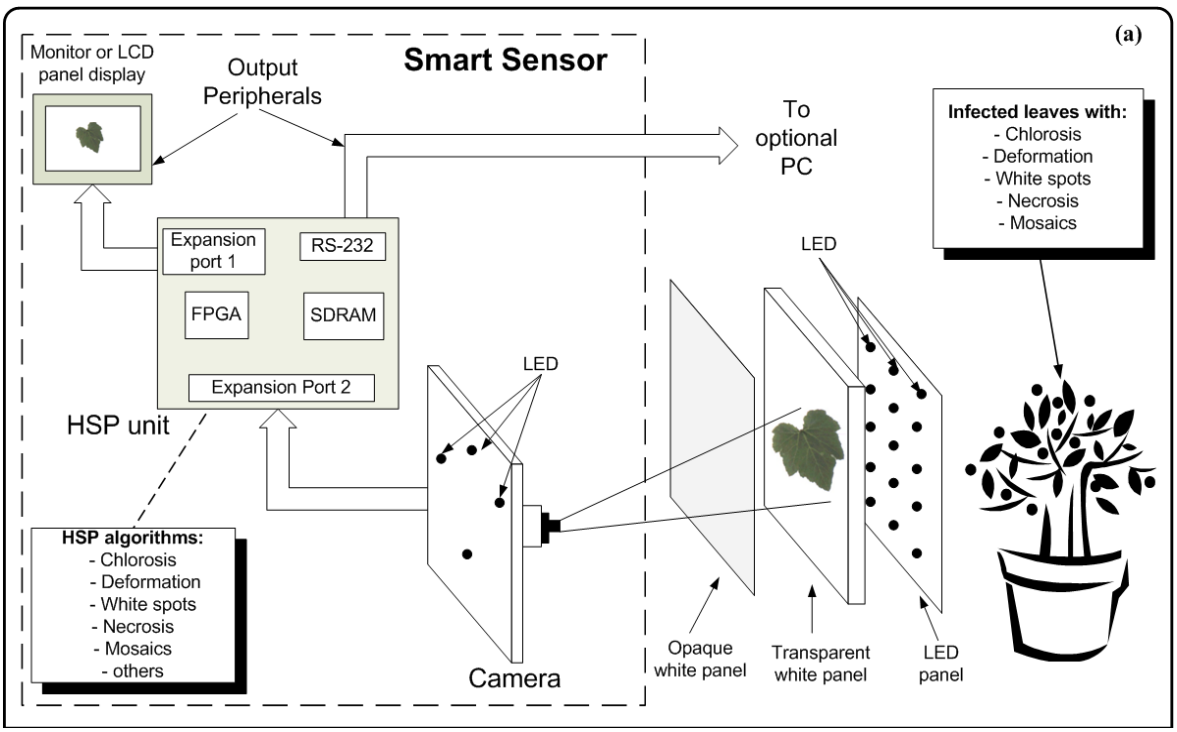

Figure 11. *Cont.*

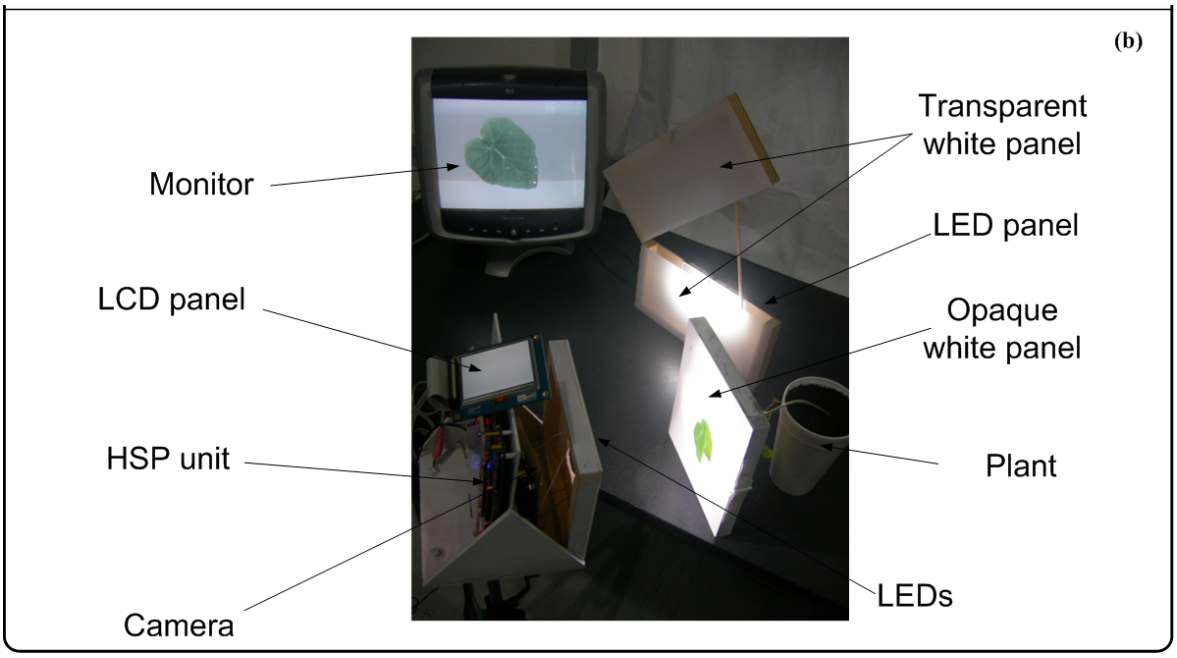

The second stage is where the image is processed to quantify chlorotic area, deformation, white-spots area, necrotic area, and mosaic symptoms. Finally, the third stage displays the original or processed image through an LCD panel showing the results of the symptom quantification. Optionally, the image can be sent to the PC through an RS232 port to create a database in order to perform further analysis (Figure 11(a)). The three panels consist of an opaque white panel used to quantify chlorosis, leaf deformation, white spots, and necrosis; and the transparent-white and LED panel are used jointly to quantify the mosaic symptoms. The LED panel generates the high-intensity back-light that, jointly with the transparent white panel, allows that light passes through the leaf; this amplifies the visibility of the leaf venation. Figure 11(b) shows the experimental setup where all the parts can be identified in the block diagram of the proposed system. The smart sensor is mounted on a mobile mechanism that permits moving the system in order to perform *in-situ* assessments.

HSP Unit

The HSP unit is in charge of controlling the dataflow coming from the camera and performing the image processing to quantify the symptoms. The HSP unit is composed principally by four parts: FPGA, an 8M-byte SDRAM, peripheral ports (RS232) and expansion ports. The FPGA is the key component of HSP unit and it is where the image is processed and the controllers are implemented as shown in Figure 12. The controllers and processing blocks consist of Intellectual Property (IP) cores that control the devices connected to FPGA and process the image; these blocks work at different clock frequencies in order to avoid data-transfer bottlenecks between camera, SDRAM, processing blocks and peripheral ports and to accomplish the specification of the peripheral devices such as the LCD panel that operates using a 33.2-MHz clock. The SDRAM interfacing works at 100 MHz, whereas the camera interface clock is set to 25 MHz. The processing blocks, working with a 25 MHz clock, comprise five modules in charge of quantifying the symptoms by giving the values of absolute chlorosis level intensity R_n; the differences between the four sections in the leaf R_{diff}; the deformation

index I; the percentage of necrotic leaf area A_n; the leaf area percentage with white spots A_{ws}; and the percentage of leaf area affected by mosaic symptom on the leaf A_{mosaic}.

Figure 12. HSP-unit hardware structure.

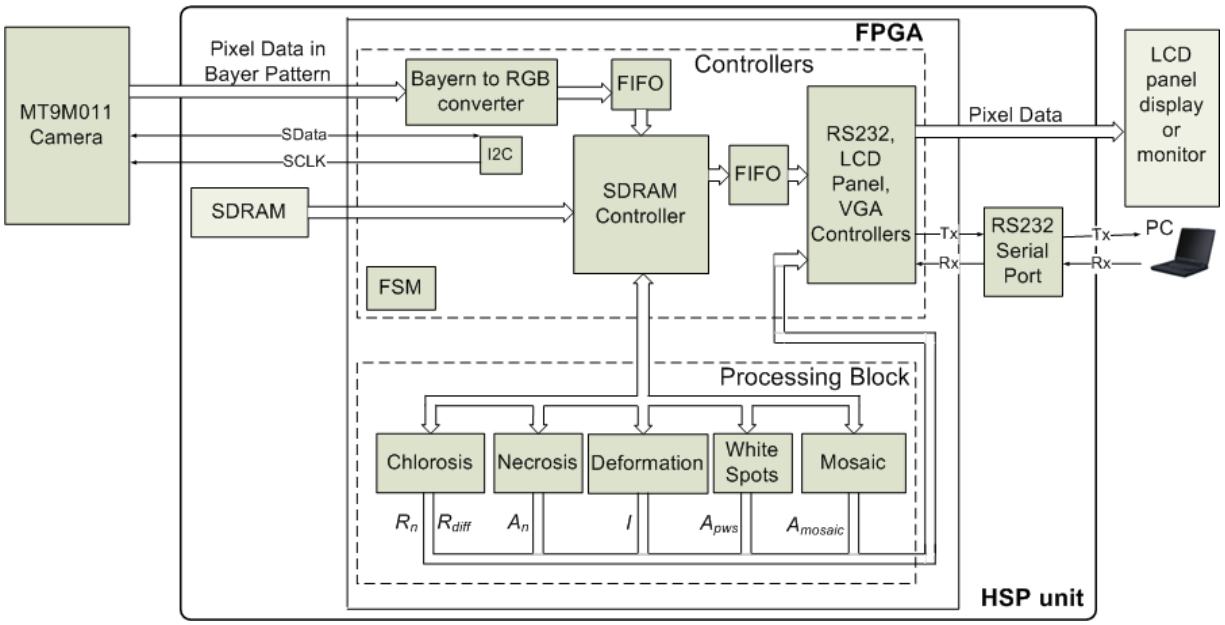

5. Results and Discussion

5.1. Chlorosis

To test the chlorosis quantification methodology, pumpkin and pepper plants were used. On the one hand, pumpkin plants were put into pots for four weeks without adding any nutritional solution, provoking nutritional deficiencies in the plants that result in the development of chlorotic areas on the leaves. On the other hand, pepper plants were infected with the common viral pathogen, causing chlorosis in the leaves. Figure 13 shows leaves of pumpkin and pepper with different chlorosis levels. According to R_n and R_{diff} (values shown at the bottom of each figure) the leaf of Figure 13(a) presents the lowest values of R_n and a low value of R_{diff}, these values suggest that the leaf is almost completely covered by a green colour as can be seen in the Figure. The leaf in Figure 13(b) still has a low value of R_n but has the highest value of R_{diff}, meaning that the leaf has a high-localized chlorosis and a low-generalized chlorosis; this fact can be easily corroborated through VE done over this leaf. The leaf in Figure 13(c) show a high value of R_n and a low value of R_{diff}, indicating that the leaf has been covered almost completely by chlorotic areas (generalized chlorosis) as can be corroborated in this figure; in the same way, the leaf in Figure 13(d) show the highest value of R_n and the lowest value of R_{diff}, and these values indicate that the leaf exhibits a high level of generalized chlorosis.

5.2. Necrosis

The necrosis algorithm was tested using bean plants infected by the common bean mosaic virus and pepper plants infected with a necrotic and bacterial disease caused by *Xanthomonas campestri*s. Bean (Figure 14(a,b)) and Pepper leaves (Figure 14(c,d)) were photographed according to the methodology

depicted in Section 4. According to the values shown in Table 1, A_n suggests that leaf of Figure 14(a) presents the major necrotic area and leaf of Figure 14(c) presents the minor necrotic area. The differences between each value of A_n are difficult to be detected by using VE.

Figure 13. Different levels of generalized and localized chlorosis in pumpkin and pepper leaves. (**a**) Pumpkin leaf with the low-generalized and localized chlorosis. (**b**) Pumpkin leaf with high-localized chlorosis. (**c**) Pumpkin leaf with high-generalized chlorosis. (**d**) Pepper leaf with high-generalized chlorosis.

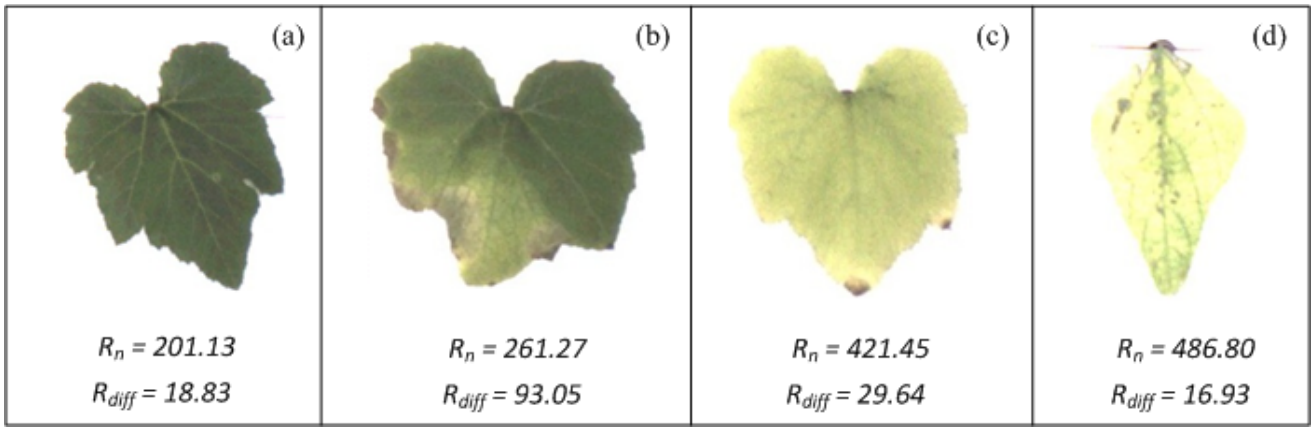

Figure 14. Bean and pepper leaves with different level of necrosis. (**a**) Bean leaf with necrotic and low-chlorotic areas. (**b**) Bean leaf with necrosis and high-generalized chlorosis. (**c**) and (**d**) Pepper leaves with necrosis and high-generalized chlorosis.

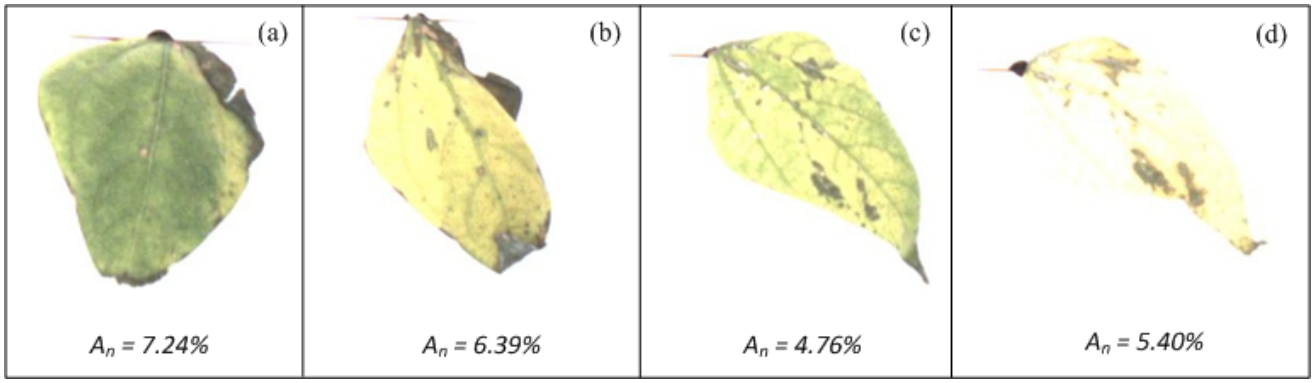

5.3. Leaf Deformation

The Leaf-deformation algorithm was tested using healthy and unhealthy pepper plants infected by the bacteria *Xanthomonas campestris*. Images from these plants were processed according to the methodology presented in Section 4. Figure 15 shows the shape contour of pepper leaves marked in black. According to the deformation index estimation (shown at the bottom of each figure) the leaf in Figure 15(a) has a deformation index of 1.02, which is the lowest value compared against deformation index values of leaves shown in the remaining figures (Figure 15(b–d)); similarly, the leaf in Figure 15(d) presents the highest deformation index (I = 1.16), while the leaf in Figure 15(b) and leaf in Figure 15(c) present an equal deformation value (I = 1.11), suggesting that both leaves have similar deformations. The difference between I value of healthy and unhealthy leaves indicate that leaves in

Figure 15(b–d) are more deformed than the leaf in Figure 15(a). It can be noticed that VE can be used to identify the differences of deformation between Figure 15(a) and Figures 15(b–d); however, it cannot be used to identify the differences between Figure 15(b–d), because they have very similar forms.

Figure 15. Pepper leaves with different level of deformation index. (**a**) Leaf with the lowest deformation index. (**b**) and (**c**) Leaves with intermediate deformation index. (**d**) Leaf with the highest deformation index.

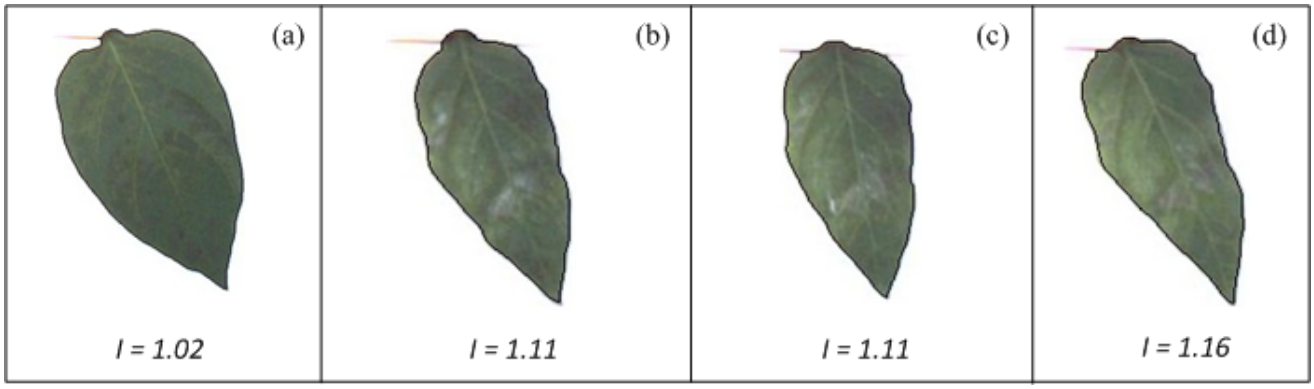

5.4. White Spots

The algorithm for evaluating white-spot areas was tested using bean plants infected with the common bean mosaic virus. Figure 16 shows bean leaves with white-spots symptoms.

Figure 16. Bean leaves with different percentages of leaf area occupied by white spots. (**a**) Bean leaf with the lowest percentage of leaf area occupied by white spots. (**b**) Bean leaf with intermediate percentage of leaf area occupied by white spots. (**c**) Chlorotic-bean leaf with intermediate percentage of leaf area occupied by white spots. (**d**) Chlorotic-bean leaf with the highest percentage of leaf area occupied by white spots.

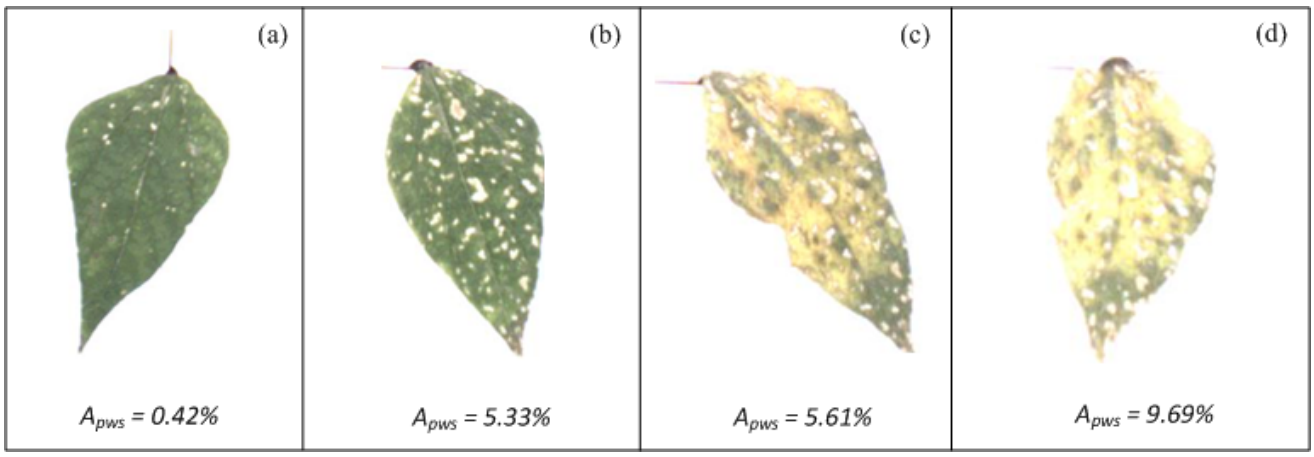

White-spot values A_{pws}, shown at the bottom of each figure, suggest an incremental tendency of white spots in leaves. The leaf in Figure 16(a) is the one with the least percentage of white-spots area according to A_{pws} and the leaf in Figure 16(d) is the leaf with the highest percentage of white-spots area. Leaves shown in Figure 16(b,c) have intermediate values. The differences between Figure 16(a)

and Figure 16 (b–d) are easily identified through VE; however, VE cannot be used as reliable tool to indicate the differences between the leaves in Figure 16(b–d).

5.5. Mosaic

The Mosaic-algorithm was tested using bean plants infected with the common bean mosaic virus that causes the mosaic veinclearing symptom. Figure 17 shows leaves with and without mosaic symptoms; A_{mosaic} values shown in Figure 17 suggest that the leaves of Figure 17(a,b), which are the healthy leaves, have a lesser percentage of area covered by mosaic symptoms than the unhealthy leaves of the Figure 17(c,d). It is important to mention that, the differences of mosaic symptoms between Figure 17(a,b) and between Figure 17(c,d) cannot be easily identified through VE.

Figure 17. Bean leaves with different percentages of area covered by mosaic symptom. (**a**) and (**b**) Healthy bean leaves with the lowest percentage of area covered by mosaic symptom. (**c**) and (**d**) Unhealthy bean leaves with the highest percentages of area covered by mosaic symptom.

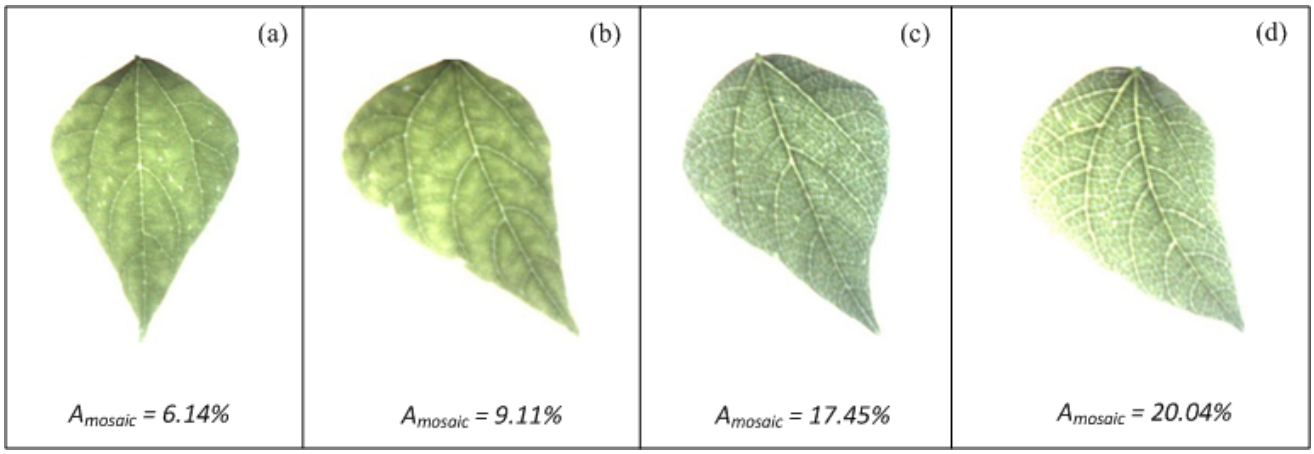

5.6. FPGA Implementation

The processing blocks implemented in the FPGA of the HSP unit (Figure 12) use a 25-MHz clock; the processing times employed by each block to accomplish their corresponding function are shown in Table 1.

Table 1. Processing times of the blocks implemented in the FPGA.

Processing block	Processing time (ms)
Chlorosis	123.398
Necrosis	12.289
Deformation	48.490
White spots	264.192
Mosaic	354.080

The implementation makes use of 7,403 logic elements, 34 9-bit multipliers, and 235,616 memory bits from the FPGA, corresponding to 22.29%, 48.57%, and 48.70% usage, respectively. It can be noticed that all image processing algorithms are below 1 s in execution time, which guarantees the *in situ* and online processing capabilities of the implemented system. Besides, the FPGA has more than 50% of resources available for incorporating further processing algorithms.

6. Conclusions

The present work describes a smart sensor capable of providing precise, reliable and robust quantification of common symptoms presented in leaves of diseased and malnourished plants; these symptoms are: chlorosis, necrosis, deformation, white spots and mosaics. The smart sensor employs a 1/3-inch megapixel CMOS active-pixel digital image sensor (camera) that acts as primary sensor and a Altera-DE2 development card containing an EP2C35F672C6N-Cyclone II FPGA that serves as processing element because it contains enough embedded resources to satisfy the high-computational demand of the proposed algorithms. Novel colour-based methodologies and FPGA characteristics are exploited by the smart sensor to give quantitative, *in-situ*, precise, real-time, and non-destructive symptom assessments. The functionality of the smart sensor was successfully tested by analyzing the aforementioned five common symptoms present in leaves of diseased and malnourished plants. The comparative analysis of the results shows that the quantitative values of Figures 13–17 prove the reliability and precision of the smart sensor in giving quantitative assessments of symptoms that are present in leaves of plants; in consequence, the proposed system could be employed in future works as a practical and powerful tool to give, through plant-leaf symptom quantification, a precise and reliable quantitative description of syndrome development of diseased plants or to determine quantitatively the nutritional deficiencies of plants. This work can also serve as a tool to know the resistance of specific plant varieties to certain pathogens and by consequence help develop new more resistant varieties. For further development, the FPGA reconfigurability capabilities allow the incorporation of different algorithms able to estimate other symptoms not considered in this work.

Acknowledgements

This project was partially supported by CONACYT scholarship 201401, UAQ FIFI 2011, PROMEP/103.5/10/0176, SEP-CONACYT 60481 and SEP-CONACYT 84723. The authors wish to thank INIFAP (*Instituto Nacional de Investigaciones Forestales, Agricolas y Pecuarias*; National Institute of Forestal, Agricultural and Livestock Investigations, Mexico) for having provided the plants and plant pathogens, used during experimentation.

References

1. Agrios, G.N. *Plant Pathology*, 5th ed.; Elsevier: London, UK, 2005; pp. 65–74.
2. Taiz, L.; Zeiger, E. *Plant Physiology*, 4th ed.; Sinauer Associates: Sunderland, MA, USA, 2006; pp. 67–86.

3. Bock, C.H.; Cook, A.Z.; Parker, P.E.; Gootwald, T.R. Characteristics of the perception of different severity measures of citrus canker and the relationships between the various symptom types. *Plant Dis*. **2008**, *92*, 927–939.
4. Contreras-Medina, L.M.; Torres-Pacheco, I.; Guevara-González, R.G.; Romero-Troncoso, R.J.; Terol-Villalobos, I.T.; Osornio-Rios, R.A. Mathematical modelling tendencies in plant pathology. *Afr. J. Biotechnol.* **2009**, *8*, 7399–7408.
5. Bock, C.H.; Cook, A.Z.; Parker, P.E.; Gootwald, T.R. Automated image analysis of the severity of foliar citrus canker symptoms. *Plant Dis.* **2009**, *93*, 660–695.
6. Nutter, F.W.; Esker, P.D.; Coelho, N. Disease assessment concepts in plant pathology and the advancements made in improving the accuracy and precision of plant disease data. *Eur. J. Plant. Pathol*. **2006**, *115*, 95–103.
7. Bock, C.H.; Parker, P.E.; Cook, A.Z. Visual rating and the use of image analysis for assessing different symptoms of citrus canker of grapefruit leaves. *Plant Dis.* **2008**, *92*, 530–541.
8. Miklas, P.N.; Seo, Y.S; Gilbertson, R.L. Quantitative resistance to *Bean dwarf mosaic virus* in common bean is associated with the *Bct* gene for resistance to *Beet curly top virus*. *Plant Dis.* **2009**, *93*, 645–648.
9. Anaya-Lopez, J.L.; Torres-Pacheco, I.; Gonzalez-Chavira, M.; Garzon-Tiznado, J.A.; Pons-Hernandez, J.L.; Guevara-Gonzalez, R.G.; Muñoz-Sánchez, C.J.; Guevara-Olvera, L.; Rivera-Bustamante, B.F.; Hernandez-Verdugo, S. Resistence to geminivirus mixed infections in Mexican wild peppers. *Hort. Sci.* **2003**, *38*, 251–255.
10. Díaz-Lago, J.E.; Stuthman, D.D.; Leonard, K.J. Evaluation of component partial resistance to oat crown rust using digital image analysis. *Plant Dis.* **2003**, *87*, 667–674.
11. Martin, D.P.; Rybicki. E.P. Microcomputer-based quantification of maize streak virus symptoms in *Zea mays*. *Phytopathology* **1998**, *88*, 422–427.
12. Camargo, A.; Smith, J.S. Image pattern classification for the identification of disease causing agents in plants. *Comput. Electron. Agr*. **2009**, *66*, 121–125.
13. Camargo, A.; Smith, J.S. An image-processing algorithm to automatically identify plant disease visual symptoms. *Biosyst. Eng*. **2008**, *102*, 9–21.
14. Wijekoon, C.P.; Goodwin, P.H.; Hsiang, T. Quantifying fungal infection of plant leaves by digital image analysis using Scion Image software. *J. Microbiol. Methods* **2008**, *74*, 94–101.
15. James, W.C. An illustrated series of assessment keys for plant diseases, their preparation and usage. *Can. Plant Dis. Surv*. **1971**, *51*, 39–65.
16. Al-Hiary, H.; Bani-Hamad, S.; Reyelat, M.; Braik, M.; Alrahamneh, Z. Fast and accurate detection and classification of plant diseases. *Int. J. Comput. Appl*. **2011**, *17*, 31–38.
17. Sankaran, S.; Mishra, A.; Ehsani, R.; Davis, C. A review od advanced techniques for detecting plant diseases. *Comput. Electron. Agr*. **2010**, *72*, 1–13.
18. Chaerle, L.; Hagenbeek, D.; Bruyne, E.D.; Valcke, R.; Van Der Straeten, D. Thermal and chlorophyll-fluorescence imaging distinguish plant-pathogen interactions at early stage. *Plant Cell. Physiol*. **2004**, *45*, 887–896.
19. Delaieux, S.; Auwerkerken, A.; Verstraeten, W.; Somers, B.; Valcke, R.; Lhermitte, S.; Keulemans, J.; Coppin, P. Hyperspectral reflectance and fluorescence imaging to detect scab induced stress in apple leaves. *Remote Sens*. **2009**, *27*, 858–874.
20. Belasque, L.; Gasparoto, M.C.G.; Marcassa, L.G.; Detection of mechanical and disease stresses in citrus plants by fluorescence spectroscopy. *Appl. Opt*. **2008**, *47*, 1922–1926.

21. Bravo, C.; Moshou, D.; Oberti, R.; West, R.; McCartney, A.; Bodria, L.; Ramon, H. Foliar disease detection in the field using optical sensor fusion. *CIGR J. Sci. Res. Dev.* **2004**, *6*, 1–14.
22. Williamson, B.; Goodman, B.A.; Chudek, J.A. Nuclear magnetic resonance (NMR) mirco-imaging of ripening red raspberry fruits. *New Phytol.* **1992**, *120*, 21–28.
23. Goodman, B.A.; Williamson, B.; Chudek, J.A. Non-invasive observation of the development of fungal infection in fruit. *Protoplasma* **1992**, *166*, 107–109.
24. Navakar, D.S.; Singh, C.B.; Jayas, D.S.; White, N.D.G. Assessment of soft X-ray imaging for detection of fungal infection in wheat. *Biosist. Eng*. **2009**, *103*, 49–56.
25. Laothawornkitkul, J.; Moore, J.P.; Taylor, J.E.; Possel, M.; Gibson, T.D.; Hewitt, C.N.; Paul, N.D. Discrimination of plant volatile signatures by an electronic nose: A potential technology for plant pest and disease monitoring. *Environ. Sci. Technol*. **2008**, *42*, 8433–8439.
26. Liu, L.; Vikram, A.; Hamzehzarghani, H.; Kushalappa, A.C. Discrimination of three fungal disease of potato tubers based on volatile metabolic profiles developed using GC/MS. *Potato Res*. **2005**, *48*, 85–96.
27. Heuser, T.; Zimmer, W. Genus- and isolate-specific real-time PCR quantification of Erwinia on leaf surface of English oaks (*Quercus robur L.*). *Curr. Microbiol*. **2003**, *47*, 214–219.
28. Gutiérrez-Aguirre, I.; Mehle, N.; Delic, D.; Gruden, K.; Mumford, R.; Ravnikar, M. Real-time quantitative PCR based sensitive detection and genotype discrimination of *Pepino mosaic virus*. *J. Virol. Meth.* **2009**, *162*, 46–55.
29. Lindow, E.; Webb, R.R. Quantification of foliar plant disease symptoms by microcomputer—Digitized video image analysis. *Phytopatology* **1983**, *73*, 520–524.
30. Frank, R. *Understanding Smart Sensors*, 2nd ed.; Artech House: Norwood, MA, USA, 2000.
31. Rivera, J.; Herrera, G.; Chacón, M.; Acosta, P.; Carrillo, M. Improved progressive polynomial algorithm for self-adjustment and optimal response in intelligent sensors. *Sensors* **2008**, *8*, 7410–7427.
32. Contreras-Medina, L.M.; Romero-Troncoso, R.J.; Cabal-Yepez, E.; Rangel-Magdaleno, J.J.; Millan-Almaraz, J.R. FPGA based multiple-channel vibration analyzer for industrial application in induction motor failure detection. *IEEE Trans. Instrum. Meas.* **2010**, *59*, 63–72.
33. Pearson, T. Hardware-based image processing for high-speed inspection of grains. *Comput. Electron. Agr.* **2009**, *69*, 12–18.
34. Millan-Almaraz, J.R.; Romero-Troncoso, R.J.; Guevara-Gonzalez, R.G.; Contreras-Medina, L.M.; Carrillo-Serrano, R.V.; Osornio-Rios, R.A.; DuarteGalvan, C.; Rios-Alcaraz M.A.; Torres-Pacheco, I. FPGA-based fused smart sensor for real-time plant-transpiration dynamic estimation. *Sensor* **2010**, *10*, 8316–8331.
35. *MT9M011 Data Sheet*; Micron Technology Inc.: Boise, ID, USA, 2004.
36. Trigiano, R.N.; Windham, M.T.; Windham, A.S. *Plant Pathology: Concepts and Laboratory Exercises*, 5th ed.; CRC Press: Boca Raton, FL, USA, 2004; pp. 132–158.
37. Pratt, W.K. *Digital Image Processing*, 3rd ed.; John Wiley & Sons: New York, NY, USA, 2001; pp. 623–650.
38. Gonzalez, R.C.; Woods, R.E. *Digital Image Processing*, 2nd ed.; Prentice Hall: Upper Saddle River, NJ, USA, 2002; pp. 519–560.

39. Sonka, M.; Hlavac, V.; Roger, Boyle. *Image Processing, Analysis and Machine Vision*, 3rd ed.; Thomson: Toronto, ON, Canada, 2008; pp. 657–693.
40. Canny, J. A computational approach to edge detection. *IEEE Trans. Patt. Anal. Mach. Intell.* **1986**, *8*, 679–698.
41. *Altera Section I. Cyclone II Device Family Datasheet*; Altera Corp.: San Jose, CA, USA, 2010.

Available online at www.sciencedirect.com

SciVerse ScienceDirect

journal homepage: www.elsevier.com/locate/issn/15375110

Research Paper

Estimating the response of tomato (*Solanum lycopersicum*) leaf area to changes in climate and salicylic acid applications by means of artificial neural networks

M.A. Vazquez-Cruz [a], R. Luna-Rubio [b], L.M. Contreras-Medina [a], I. Torres-Pacheco [a], R.G. Guevara-Gonzalez [a,*]

[a] Division de Estudios de Posgrado, C.A. Ingenieria de Biosistemas, Facultad de Ingenieria, Universidad Autonoma de Queretaro, C.U. Cerro de las Campanas S/N, Colonia Las Campanas, C.P. 76010 Santiago de Queretaro, Queretaro, Mexico

[b] Division de Investigacion y Posgrado, Facultad de Ingenieria, Universidad Autonoma de Queretaro, Cerro de las Campanas s/n, C.P. 76010 Santiago de Queretaro, Queretaro, Mexico

ARTICLE INFO

Article history:
Received 25 November 2011
Received in revised form
14 April 2012
Accepted 6 May 2012
Published online 12 June 2012

Leaf area (LA) is a crucial biophysical variable that is indispensable for many physiological and agronomic models. A reliable and accurate model based on artificial neural networks (ANNs) is proposed to estimate LA of tomato growth under greenhouse conditions. The multi-layer perceptron (MLP) ANN topology was selected for the present study with 5 (ANN5) and three (ANN3) input variables, the architectures were 5-10-1 and 3-9-1, respectively. These MLPs were trained and tested to simulate the response of leaf area with linear measurements leaf length and width. In order to prove the selected topology the ANN was tested with data (leaf length and width) from different experimental growth conditions. Both models had good precision with root mean square errors (RMSEs) of 14.86 and 22.56 cm^2, and mean absolute errors (MAEs) of 10.29% and 16.74%, and coefficients of determination (R^2) of 0.94 and 0.89, respectively, indicating that the ANN5 model can accurately describe the complex relationship between climate factors (CO_2, temperature, and radiation) in different treatments. LA development varied with the different treatments. For high levels of CO_2 and temperature, the LA tends to increase highly with respect to the observed area. Variable impact analysis was performed on the input variables; width and length were the variables which impacted the most on LA estimation. Temperature and salicylic acid (SA) concentration were the variables which affect the tomato LA development during the simulations. Overall, ANN models are a useful tool in investigating and understanding the relationships between LA development and climate factors under greenhouse conditions.

1. Introduction

Leaf area (LA) plays an important role in plant growth analysis. LA is required in several physiological and agronomic models to calculate growth indices as leaf area index (LAI), net assimilation rate (NAR), specific leaf area (SLA), and leaf area duration (LAD), as well as variables involved in studies of plant development, light interception, photosynthetic efficiency,

* Corresponding author. Tel.: +52 01 442 1921200x6093.
E-mail address: ramon.guevara@uaq.mx (R.G. Guevara-Gonzalez).
1537-5110/$ – see front matter © 2012 Published by Elsevier Ltd on behalf of IAgrE.
doi:10.1016/j.biosystemseng.2012.05.003

evapotranspiration, and responses to fertilisers, elicitors and irrigation (Blanco & Folegatti, 2005; Lizaso, Batchelor, & Westgate, 2003). Therefore, LA strongly influences crop growth, development rate, yield potential, radiation use efficiency, and water and nutrient use (Bhatt & Chanda, 2003). When plants are exposed to elevated atmospheric CO_2, radiation, and temperature, photosynthesis and the accumulation of plant biomass are often increased affecting significantly the LA development (Taylor et al., 2001). Exogenous application of elicitors is effective in present-day agricultural practices, allowing the crops to be grown successfully under different stress conditions (Hussain, Malik, Farroq, Ashraf, & Cheema, 2008). Salicylic acid (SA) is a phenolic compound and is used for rising plant resistance to undesirable effects of biotic and abiotic stresses and participates in regulation of plant physiological stages. SA also has significant effect on different aspects of plant life like plant growth and development, photosynthesis, evaporation, ion transmission and absorption; also causes to special changes in leaf anatomy and chloroplast structure (Sakhabutdinova, Fatkhutdinova, Bezrukova, & Shakirova, 2003). LA determination can be done by direct methods, which involve measuring all the individual leaf areas, or direct methods, which are based on the relationship between some plant characteristics and the true leaf area obtained in destructive tests, but during this process the canopy is damaged, which can cause problems to other organs of the plant. According to Vieira Junior et al. (2006) and Femat-Diaz, Vargas-Vazquez, Huerta-Manzanilla, Rico-Garcia, and Herrera-Ruiz (2011), many traditional methods and associated equipment have been replaced by computational approaches using digital image analysis and this has been found to be a reliable tool to provide indirect measurements. An inexpensive, fast, reliable, and non-destructive method for measuring LA is required to make this type of determinations (Lu, Lu, Wei, & Chan, 2004). Decision-making processes in agriculture often require reliable crop response models to assess the impact of specific management practices and environmental conditions. Mathematical models have proved to be a useful tools to define the LA development on crops based on relationships between LA and one or more dimensions of the leaf lamina (length and width) (Mokhtarpour et al., 2010; Rouphael et al., 2010). In this sense, a common mathematical approach has been the allometric relationships, which are regression-based empirical models, but these models lack a non-linear modelling ability for complex climate-plant interactions, which is apparent in crop responses to agro-ecological conditions (Dai, Huo, & Wang, 2011). Authors commonly use allometric relationships to estimate LA with good results, but these equations are case-sensitive and tend to over- and underestimate LA depending on the shape of leaves growth under different climate conditions (Antunes, Pompelli, Carretero, & DaMatta, 2008; Beyhan, Uzun, Kandemir, Ozer, & Demirsoy, 2008; Kandiannan, Kailasam, Chandaragiri, & Sankaran, 2002; Olfati et al., 2009). The more serrated, lobed, or irregular the shape or pattern of the leaf lamina, the more difficult is to estimate its area by allometry (Akorda, 1993; Schwarz & Kläring, 2001). In addition, the influence of other growth determining factors such as radiation, temperature, CO_2, and agronomic management on leaf area has not been investigated (Schwarz & Kläring, 2001).

Artificial intelligence (AI) techniques such as expert systems, artificial neural networks (ANNs), fuzzy logic, and genetic algorithms, have been used to solve complex problems in various areas and are becoming more popular nowadays, mainly because their symbolic reasoning, flexibility, and explanation capabilities (Mellit & Kalogirou, 2008). In areas of prediction and classification, neural networks are being used over different fields of study. According to published literature, a widely network topology used has been the known multi-layer perceptron (MLP). This is because it consistently outperforms the more traditional statistical techniques namely regression analysis, logistic regression, and discriminant analysis (Paliwal & Kumar, 2009).

In agronomic research, ANNs are presented as an alternative methodology to modelling and simulating crop biophysical properties, ANN models are specially designed for dynamic non-linear systems (Rahimikhoob, 2010) inspired in studies of biological neural systems (Hopfield, 1982; Lekouch, El Jazouli, & Bouirden, 2010; McCulloch & Pitts, 1943). ANNs are now used in many computer-based applications where there is a need to identify patterns or 'learn' relationships between a set of input variables and a set of output variables (Danson & Rowland, 2003). One of the most important traits of ANN models is their ability to adapt to current changes and detect patterns in complex natural systems. During the last decade, there has been a significant increase in agronomic ANN application (Dreyfus, 2004; Huang et al., 2010), including crop development modelling (Fortin, Anctil, Parent, & Bolinder, 2010; Zhang, Zhang, Zhang, & Watson, 2009), crop yield prediction (Green, Salas, Martinez, & Erskine, 2007; Khazaei, Naghavi, Jahansouz, & Salimi-Khorshidi, 2008; Park, Hwang, & Viek, 2005), evapotranspiration estimations (Dai, Shi, Li, Ouyang, & Huo, 2009; Liu, Kang, & Li, 2009), and soil water and salt content assessments (Zou, Yang, Fu, Liu, & Li, 2010). However, there have been a few attempts to produce leaf area estimations models predicting leaf area by means of using simple linear measurements (Beyhan et al., 2008). Tomato is one of the most important products worldwide. As a commodity, its production is monitored in order to estimate its availability, and a predictor can be provided by estimation of leaf area in whole plants in a crop. The challenge is then to present a methodology or equipment to improve estimation of leaf area responses to different climate conditions, especially to CO_2, radiation, temperature, and applications of SA in tomato plants as it is proposed in this work. Some approaches had been established to prove the utilisation of ANN in improving some crop growth parameters as leaf area index (LAI) in other crops (Dunea & Moise, 2008). From the aforementioned it can be seen that ANN have the ability to associate climate information with targets attributes of the crops such as LA without any constraints on the sample distribution make them ideal for describing the intricate and complex non-linear relationships that exist between leaf level and various biophysical crop conditions (Yi, Huang, Wang, & Wang, 2010).

The objective of this study is to develop an ANN model to determine the response of LA development to different climate conditions such as CO_2 concentration, radiation and temperature, also including the effect of SA applications.

2. Material and methods

Experiments were carried out in an experimental plastic-covered greenhouse (Fig. 1), located at the Universidad Autonoma de Queretaro, Queretaro, Mexico. The total ground area of the greenhouse was 1012 m^2. The greenhouse was also equipped with side windows. The greenhouse soil was completely covered with a plastic film in order to avoid the emergence of weeds. Samples consisted of tomato Roma var. Rafaello grown from April to October 2011. The seeds were germinated in a mixture of peat-moss, vermiculite, and perlite as substrate (2:1:1). The seedlings were transplanted to the greenhouse when they developed two true leafs. The substrate for the transplanting was tezontle, the apparent density was evaluated to ensure the correct conditions for the root growth and it was 0.605 mg m^{-3}. A total of 990 plants were distributed in 16 rows, with planting distances of 1.5 m between the rows and 0.5 m between plants within the row, with a plant density of 0.97 plants m^{-2}. The total duration of the experiment was 180 days. The plants were grown under different climate conditions, the effect of radiation, temperature, CO_2 concentration, and addition of SA as elicitor for growth were evaluated according to the treatment design described below.

2.1. Experimental design

In this experiment a factorial incomplete design was applied (Turrent & Laird, 1985). Treatment factors in this experiment were CO_2 concentration, radiation, temperature and SA concentration (Table 1). A total of 20 treatments resulted from the combination of these four factors (Table 2). Only SA was evaluated in four levels, the other factors were evaluated only in three levels.

The experiment was laid out in randomised complete block design and replicated three times. In addition, measurements of climate variables above mentioned were taken daily during the whole development of tomato plants (from seedling to fruit stage) with a WatchDog® data logger (Spectrum Technologies, Plainfield, IL, USA).

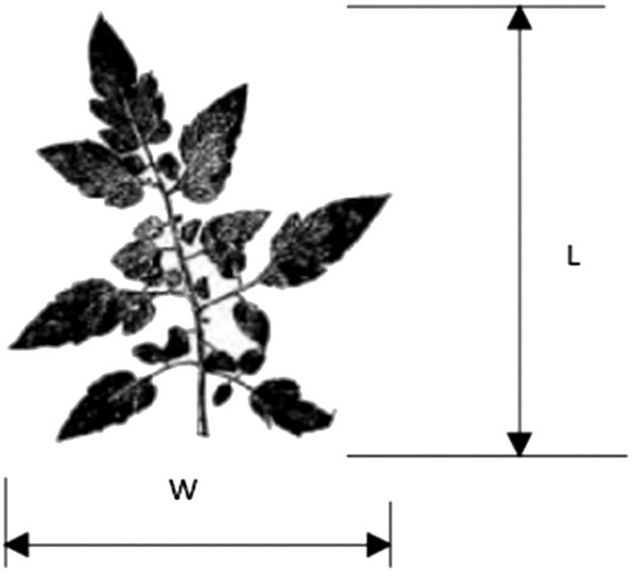

Fig. 1 – Length (*L*) and width (*W*) taken in each leaf.

2.2. Physical measurements and statistical analysis

One single leaf from three plants in each treatment was cut and measured each seven days. A total of 1914 leaves were analysed from the whole experiment. The plants were selected randomly in each repetition. In these leaves, the maximum length (*L*) from the petiole to the central leaflet, and the maximum width of each leaf (*W*) perpendicularly to the maximum length were measured with a hand ruler (Fig. 1).

The real LA (RLA) of individual leafs, taken as a reference, was measured using a camera based on a CCD sensor MT9M011 (Micron Technology, Boise, ID, USA) to capture the image. These data were used to ANN models. All the statistical analyses were performed using the StatTools® Software (Palisade Corporation, Ithaca, NY, USA).

2.3. Artificial neural network model

The multi-layer perceptron or feed-forward network (MLP or MLF) ANN topology was selected for the study. This architecture consists of artificial neurons, called nodes, arranged into three layers: input, hidden, and output. The input layer receives the data of leaf width and length, climate conditions, and SA concentrations; one or more hidden layers connect the input and output layers and the output layer is interpreted as the prediction, in this case the output is the leaf area. A number of interconnected processing nodes or neurons are logically organised in these layers. The neurons in the hidden layers, which are linked to the neurons in the preceding layer and the succeeding layer by adjustable weights, enable the network to compute complex associations between the inputs and outputs. The process of determining these weights is known as training. Basically, the network is taught to model an input-output relationship during a supervised training procedure by using a series of input and associated output data.

The number of nodes in the input and output layers depends on the number of input and output variables, respectively. The performance of the ANN depends on the number of nodes in the hidden layer. Because no specific guidelines exist for choosing the optimum number of hidden nodes for a given problem, this network parameter is often optimised using a combination of empirical rules and trial and error. Figure 2 shows the general layout of three-layer neural network used in this study. In this structure, there are two neurons in the input layer (representing the *W* and *L*

Table 1 – Experimental factors.

Factor	Level			
CO_2	400 ppm	550 ppm	1100 ppm	–
Temperature	25 °C	33 °C	40 °C	–
Radiation	73	221	295	–
Salicylic acid	0 μM	0.01 μM	0.1 μM	1 μM

Table 2 – Summary of treatments applied to tomato under greenhouse conditions.

Treatment	CO_2 (ppm)	SA (μM)	Radiation ($\mu M\,m^{-2}\,s^{-1}$)	Temperature (°C)
T1	550	0.01	295.14	33
T2	550	0.1	295.14	33
T3	550	0.1	295.14	33
T4	550	0.01	295.14	33
T5	550	0.01	295.14	33
T6	550	0.1	295.14	33
T7	550	0.01	295.14	33
T8	550	0.1	295.14	33
T9	550	0	295.14	33
T10	550	0.01	295.14	33
T11	550	0.01	295.14	33
T12	550	1.0	295.14	33
T13	550	0.1	295.14	33
T14	550	0.1	295.14	33
RH	550	0.1	221.35	33
TH	550	0.1	295.14	40
RL	550	0.1	73.78	33
TL	550	0.1	295.14	25
COH	1100	0.1	295.14	33
COL	400	0.1	295.14	33

R = radiation; T = temperature; CO = carbon dioxide; H and L means high and low levels, respectively.

variables), i neurons in a single hidden layer, and one neuron in the output layer (representing the LA). Inside each hidden neuron, a weighted sum of inputs is processed using a transfer function. The transfer or activation function in the networks was the hyperbolic tangent in this study.

Training constitutes the first stage in implementation of a neural network designed to identify the relationship between the independent and dependent variables of a given process. Training of a neural network with the above topology is achieved by adjusting the weights of the neurons through an iterative algorithm that minimises the error between the network-predicted outputs and actual data. A second order optimisation method is used for training connection networks in MLF, particularly the conjugate gradient descent. This deterministic optimisation method was designed to find the local minimum of a function: it proceeds efficiently down the slope of the error function. For the training, the data were divided into two sets. The first set was the training set for determining the interconnection weights of the network. The second set was the validation set for evaluating the interconnection weights in the ANN trained previously.

To suit the consistency of the model, all source data were initially normalised in the range of 0.0–1.0 and then returned to the original values after simulation using the following equation:

$$X_{norm} = \frac{X - X_{min}}{X_{max} - X_{min}}$$

where X_{norm} is the normalised dimensionless variable, X is the original value of the variable, and X_{min} and X_{max} are the minimum and maximum original values of the variable.

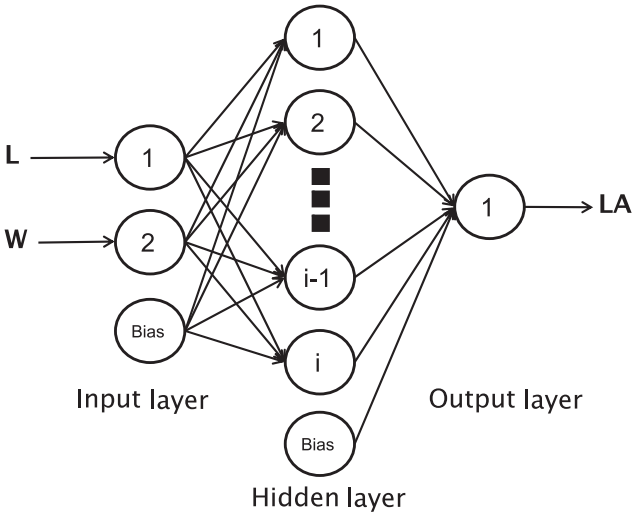

Fig. 2 – General layout of the neural network used in this study with two input variables, one hidden layer, and one output variable estimation of LA.

3. Results

3.1. Artificial neural network development

3.1.1. Input and output variables

One of the most important steps in the ANN development process is to determine input variables. In this study width and length were considered as input variables along with CO_2 concentration, temperature, and radiation evaluated in three levels during the whole development of the tomato plant. As a result 5 input variables were included in the ANN. Furthermore, tomato plant is significantly sensitive to SA (Zahra, Amin, & Mehdi, 2010). Thus, an ANN with 3 input variables was also developed in this study. The output of the ANNs was leaf area (LA). The experimental data (200 samples) including leaf length, width, and area were randomly averagely divided into 3 groups in which two groups were chosen to train ANN and the remainder was used to test ANN.

3.1.2. Network architecture

The neurons in the hidden layer in the neural network were determined by trial and error (Table 3). For training and testing results from ANNs, the root mean square error (RMSE), mean absolute error (MAE), and coefficient of determination (R^2) with different node numbers of the hidden layer were compared to select the optimal node number in the hidden layer (Table 4). For the testing data, the ANN5 with 5–8 nodes in hidden layer produced the lowest RMSE and MAE, and the highest R^2 was observed in the ANN5 with 10 nodes in the hidden layer. After node 7 the value of R^2 decreased and the RMSE and MAE increased. For the testing data of the ANN3, the model with 9 nodes had the lowest RMSE and MAE, and the highest R^2. After 9 hidden neurons in both ANNs the values of RMSE and MAE tend to increase and R^2 was decreased. In addition, more hidden neurons increased the network training time significantly. Therefore, the optimal network structures were 5-10-1 and 3-9-1 for the two ANNs, respectively.

Table 3 – Test errors (RMSE, MAE, and R^2) of ANN5 and ANN3 models.

Nodes ANN5		4	5	6	7	8	9	10	11
Testing data	RMSE	24.77	16.33	18.32	9.542	11.89	18.45	8.703	10.87
	MAE	17.14	10.76	12.73	7.177	8.685	12.65	6.084	7.101
	R^2	0.86	0.94	0.92	0.98	0.96	0.92	0.98	0.97
Nodes ANN3		4	5	6	7	8	9	10	11
Testing data	RMSE	23.77	21.42	27.28	24.55	22.49	18.07	21.19	21.41
	MAE	17.20	16.20	19.40	18.09	17.63	13.81	15.12	16.43
	R^2	0.87	0.9	0.83	0.86	0.89	0.93	0.9	0.9

After training data, testing data were used to determine the errors of the model. The RMSE range of ANN5 was from 8.7 to 24.77 cm^2, and the MAE was from 6.08 to 17.14%, whereas the ANN3 produced a bigger RMSE and MAE range, which was 18.07–27.28 cm^2 and 13.81–19.4%, respectively (Table 4). Comparably, the ANN5 had a lower RMSE and MAE, and a larger R^2 than the ANN3 model (Table 4 and Fig. 3).

3.1.3. *Relative variable impacts*

The purpose of variable impact analysis is to measure the sensitivity of net predictions to changes in independent variables. In ANN5 and ANN3, the relative variable impacts of the input variables were calculated during the training process and were listed in Table 5. For ANN5, the leaf width had the highest impact among all input variables, which accounted for 90.8%. Secondly was the length with an impact of 4.7%. The climate variables temperature, CO_2 concentration, and photosynthetic active radiation (PAR) had a low impact on LA development (<3%). These results indicate that tomato LA estimation is more sensitive to linear measurements (length and width) than the variations induced for different levels in climate factors. Among climate factors, temperature had the highest impact on LA estimations (2.55%), but is relatively low compared with the impact of leaf width. These results suggest that temperature, CO_2 concentration, and PAR had an important effect on leaf width development.

For the ANN3, the length of leaf was the variable with the highest impact, accounting for 50.3%, indicating that SA had an important effect on leaf length than on leaf width. As an input variable the SA concentration had an important impact (34.5%) on leaf area estimations. This also proved the importance of the precision in measurements to estimate LA by means of

Table 4 – Error comparison of the ANN models.

		ANN5	ANN3
RMSE (cm^2)	Max	24.77	27.28
	Min	8.703	18.07
	Average	14.86	22.52
MAE	Max	17.14	19.4
	Min	6.084	13.81
	Average	10.29	16.74
R^2	Average	0.94	0.89

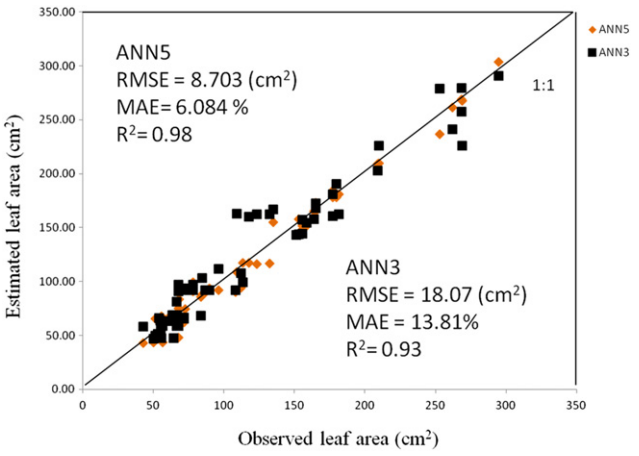

Fig. 3 – Observed versus estimated leaf area from ANN5 and ANN3.

ANNs, the changes in leaf shape due to the climate factors could have an important effect on this precision and needs to be taken into account to improve the accuracy on estimations.

3.2. *Simulation of tomato leaf area using both ANNs*

ANN5 and ANN3 were used to simulate tomato LA changes, under different climate conditions from those evaluated in the experiment, in order to evaluate the effectiveness of ANNs to predict leaf area. The climate conditions evaluated were temperature (30 and 35 °C), CO_2 concentration (600 and 900 ppm), and radiation (100 and 200 $\mu M\, m^{-2}\, s^{-1}$) (Fig. 4).

For the PAR response, at 300 and 100 $\mu M\, m^{-2}\, s^{-1}$, the LA remained constant from the day 35 and on. According to the ANN results, the increment in PAR did not increased the leaf area. With a reduced quantity of PAR, the LA showed a significant reduction. In both cases LA development diminished, although during the first 35 days after transplanting the behaviour of observed and predicted LA was closely related.

The high temperature (45 °C) showed an important influence on the LA development. LA was increased in the day 28 after transplanting, with an important increment in the day 35, reaching a final area above the 500 cm^2 on the 70 day after transplanting (DAT). LA development decreased when the temperature was low. A temperature of 20 °C there was little

Table 5 – Variable impact analysis (%) of the input variables in each ANN.

Variables	Variable impact analysis	
	ANN5	ANN3
Width (cm)	90.8734	15.1093
Length (cm)	4.7275	50.3785
TEMP (°C)	2.5582	–
PAR ($\mu M\, m^{-2}\, s^{-1}$)	1.7073	–
CO2 (ppm)	0.1336	–
Salicylic acid ($mM\, ml^{-1}$)	–	34.5122

–, no value because the variable was not an input for the ANN.

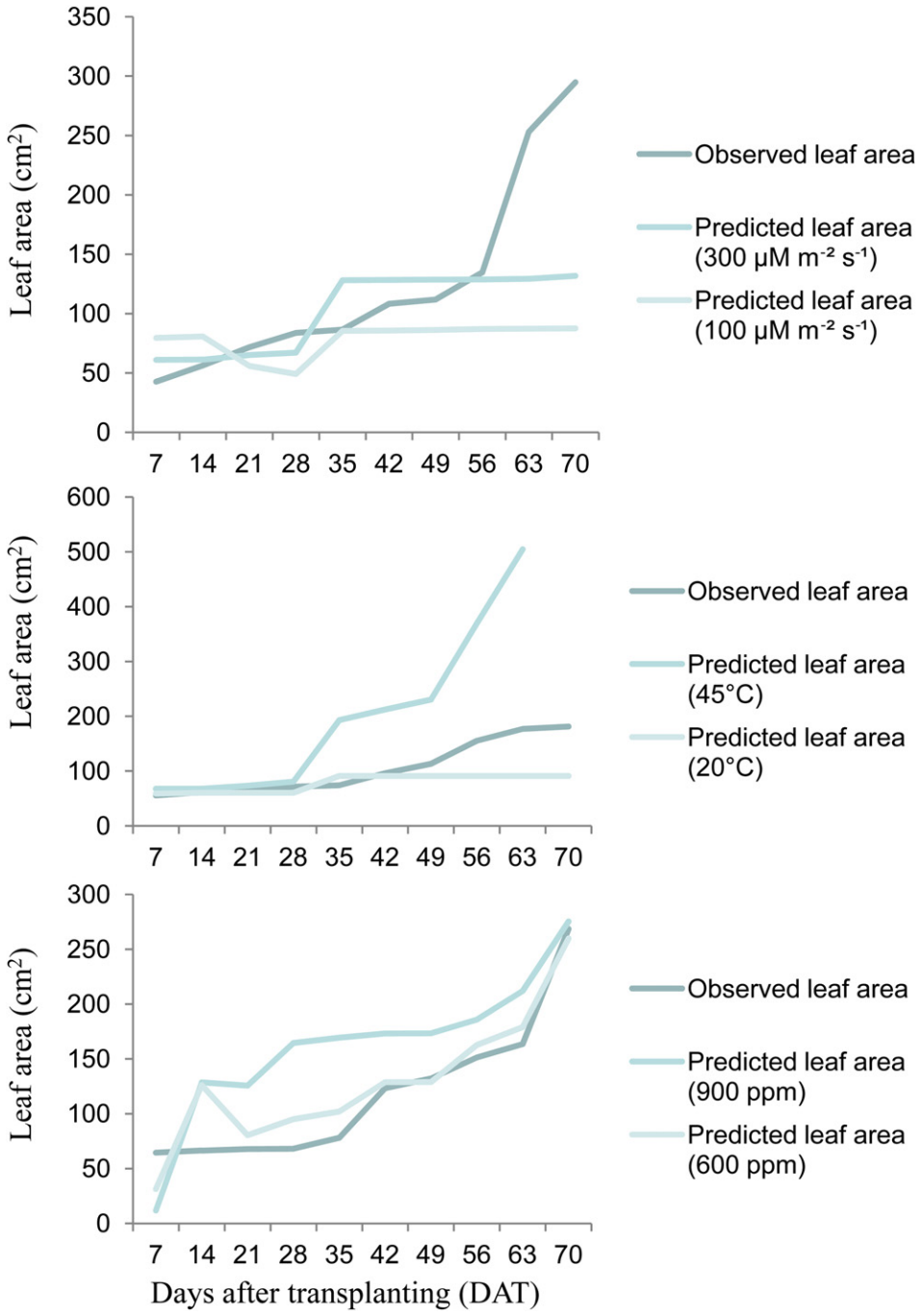

Fig. 4 – ANN5 predicted leaf area response to temperature, PAR, and CO_2 concentration.

LA development, the maximum area was close to 90 cm^2, remaining constant until the 70 DAT. It is important to note that in the case of 20 °C and 45 °C, the increment in LA was from 28 DAT, and a second increment at the 35 DAT. The behaviour of the predicted LA was very similar to the observed LA during the first 28 days.

The effect of CO_2 concentration was also evaluated. A concentration of 900 ppm produced an important increment in LA during the second week of growth period. The LA was higher from the 21st day after transplanting. The final LA in the three CO_2 concentrations was between 259 and 275 cm^2. With a concentration of 600 ppm LA development was very similar to the observed data during the last four weeks; the LA was higher during the first 5 weeks of the growing period with 600 ppm of CO_2. The LA was more sensitive to high levels of temperature and CO_2 concentration.

4. Discussion

Tomato is sensitive to a number of environmental stresses, especially at extreme temperatures, radiation, drought,

salinity, and concentrations of CO_2 and also at low relative humidity (Nahar, Ullah, & Islam, 2011). Many previous studies have already shown that the crop response to these factors is very complex, and should be modelled using cubic or quadratic functions (Starr, Rowland, Griffin, & Olanya, 2008). Other rapid and non-destructive methods to estimate LA in other crops had been developed (Astegiano, Favaro, & Bouzo, 2001; Gutierrez & Lavin, 2000; Kandiannan et al., 2002; Schwarz & Kläring, 2001). These methods consist of equations which needs leaf dimensions (length and width) as input variables. However, these equations do not take into account the interaction of leaf development to climate factors.

Allometric relationships have shown accurate results in predicting LA. Olfati et al. (2009) evaluated an allometric equation for LA prediction in red cabbage from linear measurements of leaf length and width, in their study a strong relationship between LA and leaf width was reported. Antunes et al. (2008) also showed that there was a high correlation between LA and leaf width in coffee leaves through an allometric model. Kandiannan et al. (2002) found that estimation of LA in black pepper (*Piper nigrum* L.) can be done with high accuracy using leaf length with R^2 ranging between 0.86 and 0.96. In this study, the ANN models were very suitable and accurate for modelling LA responses to climate factors and SA. The ANN with 5 input variables showed superior results to those of the ANN with three input variables. Furthermore, ANN model with five input variables allowed predictions of LA development taking into account the complex interactions of LA with climatic factors such as radiation, temperature, and CO_2 concentrations. Improvement in the estimations with allometric models sometimes is not possible because LA can be underestimated due to the irregular shape of tomato leaves (unpaired pinnate leaves). The more serrated, lobed, or irregular the shape or pattern of the leaf lamina, the more difficult it is to estimate its area by allometry (Akorda, 1993; Schwarz & Kläring, 2001). ANN methods have an advantage over the empirical modelling techniques since they do not assume a prior structure for the data, are well suited for fitting non-linear relationships and complex interactions, and can expose hidden relationships among the input variables.

Also, ANN5 performed better than ANN3. The error in ANN models increased with the decrease in the number of input variables. Considering the simplicity of the model, ANN5 was more useful for simulating the leaf area development in response to climate factors.

The results for ANN5 indicated that LA is more sensitive to temperature and CO_2 concentration. During the first 28 days the leaf area development was very similar, important changes in leaf area could be observed from the day 35 onwards. The modelling proved that increasing CO_2 concentration resulted in increased tomato LA. In this study the simulated LA in 900 ppm of CO_2 was higher than that at 600 ppm, and mostly higher than the observed LA.

The modelling also showed that increasing the temperature increases the predicted more than the observed LA. In fact, this increment was constant from the day 49 onwards; further days were needed to prove that this growth continues during the whole development of the plant. The same situation was observed for the LA at temperatures below 20 °C, from the day 35 onwards since the LA was constant (approximately 100 cm^2) and no further effect of temperature on LA development was observed during the period of time used in this study. In fact, length and width were the input variables with the highest effect on LA estimations, along with temperature and SA concentration. Accurate knowledge of the relative impact of the input variables in ANN models would be useful in guiding climate control in greenhouse to enhance the LA development. However, crop growth response to climate factors is more complex. Temperature and CO_2 dynamics, as well as radiation distribution patterns change with crop growth, climate control, and management.

The ANN with three input variables (ANN3) showed that the SA effect on leaf area development was not important enough, in this case the leaf width was more important to estimate LA development. In other studies using SA as an elicitor it has not been reported that this could affect the LA architecture (Esmailzadeh, Soleimani, & Rouhani, 2008). Thus, ANN3 was not used for simulation purposes because the different concentrations of SA did not affect LA development.

In future, ANN technology could be used to model more complex relationships between crop growth, management, and climatic factors which are more important for the prediction of LA development.

5. Conclusions

Two ANN models, with 5 inputs (ANN5) and with three inputs (ANN3), were used to simulate the response of tomato LA to different climate conditions in greenhouse cultivation. Both ANN models have good precision with RMSEs of 14.86 and 22.56 cm^2, MAEs of 10.29% and 16.74%, and R^2 of 0.94 and 0.89, respectively, indicating that ANN5 model can accurately describe the complex relationship between climate factors (CO_2, temperature, and radiation) in different treatments. The response of LA development to climate factors can be understood through the simulation results of the ANN models. At high temperatures and CO_2 concentrations the LA tended to increase. In the case of high and low PAR, the observed LA was higher than the predicted LA. The variables which impacted the most on the estimated LA were width and length for ANN5 and ANN3, respectively. Among the climatic factors, LA was more sensitive to temperature and SA concentrations. The response of LA to climatic factors in the different treatments can be understood through the simulated results of ANN5. Therefore, an ANN model is a useful tool in investigating and understanding the complex relationships between the development of tomato plants grown under greenhouse conditions, particularly LA development, and climatic factors.

Acknowledgements

The authors wish to acknowledge to PROMEP, Ciencia Basica (SEP-CONACyT) and FOMIX Queretaro for supporting this research. M.A. Vazquez-Cruz also thanks to CONACyT for the PhD scholarship support contract number 218413, and the respective reviewers for their valuable comments and criticisms.

REFERENCES

Akorda, M. O. (1993). Non destructive estimation of area and variation in shape of leaf lamina in the fluted pumpkin (*Telfairia occidentalis*). *Scientia Horticulturae, 53*, 261–267.

Antunes, W. C., Pompelli, M. F., Carretero, D. M., & DaMatta, F. M. (2008). Allometric models for non-destructive leaf area estimation in coffee (*Coffea arabica* and *Coffea canephora*). *Annals of Applied Biology, 153*, 33–40.

Astegiano, E. D., Favaro, J. C., & Bouzo, C. A. (2001). Estimación del área foliar en distintos cultivares de tomate (*Lycopersicon esculentum* Mill) utilizando medidas foliares lineales. *Investigación Agraria, Producción y Protección Vegetales, 16*, 249–256.

Beyhan, M. A., Uzun, S., Kandemir, D., Ozer, H., & Demirsoy, M. (2008). A model for predicting leaf area in young and old leaves of greenhouse type tomato (*Lycopersicon esculentum*, Mill.) by linear measurements. *Journal of Faculty of Agriculture, 23*, 154–157.

Bhatt, M., & Chanda, S. V. (2003). Prediction of LA in *Phaseolus vulgaris* by non destructive method. *Bulgarian Journal of Plant Physiology, 29*, 96–100.

Blanco, F. F., & Folegatti, M. V. (2005). Estimation of LA for greenhouse cucumber by linear measurements under salinity and grafting. *Scientia Agricola, 62*, 305–309.

Dai, X., Huo, Z., & Wang, H. (2011). Simulation for response of crop yield to soil moisture and salinity with artificial neural network. *Field Crops Research, 121*, 441–449.

Dai, X., Shi, H., Li, Y., Ouyang, Z., & Huo, Z. (2009). Artificial neural networks models for estimating reference evapotranspiration based on climate factors. *Hydrological Processes, 23*, 442–450.

Danson, F. M., & Rowland, C. S. (2003). Training a neural network with canopy reflectance model to estimate crop leaf area index. *International Journal of Remote Sensing, 24*, 4891–4905.

Dreyfus, G. (2004). *Réseux de neurons méthodologie et applications* (2éme ed.). ISBN: 2-212-11464-8.

Dunea, D., & Moise, V. (2008). Artificial neural networks as support for leaf area modeling in crop canopies. In *12th WSEAS international conference on computers*, Heraklion, Greece, July 23–25.

Esmailzadeh, M., Soleimani, M. J., & Rouhani, H. (2008). Exogenous applications of salicylic acid for inducing systemic acquired resistance against tomato stem canker disease. *Journal of Biological Sciences, 8*, 1039–1044.

Femat-Diaz, A., Vargas-Vazquez, D., Huerta-Manzanilla, E., Rico-Garcia, E., & Herrera-Ruiz, G. (2011). Scanning image methodology (SIM) to measure dimensions of leaves for agronomical applications. *African Journal of Biotechnology, 10*, 1840–1847.

Fortin, J. G., Anctil, F., Parent, L., & Bolinder, M. A. (2010). A neural network experiment on the site-specific simulation of potato tuber growth in Eastern Canada. *Computers and Electronics in Agriculture, 73*, 267–272.

Green, T. R., Salas, J. D., Martinez, A., & Erskine, R. H. (2007). Relating crop yield to topographic attributes using spatial analysis neural networks and regression. *Geoderma, 139*, 23–27.

Gutierrez, T., & Lavin, A. (2000). Linear measurements for non destructive estimation of leaf area in Chardonnay vines. *Agricultura Tecnica, 60*, 69–73.

Hopfield, J. J. (1982). Neural networks and to physical systems with emergent collective computational abilities. *Proceedings of the National Academy of Sciences of the United States of America, 79*, 2554–2558.

Huang, Y., Lan, Y., Thomson, S. J., Fang, A., Hoffmann, W. C., & Lacey, R. E. (2010). Development of soft computing and applications in agricultural and biological engineering. *Compouters and Electronics in Agriculture, 71*, 107–127.

Hussain, M., Malik, M. A., Farroq, M., Ashraf, M. Y., & Cheema, M. A. (2008). Improving drought tolerance by exogenous application of glycinebetaine and salicylic acid in sunflower. *Journal of Agronomy and Crop Science, 194*, 193–199.

Kandiannan, K., Kailasam, C., Chandaragiri, K. K., & Sankaran, N. (2002). Allometric model for leaf area estimation in black pepper (*Piper nigrum* L.). *Journal of Agronomy and Crop Science, 188*, 138–140.

Khazaei, J., Naghavi, M. R., Jahansouz, M. R., & Salimi-Khorshidi, G. (2008). Yield estimation and clustering of chickpea genotypes using soft computing techniques. *Agronomy Journal, 100*, 1077–1087.

Lekouch, K., El Jazouli, M., & Bouirden, L. (2010). Predicting air temperature in a natural ventilated greenhouse with tomato crop. *International Review of Physics, 4*, 76–82.

Liu, X., Kang, S., & Li, F. (2009). Simulation of artificial neural network model for trunk sap flow of *Pyrus pyrifolia* and its comparison with multiple-linear regression. *Agricultural Water Management, 96*, 939–945.

Lizaso, J. I., Batchelor, W. D., & Westgate, M. E. (2003). A LA model to simulate cultivar-specific expansion and senescence of maize leaves. *Field Crops Research, 80*, 1–17.

Lu, H. Y., Lu, C. T., Wei, M. L., & Chan, L. F. (2004). Comparison of different methods for non-destructive LA estimation in taro. *Agronomy Journal, 96*, 448–453.

McCulloch, W. S., & Pitts, W. A. (1943). A logical calculus of the ideas imminent in nervous activity. *Bulletin of Mathematical Biology, 52*, 99–115.

Mellit, A., & Kalogirou, S. A. (2008). Artificial intelligence techniques for photovoltaic applications: a review. *Progress in Energy and Combustion Science, 34*, 574–632.

Mokhtarpour, H., Teh, C. B. S., Saleh, G., Selamat, A. B., Asadi, M. E., & Kamkar, B. (2010). Non-destructive estimation of maize leaf area, fresh weight, and dry weight using leaf length and leaf width. *Communications in Biometry and Crop Science, 5*, 19–26.

Nahar, K., Ullah, S. M., & Islam, N. (2011). Osmotic adjustment and quality response of five tomato cultivars (*Lycopersicon esculentum* Mill) following water deficit stress under subtropical climate. *Asian Journal of Plant Sciences, 10*, 153–157.

Olfati, J. A., Peyvast, G., Sanavi, M., Salehi, M., Mahdipour, M., & Nosratie-Rad, Z. (2009). Comparisons of leaf area estimation from linear measurements of red cabbage. *International Journal of Vegetable Science, 15*, 185–192.

Paliwal, M., & Kumar, U. A. (2009). Neural networks and statistical techniques: a review of applications. *Expert Systems and Applications, 36*, 2–17.

Park, S. J., Hwang, C. S., & Viek, P. L. G. (2005). Comparison of adaptive techniques to predict crop yield response under varying soil and land management conditions. *Agricultural Systems, 85*, 59–81.

Rahimikhoob, A. (2010). Estimation of evapotranspiration based on only air temperature data using artificial neural networks for a subtropical climate in Iran. *Theoretical and Applied Climatology, 101*, 83–91.

Rouphael, Y., Mouneime, A. H., Ismail, A., Mendoza-De Gyves, E., Rivera, C. M., & Colla, G. (2010). Modeling individual leaf area of rose (Rosa hybrida L.) based on leaf length and width measurement. *Photosynthetica, 48*, 9–15.

Sakhabutdinova, A. R., Fatkhutdinova, D. R., Bezrukova, M. V., & Shakirova, F. M. (2003). Salicylic acid prevents the damaging action of stress factors on wheat plants. *Bulgarian Journal of Plant Physiology*, (Special issue), 314–319.

Schwarz, D., & Kläring, H. S. (2001). Allometry to estimate leaf area of tomato. *Journal of Plant Nutrition, 24*, 1291–1309.

Starr, G. C., Rowland, D., Griffin, T. S., & Olanya, O. M. (2008). Soil water in relation to irrigation, water uptake, and potato yield in a humid climate. *Agricultural Water Management,* 95, 292–300.

Taylor, G., Ceulemans, R., Ferris, R., Gardner, S. D. L., & Shao, B. Y. (2001). Increased leaf are expansion of hybrid poplar in elevated CO2. From Controlled environments to open-top chambers and to FACE. *Environmental Pollution,* 115, 463–472.

Turrent, F. A., & Laird, R. J. (1985). *La matriz experimental plan Puebla, para ensayos sobre prácticas de producción de cultivos. Volumen 1 de Escritos sobre la metodología de la investigación en productividad de agrosistemas*. Ed. 3 (28 pp.). ISBN 9688390127, 9789688390122.

Vieira Junior, P. A., Dourado Neto, D., Cicero, S. M., Cstro Jorge, L. A., Manfron, P. A., & Martin, T. N. (2006). Estimativa da area foliar em milho atraves de analise de imagens. *Revista Brasileira de Milho e Sorgo,* 5, 58–66.

Yi, Q., Huang, J., Wang, F., & Wang, X. (2010). Evaluating the performance of PC-ANN for the estimation of rice nitrogen concentration from canopy hyperspectral reflectance. *International Journal of Remote Sensing,* 31, 931–940.

Zahra, S., Amin, B., & Mehdi, Y. (2010). The salicylic acid effect on the tomato (*Lycopersicon esculentum* Mill.) germination, growth, and photosynthetic pigment under salinity stress (NaCl). *Journal of Stress Physiology & Biochemistry,* 6, 4–16.

Zhang, J. Q., Zhang, L. X., Zhang, M. H., & Watson, C. (2009). Prediction of soybean growth and development using artificial neural network and statistical models. *Acta Agronomica Sinica,* 35, 341–347.

Zou, P., Yang, J., Fu, J., Liu, G., & Li, D. (2010). Artificial neural network and time series model for predicting soil salt and water content. *Agricultural Water Management,* 97, 2009–2019.

Sensors **2010**, *10*, 8316-8331; doi:10.3390/s100908316

OPEN ACCESS

sensors

ISSN 1424-8220

www.mdpi.com/journal/sensors

Article

FPGA-based Fused Smart Sensor for Real-Time Plant-Transpiration Dynamic Estimation

Jesus Roberto Millan-Almaraz [1], Rene de Jesus Romero-Troncoso [2], Ramon Gerardo Guevara-Gonzalez [1], Luis Miguel Contreras-Medina [1,3], Roberto Valentin Carrillo-Serrano [4], Roque Alfredo Osornio-Rios [3], Carlos Duarte-Galvan [1], Miguel Angel Rios-Alcaraz [1] and Irineo Torres-Pacheco [1,*]

[1] CA Ingenieria de Biosistemas, Division de Investigacion y Posgrado, Facultad de Ingenieria, Universidad Autonoma de Queretaro, Cerro de las Campanas s/n, 76010, Queretaro, Qro., Mexico; E-Mails: roberto.millan@uaq.mx (J.R.M.-A.); ramon.guevara@uaq.mx (R.G.G.-G.); mcontreras@hspdigital.org (L.M.C.-M.); cduarte20@alumnos.uaq.mx (C.D.-G.); mrios24@alumnos.uaq.mx (M.A.R.-A.)

[2] HSPdigital-CA Telematica, DICIS, Universidad de Guanajuato, Carr. Salamanca-Valle km 3.5+1.8, Palo Blanco, 36885 Salamanca, Gto., Mexico; E-Mail: troncoso@hspdigital.org (R.J.R.-T.)

[3] HSPdigital-CA Mecatronica, Facultad de Ingenieria, Universidad Autonoma de Queretaro, Campus San Juan del Rio, Rio Moctezuma 249, 76807 San Juan del Rio, Qro., Mexico; E-Mail: raosornio@hspdigital.org (R.A.O.-R.)

[4] Division de Investigacion y Posgrado, Facultad de Ingenieria, Universidad Autonoma de Queretaro, Cerro de las Campanas s/n, 76010, Queretaro, Qro., Mexico; E-Mail: roberto.carrillo@uaq.mx (R.V.C.-S.)

* Author to whom correspondence should be addressed; E-Mail: irineo.torres@uaq.mx; Tel.: +52-442-192-1200 ext. 6096; Fax: +52-442-192-1200 ext. 6005.

Received: 21 July 2010; in revised form: 6 August 2010 / Accepted: 20 August 2010 / Published: 2 September 2010

Abstract: Plant transpiration is considered one of the most important physiological functions because it constitutes the plants evolving adaptation to exchange moisture with a dry atmosphere which can dehydrate or eventually kill the plant. Due to the importance of transpiration, accurate measurement methods are required; therefore, a smart sensor that fuses five primary sensors is proposed which can measure air temperature, leaf temperature, air relative humidity, plant out relative humidity and ambient light. A field programmable gate array based unit is used to perform signal processing algorithms as

average decimation and infinite impulse response filters to the primary sensor readings in order to reduce the signal noise and improve its quality. Once the primary sensor readings are filtered, transpiration dynamics such as: transpiration, stomatal conductance, leaf-air-temperature-difference and vapor pressure deficit are calculated in real time by the smart sensor. This permits the user to observe different primary and calculated measurements at the same time and the relationship between these which is very useful in precision agriculture in the detection of abnormal conditions. Finally, transpiration related stress conditions can be detected in real time because of the use of online processing and embedded communications capabilities.

Keywords: smart sensor; transpiration; stomatal conductance; precision agriculture; phytomonitoring; water stress; field programmable gate array

1. Introduction

Plant transpiration is the process in which plants exchange moisture with the atmosphere [1]. This process is carried out when plants perform photosynthesis. While the plants are absorbing the carbon dioxide (CO_2) they also lose a certain amount of water and release oxygen O_2 [2]. Also, transpiration is performed to maintain temperature equilibrium between plants and their environments, dissipating undesirable heat in the lost water vapor. Plant monitoring commonly includes the estimation of photosynthesis itself, the assimilation or CO_2 uptake and water thermodynamic relations such as: transpiration (E), stomatal conductance (C_{leaf}), vapor pressure deficit (VPD), and leaf-air temperature difference ($LATD$) [3]. Those variables constitute transpiration dynamic indicators which are often used in agriculture to optimize the available water resources [4].

E is considered one of the most important plant physiological functions because it encompasses plants evolving and adapting to exchange moisture in a very dry atmosphere that can dehydrate or eventually kill the plant [1]. C_{leaf} is a transpiration variable that represents a quantitative measurement of the stomatal resistance (r_s) inverse of plant guard cells plus the inverse boundary resistance (r_b) against water vapor flux. Those guard cells act as flux valves to control the water vapor movement from plant to the atmosphere and CO_2 movement in an inverse way [5]. $LATD$ is the difference between air temperature (T_a) and leaf temperature (T_{leaf}) in relation to the global transpiration process which is proportional to E. Furthermore, VPD is also a response variable that is calculated by subtracting air vapor pressure (e_i) content from saturation vapor pressure (e_s). These variables are very important because they can indicate drought stress conditions and condensation problems that may cause dangerous plant diseases [2,6,7].

Because of this, transpiration dynamic measurement is crucial and necessary to establish comparisons and understand plant-soil-atmosphere relationships at leaf, plant, canopy, or community levels as well as their interaction and response to environmental [6], chemical [8], or biological [9] factors that generate different stress conditions. Therefore, continuous monitoring of the aforementioned transpiration dynamics by a single smart sensor system is highly desirable. As a

consequence, more accurate measurement methods are required to gather more knowledge about these processes. Relative humidity (*RH*) capacitive sensors and thermistors are the most commonly utilized sensors to measure these variables in environmental and agricultural research [2,6,10,11]; however, in modern instrumentation the use of intelligent sensors with *in situ* signal processing capabilities to calculate response variables equations from simple sensor measurements is necessary [12-14]. *E* and C_{leaf} calculation is based mainly on water vapor exchange measurements [2,6]. This method consists of temporally isolating a plant leaf sample in a miniature gas exchange chamber which is often used for photosynthesis measurements [15]. An air flow is introduced into the leaf chamber to measure the intake e_i and the amount of leaf out vapor (e_o). The absolute amount of water is calculated using *RH* sensors and vapor curve equations from Mollier diagrams by expressing, *E* and C_{leaf} as vapor mass for each surface unit of each time unit [6,16,17]. Previous monitoring systems have used this technique to obtain *E* and C_{leaf} from air relative humidity (RH_a) and T_a [18,19]. Temperature, light, carbon, and *RH* measurements contain merged transpiration and photosynthesis dynamics information; therefore, the extraction of those response variables is desirable for precision agriculture applications. Previously, T_a and *RH* sensors have been used in data acquisition systems for environmental monitoring and greenhouse climate controllers [2]. More advanced applications involve offline crop water stress detection based on *E* behavior analysis [20]. Forestry research has also used transpiration dynamics to investigate the properties of trees [21]. Intelligent irrigation has been investigated in order to schedule irrigation cycles according to the speaking plant concept approach, better known as phytomonitoring technique [20,22]. It takes into consideration the plant as the final user of the irrigation line, activating water delivery when plant has an excessive *E*. *VPD* has been studied in greenhouse climate controller design also in order to determine when *RH* is near to dew point to avoid excessive fogging and consequently leaf condensation that leads to plant diseases [7]. However, those systems do not fuse their sensors data with other transpiration-related response variables such as ambient light and *LATD* nor do they have online *in situ* signal processing capabilities to make real-time decisions. Consequently, it involves having an agricultural expert technician to manually download data to be analyzed offline with at least a one day delay [22]. In precision agriculture, a one day delay can sometimes represent the loss of the total crop. It makes necessary the development of a real time transpiration dynamics intelligent sensor to early detect stress and disorder conditions.

The contribution of this project is to develop a smart sensor capable of estimating plant transpiration dynamic variables: *E*, C_{leaf}, *LATD*, and *VPD*, through the fusion of five primary low-cost sensors: two *RH* capacitive sensors, two Resistance Temperature Detector (RTD) sensors, one light quantum sensor, average atmospheric pressure data, and fixed volumetric air flow. All the aforementioned instrumentation was embedded into a smart sensor system using an aluminum/acrylic leaf chamber with automatic open/close mechanism based on a miniature servomotor to perform temporal leaf isolation cycles. A vacuum pump is used to generate the air flow through the leaf chamber. Transpiration dynamic response variables are extracted from the primary sensors and its computation is performed *in situ* using digital signal processing techniques such as: average decimation filters, infinite-impulse-response (IIR) filters, polynomial fitting, and the corresponding *E*, C_{leaf}, *LATD*, and *VPD* equations. The light sensor is fused as a reference to understand daylight information which is related to the beginning of daily transpiration dynamic processes. The data acquisition systems,

aforementioned computations, data communication and leaf chamber servomotor/vacuum pump control system are implemented in a field programmable gate array (FPGA) as an embedded smart sensor approach.

2. Background

2.1. Plant Transpiration Water-Atmosphere Scheme

In Figure 1, a plant leaf cut scheme is shown where it can be noticed that the different plant tissues (parenchyma, mesophyll and guard cells) which have low CO_2 contents and a high amount of water. The atmosphere, presented as a gray cloud constitutes a relatively dry environment that can eventually dehydrate or even kill the entire plant if the environmental conditions are not adequate [1]. The stomata guard cells which are the orange ones in Figure 1, are the plant system that controls the stomatal pores open and close process to balance the CO_2 and water fluxes between the plant and its environment. Here r_b is the boundary resistance and r_s is the stomatal resistance.

2.2. Transpiration Process

As was aforementioned, E is a function that depends primarily on the difference between e_i and e_o. However, primary humidity sensors provide relative humidity measurement values [6] and need to be converted into e_i and e_o. First, it is necessary to determine e_s in order to know the maximum amount of water that air can contain at a specified T_a by using vapor curves in the Mollier thermodynamic diagrams [2] or by using the simplified equation (1) as was previously reported [19]. Then e_i and e_o can easily be obtained with (2) and (3), where RH_i is air input RH and RH_o is leaf chamber output RH.

Figure 1. Leaf cut water scheme, showing CO_2 and H_2O flows.

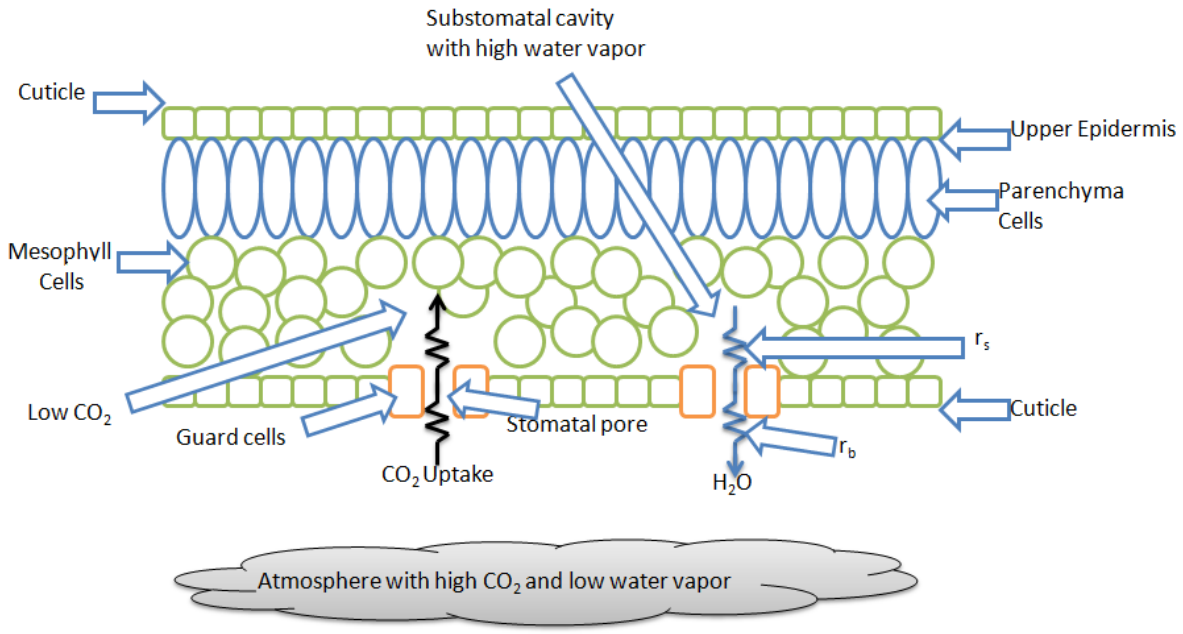

$$e_s = 6.13753 \times 10^{-3} \exp\left(T_a \quad \frac{18.564 - \frac{T_a}{254.4}}{T_a + 255.57} \right) \tag{1}$$

$$e_i = \frac{(RH_i)(e_s)}{100} \tag{2}$$

$$e_o = \frac{(RH_o)(e_s)}{100} \tag{3}$$

In order to estimate *E*; it is necessary to calculate another important factor, *W* which is the mass flow rate per leaf area, expressed in mol/m^2/s for open flow systems. *W* equation is stated in (4), where *P* is the atmospheric pressure in Bar, *V* is the volumetric air flow in liters per minute (lpm), T_aK is air temperature in Kelvin (K) and *A* is leaf area in cm^2, which is often used the effective leaf chamber area in transpiration and photosynthesis measurement systems [19]. The 2005.39 constant is an adjusted coefficient to change mass units to mol, surface to m^2 and time from minutes to seconds:

$$W = (2005.39)\frac{(V)(P)}{(T_aK)(A)} \tag{4}$$

Once e_i, e_o and *W* were estimated, *E* can be calculated as established in (5) and expressed in mg/m^2/s:

$$E = (W)(1000)(18.02)\frac{(e_o - e_i)}{(P - e_o)} \tag{5}$$

2.3. Stomatal Conductance

Stomatal conductance is another important transpiration dynamic variable that represents the guard cells vapor conductivity [1,2,5]. It can be estimated from primary temperature and *RH* sensors data. The first step is to calculate the leaf saturation vapor pressure e_{leaf} as a function of T_{leaf}. For this purpose, (1) can be used to calculate e_{leaf} substituting T_a by T_{leaf} to obtain (6). r_b is considered a constant of 0.3 m^{2}s/mol. Once e_{leaf} is obtained, stomatal conductance (C_{leaf}) can be calculated by using (7), expressing the result in mmol/m^2/s as was previously utilized [19]:

$$e_{leaf} = 6.13753 \times 10^{-3} \exp\left(T_{leaf} \quad \frac{18.564 - \frac{T_{leaf}}{254.4}}{T_{leaf} + 255.57} \right) \tag{6}$$

$$C_{leaf} = \frac{W}{\left(\frac{e_{leaf} - e_o}{e_o - e_i} \right)\left(\frac{P - e_o}{P} - R_b W \right)}(1000) \tag{7}$$

2.4. Vapor Pressure Deficit

VPD is a variable that represents the margin between air vapor pressure and air saturation vapor pressure. If air *RH* is low, *VPD* has a large margin; but if *RH* is high *VPD* is low and it is easy to get undesirable condensation conditions [6]. To calculate *VPD* it is necessary to subtract e_i from e_s. The most common units to represent *VPD* are kPa [2]:

$$VPD = e_s - e_i \tag{8}$$

3. Smart Sensor Methodology

The proposed methodology for the smart sensor can be seen in Figure 2. It consists of the following stages: primary sensors, data acquisition system (DAS), FPGA-based digital signal processing (DSP), RAM memory to storage sensors measurements, RS232 data communication module, and leaf chamber mechanism control system. In the first stage, five primary sensor signals are obtained from two RTD temperature sensors, two *RH* capacitive sensors and one light quantum sensor. The second stage consists of an eight channel DAS capable of acquiring the signals of the five primary sensors and leaving the last three channels disconnected (NC). The signal processing stage is carried out on a FPGA-based hardware signal processing (HSP) unit, as reported by [23] for CNC and [24] for robotics vibration applications. Atmospheric pressure is provided by external smart sensor input. Volumetric air flow is fixed at a constant 0.9 lpm flow rate by using a passive flow limiter. Data communication is carried out via RS232 interface embedded in the FPGA unit to send the measurement to a data server PC or another system. Finally, the leaf chamber opening mechanism and vacuum pump is controlled by the FPGA HSP unit.

Figure 2. Transpiration smart sensor architecture.

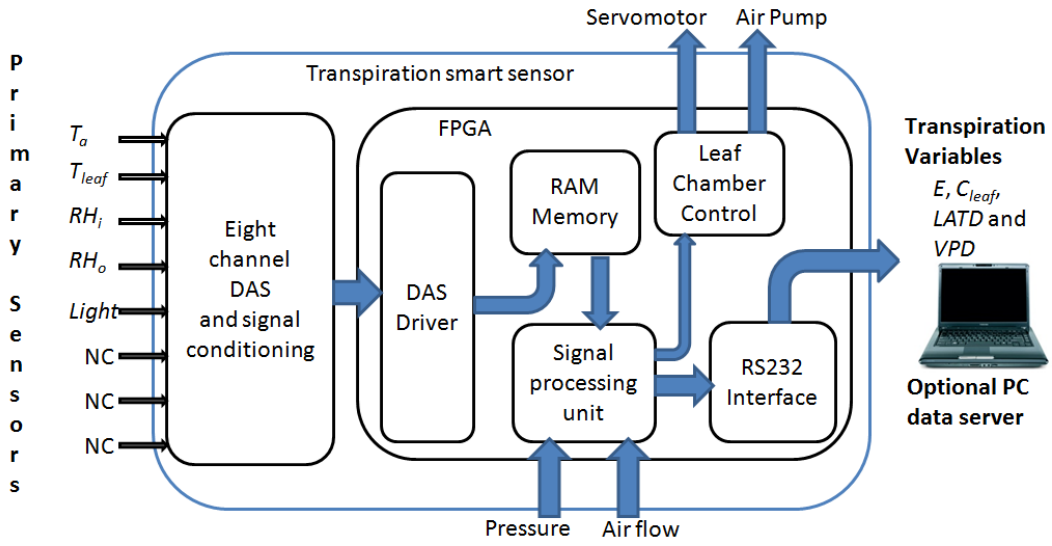

3.1. Transpiration Smart Sensing Cycle Methodology

Transpiration smart sensing cycle methodology is shown in Figure 3. Here, the green blocks represent the open leaf chamber stages and red blocks represent the closed leaf chamber; therefore,

isolating the plant leaf. Each measurement starts with the activation of the air vacuum pump and closing the leaf chamber by the servomotor controller to isolate the plant sample. The smart sensor performs a 1 min delay to wait pneumatic line flow steady state. After that, the data acquisition starts by measuring cycles of 1 Hz sampling frequency from the five primary sensors. This process is repeated to acquire 64 samples from each sensor in each transpiration measurement cycle. Once sufficient data has been acquired, the computation of transpiration dynamics are performed, data can be transferred, the leaf chamber is opened and vacuum pump is turned off to save energy. Finally, another delay is carried out to complete the 15 min duration of the entire transpiration smart sensing process. This measurement period was selected because in commercial equipment, the fastest acquisition period is 15 min and this is necessary to establish the same sampling frequency to compare both sensing techniques.

Figure 3. Block diagram of transpiration smart sensing cycle.

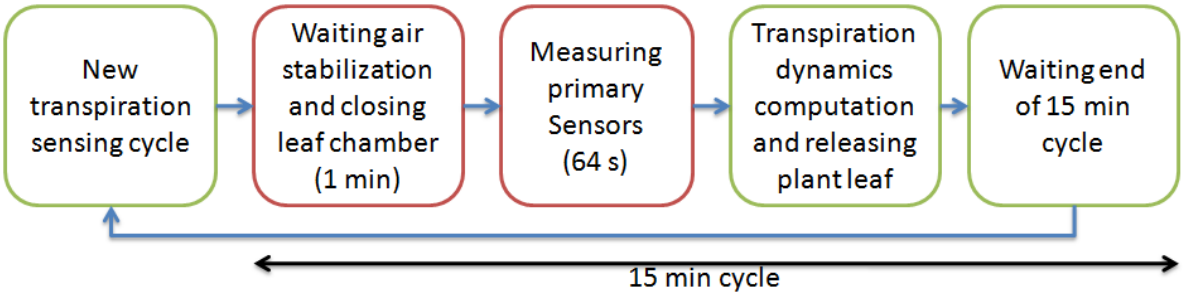

3.2. Transpiration Methodology

In order to calculate plant transpiration E, an FPGA-based signal processing methodology is proposed and described in Figure 4. Average decimation filters of 64th order are applied to all the primary sensors signals T_a, RH_i, and RH_o in order to reduce undesired quantization noise as stated in (9), (10), and (11) and presented by [14]. Once $T_{a\,os}$, $RH_{i\,os}$, and $RH_{o\,os}$ were estimated, a 1st order IIR low-pass filter (LPF) with cut-off frequency (f_c) of 1/3600 Hz is applied to obtain the filtered versions of the decimated signals known as $T_{a\,osf}$, $RH_{i\,osf}$, and $RH_{o\,osf}$. To gather E, equations (1) to (5) are computed from the filtered signals as presented in Figure 4.

$$T_{a\,os}\left(\frac{k}{64}\right)=\frac{1}{64}\sum_{i=0}^{64-1}T_a(k-i) \tag{9}$$

$$RH_{i\,os}\left(\frac{k}{64}\right)=\frac{1}{64}\sum_{i=0}^{64-1}RH_i\,(k-i) \tag{10}$$

$$RH_{o\,os}\left(\frac{k}{64}\right)=\frac{1}{64}\sum_{i=0}^{64-1}RH_o\,(k-i) \tag{11}$$

Figure 4. Transpiration estimation signal processing methodology.

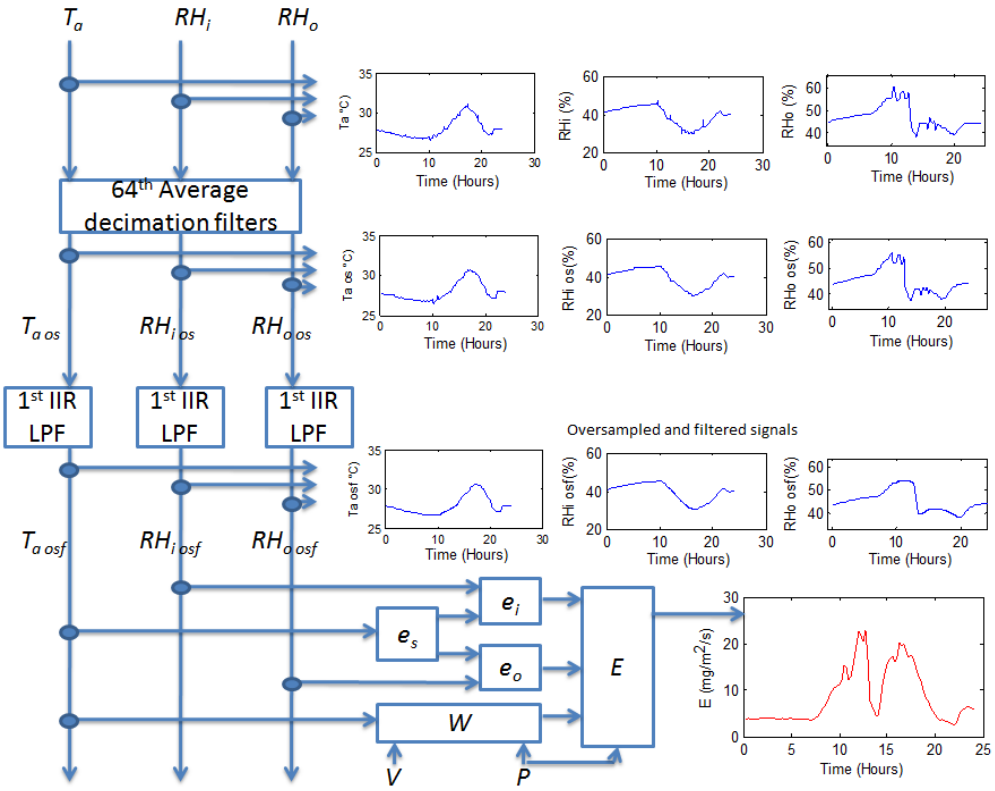

3.3. Stomatal Conductance Estimation Methodology

Stomatal conductance is advantageous because it utilizes certain factors previously calculated in the transpiration stage. A FPGA-based signal processing methodology is proposed and described in Figure 5.

Figure 5. Stomatal conductance estimation signal processing methodology.

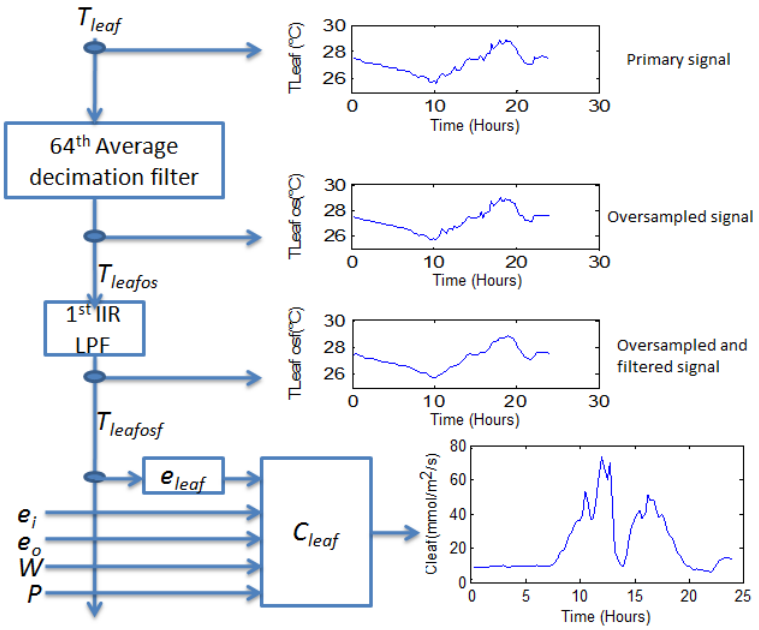

Average decimation filters of 64th order are applied to T_{leaf} sensor signals to reduce undesired quantization noise in the same manner as the previous stage according to (12). Once $T_{leaf\ os}$ was estimated, a 1st order IIR low-pass filter (LPF) stage with f_c = 1/3600 Hz is applied to obtain its filtered version $T_{leaf\ osf}$. Consequently, e_{leaf} is calculated as stated in (6) and introduced in (7) to obtain C_{leaf}:

$$T_{leaf\ os}\left(\frac{k}{64}\right)=\frac{1}{64}\sum_{i=0}^{64-1}T_{leaf}(k-i) \tag{12}$$

3.4. Vapor Pressure Deficit Methodology

VPD estimation is very simple once e_s and e_i are calculated in the transpiration calculation stage. *VPD* is obtained from the subtraction stated in (13). *VPD* implementation can be noted in Figure 6:

$$VPD = (100)(e_s - e_i) \tag{13}$$

Figure 6. *VPD*, *LATD* and *Light* estimation signal processing methodology.

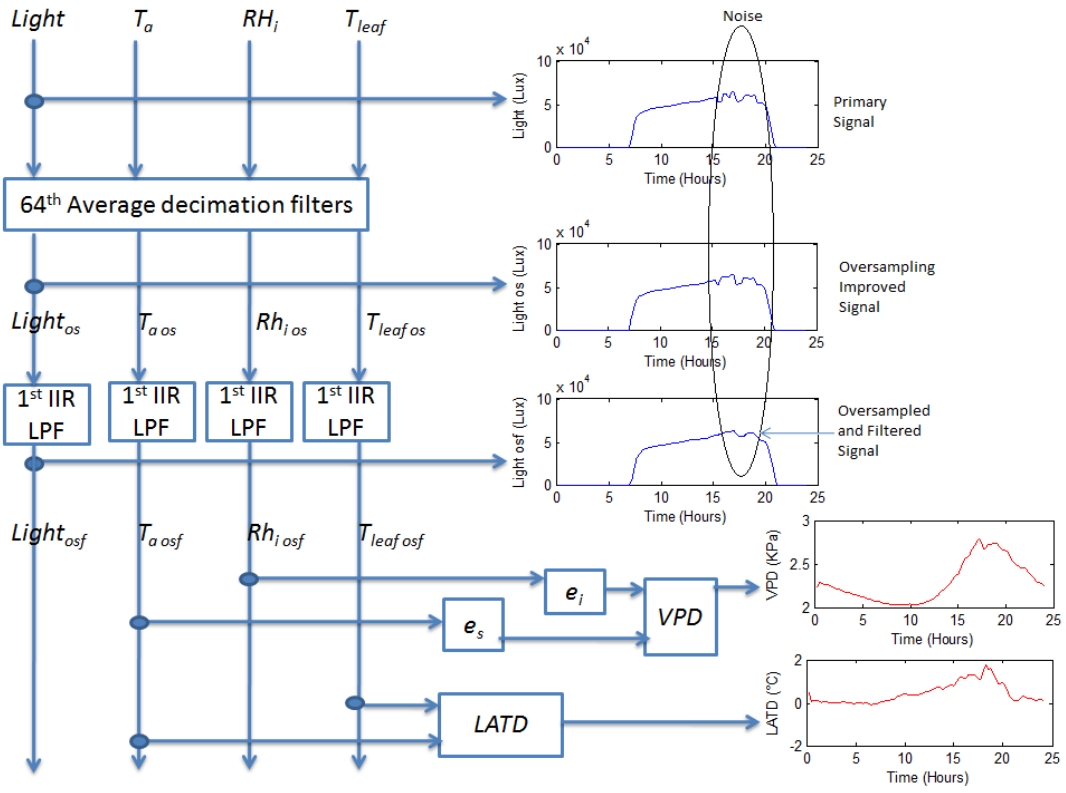

3.5. Leaf-Air Temperature Difference Methodology

LATD calculation requires subtracting the filtered air temperature and filtered leaf temperature. As occurred in previous calculation stages, once $T_{a\ osf}$ and $T_{leaf\ osf}$ was calculated, *LATD* computation is simple by using (14), as demonstrated in Figure 6:

$$LATD = T_{a\ osf} - T_{leaf\ osf} \tag{14}$$

3.6. Ambient Light Smart Sensor Methodology

To measure ambient light in a smoother signal manner, the same average decimation filter (15) plus 1st order IIR LPF with f_c = 1/3600 Hz was applied to the signal *light* in order to obtain its improved version $light_{osf}$:

$$light_{os}\left(\frac{k}{64}\right)=\frac{1}{64}\sum_{i=0}^{64-1} light(k-i) \tag{15}$$

4. Experimental Setup

4.1. Experiment Setup

The experimental setup can be seen in Figure 7, which shows the development of a smart sensor setup and the commercial Phytech PTM-48M, see Figure 7a and Figure 7b used for performance comparisons. For this experiment, tomato (*Lycopersicon esculentum*) plants were chosen as biological material to measure transpiration responses in the proposed smart sensor testing. The proposed smart sensor consists on an instrumentation platform capable of measuring T_a, T_{leaf}, RH_i, RH_o and *Light*. To measure temperature readings, Honeywell Pt1000 RTD primary sensors were used which have a measurement range from −200 ℃ to 540 ℃, but are configured for a 0 to 65 ℃ range with an accuracy rate of ±0.3 ℃ considered suitable for plant temperature ranges [10]. A RTD-signal conditioning system was developed to convert the resistance variation into a 0 to 5 volt format. For *RH* measurements, Honeywell HIH-4000 capacitive *RH* sensors with a range from 0 to 95% *RH* and accuracy of ±2.5% were selected and connected through a developed *RH*-signal conditioning system [11]. Ambient light measurement is achieved by using an OSRAM SFH-5711 light sensor with range from 0 to 100,000 lux and an accuracy of ±0.04% of its measured value, providing a 0 to 50 μA current signal [25], converted into 0 to 5 V by a designed light-signal conditioning system. The results are suitable in order to measure light intensities in rooms from total darkness to complete sunlight. Each primary sensor reading passes through a 2nd order analog anti-alias LPF with 20 Hz cut-off frequency embedded in the proposed smart sensor. An eight channel 12-bit data acquisition system based on the Burr Brown ADS7844 analog to digital converter instrumentation platform was developed to read the primary sensors [26]. An FPGA based hardware digital signal processing unit was utilized to compute the transpiration response variables from the primary sensors readings based on an Altera Cyclone III EP3C16F484C6N device with 16,000 LE [27]. For the open/close leaf chamber mechanism, a miniature servomotor model E-Sky 000155 was utilized because of its low power consumption. The air flow was induced using a dc-motor piston based vacuum pump. The FPGA IP core was implemented in VHDL language, integrating the DAS driver, leaf chamber motors control, signal processing unit and communications blocks.

The experiment was designed to monitor transpiration variables every 15 min to compare the proposed smart sensor with a Phytech PTM-48M photosynthesis and transpiration monitor configured at its fastest sampling period which is 15 min [18]. Both were connected to the same tomato plant to prove the effectiveness of the proposed smart sensor. The experiment ran for 24 hours beginning at 12:00AM and finishing at 12:00AM of the next day. It permits the acquisition of four measurement

cycles per hour for a total of 96 measurements every 24 h. As was aforementioned, each measurement cycle acquires 64 samples from each primary sensor at a sampling frequency of 1 Hz to apply the 64th averaging decimation filters. The data can be sent to a data server for massive storage via an Analog Devices ADM3232 RS232 transceiver [28].

Figure 7. (a) Transpiration smart sensor experimental setup. (b) Phytech PTM-48M setup.

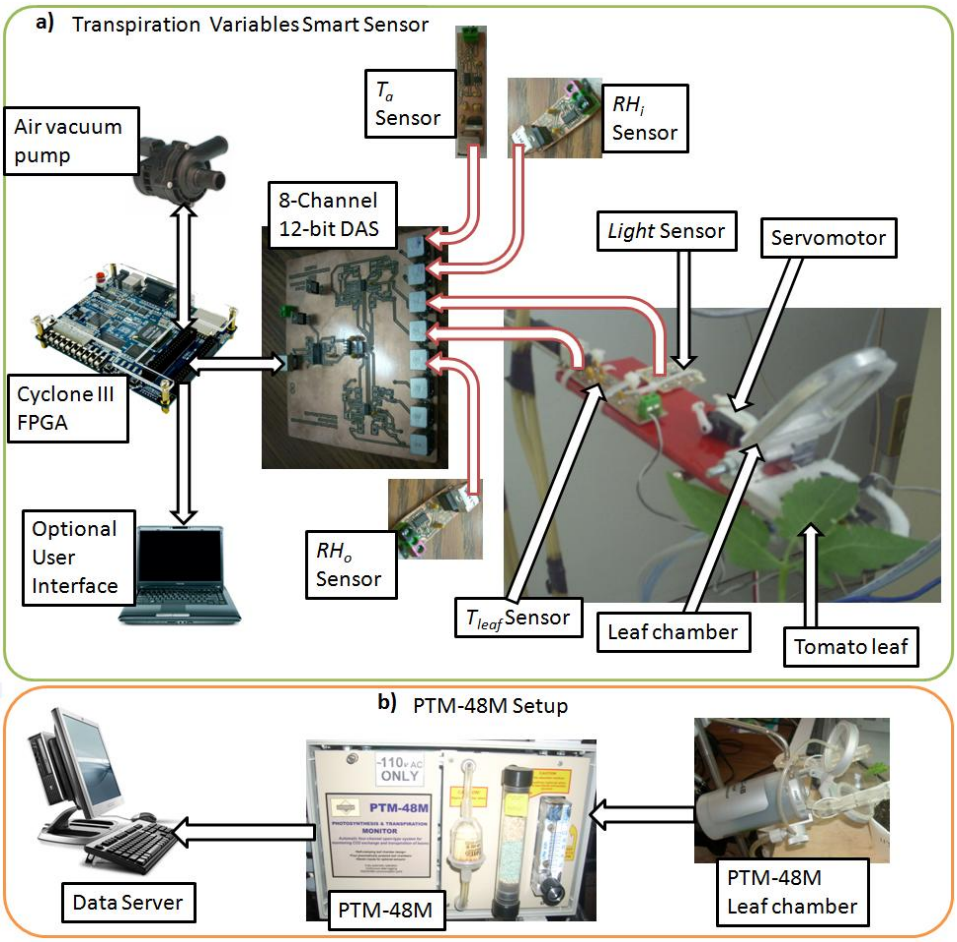

4.2. Primary Sensor Signal Improvement Results

In this subsection, a comparison between the T_a and RH_i readings from the proposed smart sensor and the commercial PTM-48M is presented. Figure 8 illustrates this comparison where blue signals correspond to PTM-48M readings and red ones to the proposed smart sensor primary readings. Here, it can be noted that a similar tendency occurs for both measurements, but a lower amount of noise in the red signals is present due to the 64-sample average decimation filters and 1st order IIR filters that reduces undesirable variations. In this manner, the filtering advantages of the smart-sensor signal processing can be clearly noticed. RH_o, T_{leaf}, and *Light* readings are not compared because PTM-48M does not provide RH_o measurement in the data output table and does not have T_{leaf} and *Light* sensors.

Figure 8. Primary sensors signal comparison. The proposed smart sensor signals are in red and Phytech PTM-48M readings in blue.

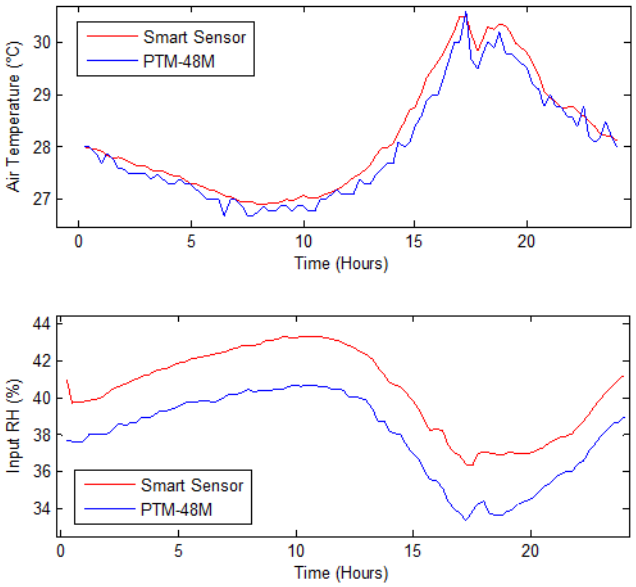

4.3. Transpiration Results and Comparison

This subsection shows a comparison between the proposed smart sensor transpiration estimation and the reference PTM-48M. In Figure 9, this comparison is represented by using blue for the PTM-48M transpiration signal and red for the smart-sensor transpiration estimation signal. Here, it is noteworthy that a similar transpiration signal behavior between both instruments occurs.

Figure 9. Comparison between the developed smart sensor and the PTM-48M transpiration estimations.

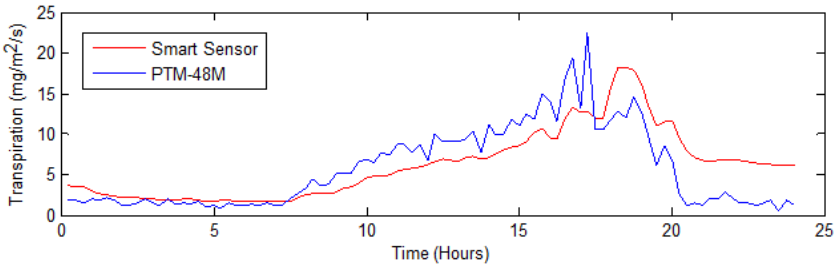

4.4. Fused Transpiration Dynamics Smart Sensing Results

The proposed smart sensor fuses T_a, T_{leaf}, RH_i, Rh_o and *Light* measurements in a single device which is considered highly desirable for precision agriculture applications to be able to monitor different environmental factors that can affect the crops. In Figure 10, the monitoring results of the primary sensors in this experiment are presented. All of these were previously oversampled 64 times for the average filtering process and passed through an IIR 1st order LPF with a cut-off frequency of $f_c = 1/(3600)$. As it can be seen, the amount of noise in these primary signals is very low.

Figure 10. Primary sensor readings of the proposed smart sensor.

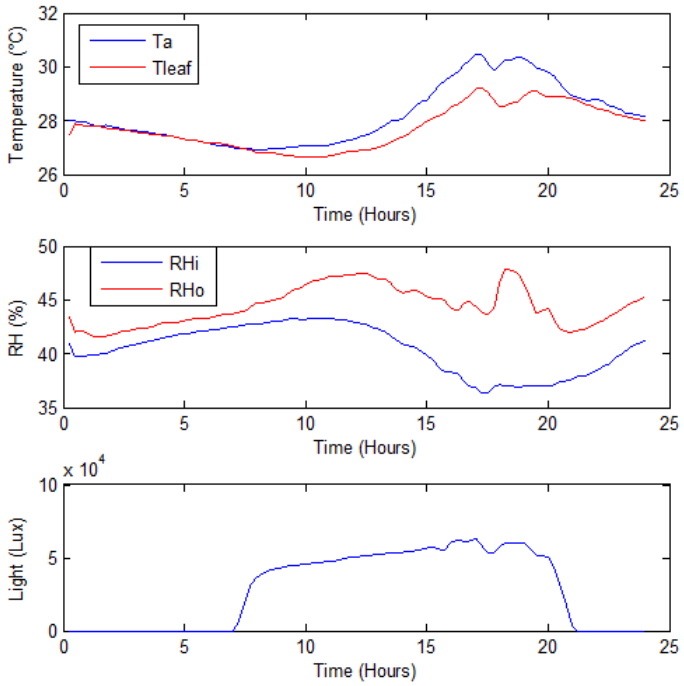

In Figure 11, transpiration dynamics response variables (*E*, C_{leaf}, *LATD*, and *VPD*) can be observed. These parameters share a similar dynamic behavior because they are related to the entire photosynthesis and transpiration processes which involve different phenomena.

Figure 11. Transpiration dynamics results.

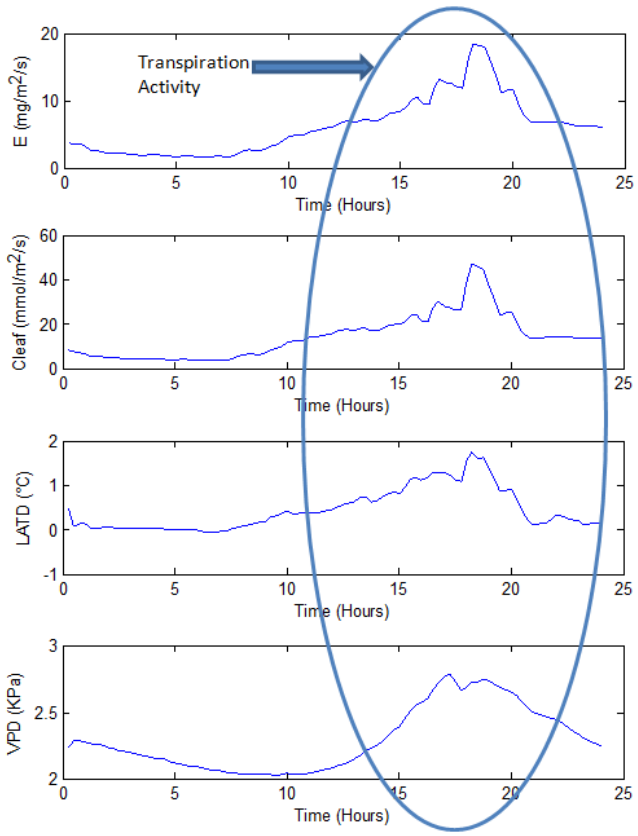

The computation of the required equations to obtain these results is achieved using FPGA reconfigurability and open architecture that permits implementation of any digital system such as data acquisition, memory management, signal processing, and data communication. The developed smart sensor fuses five primary sensors and can measure the necessary environmental variables to calculate transpiration dynamics and permits the user to observe and record different primary and response measurements at the same time and the relationship between these. This is very useful in precision agriculture in order to detect abnormal conditions. In contrast, commercial equipment as noted in [18,19] can measure time series of transpiration information; however, they do not provide the readings for all the primary sensors. In some cases, they are not equipped with the necessary sensors. The FPGA-based unit permits improvements of the primary sensor signals by oversampling and digital filtering that is consequently reflected in superior accuracy, and overall transpiration variables signal quality. The integration of these elements merge different variables at the same time that can be acquired and used to take specific control actions by communicating these transpiration measured values to other systems via RS232 interface like PC data servers, an irrigation controller, or a climatic control unit due to the online processing and remote communications capabilities of the proposed smart sensor. Taken together they constitute a smart sensor solution to monitor transpiration variables in precision agriculture applications by using a single FPGA-based system.

5. Conclusions

In this investigation the development of a novel smart sensor that can estimate plant-transpiration dynamic variables as: transpiration, stomatal conductance, leaf-air temperature difference, and water vapor deficit in real time is presented. This smart sensor fuses five primary sensors: two temperature sensors, two relative humidity sensors and one light sensor. To show the effectiveness of the proposed smart sensor, it was compared with a commercial Phytech PTM-48M transpiration monitoring system. Results show that the proposed sensor can obtain very similar results compared to the reference system with less noise due to the digital filtering applied to the primary measurements. The transpiration dynamics variables are calculated in real time from the primary sensor data providing very useful information related to the plant transpiration which is valuable to schedule irrigation, prevent diseases, and detect drought conditions in precision agriculture. Similar behavior of the estimated transpiration variables shows the relationship between these and how they depend on the primary sensor readings. The necessary computations in order to obtain the transpiration dynamics are computed in a low-cost FPGA platform in which parallel architecture is utilized to implement the transpiration equations. This permits the integration of the data communication, memory management data acquisition and signal processing in a single embedded sensor which can be used to monitor plant transpiration variables and their relationships in a wide range of precision agriculture applications. Finally, transpiration related stress conditions can be detected in real time because of the online processing and communications capabilities. All of which constitutes a very useful precision agriculture smart sensor.

Acknowledgements

This project was partially supported by CONACYT scholarship 207684, FOMIX-QRO-2008-CO2-101490 and FOMIX-QRO-2008-CO2-102123 projects. The authors wish to thank HSP Digital research group

in general but specially by the assistance in the aluminum leaf chamber machining process. Also thanks to Altera Corp. for the donation of an Altera DE2-70 3 in 1 FPGA development kit used at the beginning of this project. They also wish to thank Texas Instruments Inc. and Analog Devices Inc. for donating analog electronics samples which were tested in the data acquisition system development. Finally, the authors wish to acknowledge Silvia C. Stroet of the Engineering Faculty at Universidad Autonoma de Queretaro for editing the English content of this document.

References

1. Taiz, L.; Zeiger, E. *Plant Physiology*, 4th ed.; Sinauer Associates: Sunderland, MA, USA, 2006.
2. Bakker, J.C.; Bot, G.P.A.; Challa, H.; Braak, N.J. *Greenhouse Climate Control: An Integrated Approach*; Wageningen Academic Publishers: Wageningen, The Netherlands, 2001.
3. Field, C.B.; Ball, J.T.; Berry, J.A. *Photosynthesis: Principles and Field Techniques. Plant Physiological Ecology: Field Methods and Instrumentation*; Chapman and Hall: London, UK, 1991; pp. 209-253.
4. Bittelli, M. Measuring soil water potential for water management in agriculture: A review. *Sustainability* **2010**, *2*, 1226-1251.
5. Hubbard, R.M.; Ryan, M.G.; Stiller, V.; Sperry, J.S. Stomatal conductance and photosynthesis vary linearly with plant hydraulic conductance in ponderosa pine. *Plant Cell Environ.* **2001**, *24*, 113-121.
6. Kamp, P.G.H.; Timmerman, G.J. *Computerized Environmental Control in Greenhouses: A Step by Step Approach*; IPC Plant: Ede, The Netherlands, 1996.
7. Prenger, J.J.; Ling, P.P. *Greenhouse Condensation Control. Fact Sheet (Series) AEX-800*; Ohio State University Extension: Columbus, OH, USA, 2000.
8. Marschner, H. *Mineral Nutrition of Higher Plants*; Academic Press: San Diego, CA, USA, 1995.
9. Stout, M.J.; Fidantsef, A.L.; Duffey, S.S.; Bostock, R.M. Signal iinteractions in pathogen and insect attack: Systemic plant-mediated interactions between pathogens and hervibores of the tomato, lycopersicon esculentum. *Physiol. Molec. Plant. Pathol.* **1999**, *54*, 115-130.
10. *HEL-700 Pt1000 RTD Sensor Data Sheet*; Honeywell: Golden Valley, MN, USA, 2010.
11. *HIH-4000 RH Sensor Data Sheet*; Honeywell: Golden Valley, MN, USA, 2010.
12. Rivera, J.; Herrera, G.; Chacón, M.; Acosta, P.; Carrillo, M. Improved progressive polynomial algorithm for self-adjustment and optimal response in intelligent sensors. *Sensors* **2008**, *8*, 7410-7427.
13. Hernandez, W. A survey on optimal signal processing techniques applied to improve the performance of mechanical sensors in automotive applications. *Sensors* **2007**, *7*, 84-102.
14. Rangel-Magdaleno, J.J.; Romero-Troncoso, R.J.; Osornio-Rios, R.A.; Cabal-Yepez, E. Novel oversampling technique for improving signal-to-quantization noise ratio on accelerometer-based smart jerk sensors in CNC applications. *Sensors* **2009**, *9*, 3767-3789.
15. Millan-Almaraz, J.R.; Guevara-Gonzalez, R.G.; Romero-Troncoso, R.J.; Osornio-Rios, R.A.; Torres-Pacheco, I. Advantages and disadvantages on photosynthesis measurement techniques: A review. *Afr. J. Biotechnol.* **2009**, *8*, 7340-7349.

16. Strobel, B.R.; Stowell, R.R. *Using a Psychrometric Chart to Describe Air Properties Fact Sheet AEX-120-99*; Ohio State University Extension: Columbus, OH, USA, 1999.
17. Schmidt, U. Microclimate control in greenhouses based on phytomonitoring data and Mollier phase diagram. *Acta Hortic.* **2005**, *691*, 125-132.
18. *PTM-48M User Manual*; Phytech Inc.: Yad Mordechai, Israel, 2005.
19. *CI-340 Hand-held Photosynthesis System Instruction Manual*; CID Inc.: Camas, WA, USA, 2008.
20. Escalona, L.; Flexas, J.; Medrano, H. Comparison of heat balance and gas exchange methods to measure transpiration in irrigated and water stressed grapevines. *Acta Hortic.* **2000**, *526*, 145-156.
21. Schulze, E.D. A new type of climatized gas exchange chamber for net photosynthesis and transpiration measurements in the field. *Oecologia* **1972**, *10*, 243-251.
22. Ton,Y.; Kopyt, M.; Nilov, N. Phytomonitoring technique for tuning irrigation of vineyards. *Acta Hortic.* **2004**, *646*, 133-139.
23. Trejo-Hernandez, M.; Osornio-Rios, R.A.; Romero-Troncoso, R.J.; Rodriguez-Donate, C.; Dominguez-Gonzalez, A.; Herrera-Ruiz, G. FPGA-based fused Smart-sensor for Tool-wear area quantitative estimation in CNC machine inserts. *Sensors* **2010**, *10*, 3373-3388.
24. Rodriguez-Donate, C.; Morales-Velazquez, L.; Osornio-Rios, R.A.; Herrera-Ruiz, G.; Romero-Troncoso, R.J. FPGA-Based fused smart sensor for dynamic and vibration parameter extraction in industrial robot links. *Sensors* **2010**, *10*, 4114-4129.
25. *SFH-5711 Data Sheet*; OSRAM Opto Semiconductors Inc.: Munich, Germany, 2007.
26. *ADS7844 Data Sheet*; Burr Brown Corp: Dallas, TX, USA, 2003.
27. *Cyclone III Hand Book Volume 1*; Altera Corp: San Jose, CA, USA, 2010.
28. *ADM3232 Data Sheet*; Analog Devices Inc: Norwood, MA, USA, 2008.